DETERMINATION OF ALL FRACTIONAL-ORDER PID CONTROLLERS THAT MEET SPECIFIC STABILITY, ROBUSTNESS, AND PERFORMANCE REQUIREMENTS

A Dissertation by

Yung K. Lee

Master of Science, Wichita State University, 2008

Bachelor of Science, Korea Aerospace University, 1997

Submitted to the Department of Electrical Engineering and Computer Science
and the faculty of the Graduate School of
Wichita State University
in partial fulfillment of
the requirements for the degree of
Doctor of Philosophy

July 2013

DETERMINATION OF ALL FRACTIONAL-ORDER PID CONTROLLERS THAT MEET SPECIFIC STABILITY, ROBUSTNESS, AND PERFORMANCE REQUIREMENTS

The following faculty members have examined the final copy of this dissertation for form and content, and recommend that it be accepted in partial fulfillment of the requirement for the degree of Doctor of Philosophy.

_____
John M. Watkins, Committee Chair

_____
M. Edwin Sawan, Committee Member

_____
James E. Steck, Committee Member

_____
Ward T. Jewell, Committee Member

_____
Brian J. Driessen, Committee Member

Accepted for the College of Engineering

_____
Vish Prasad, Interim Dean

Accepted for the Graduate School

_____
Abu S.M. Masud, Interim Dean

To My Loved Ones…. Mom and K.

Living by Chance

Loving by Choice

Dying by Destiny…

ACKNOWLEDGMENTS

I would like to express the deepest appreciation to Dr. John M. Watkins in the Department of Electrical Engineering and Computer Science at Wichita State University for his support of this dissertation. Without his encouragement, guidance, and continued help this dissertation would not have been possible.

Special thanks to Dr. M. Edwin Sawan whose enthusiasm for life-long learning and research has long-lasting effects. I feel motivated and encouraged every time I meet him.

I would also like to express my gratitude to my committee members Dr. James E. Steck, Dr. Ward T. Jewell, and Dr. Brian J. Driessen for their useful comments and engagement through the learning process of this dissertation.

I would also like to thank Wilfred Nobleheart, who as a good friend, is always willing to help and give his guided input. It would have been difficult to successfully complete the experiments in Chapter 8 of my dissertation without him.

I would like to extend my gratitude to my friends, Tom McGuire, Carole Higgins, and Ken Tedder, for their helpful technical support through various forms.

I would like to thank my mom who has supported and inspired me throughout the entire process.

Finally, I would like to show my greatest appreciation to my best friend, Kristie Sheridan, for being there for me. It would have been a lonely journey without her.

ABSTRACT

In this dissertation, a broad spectrum of research in fractional-order (FO) proportional-integral-derivative (PID) controllers is directed to fundamental control problems such as stability, performance, and robustness. First, nominal stability was considered by finding all the possible FO PID controllers that stabilize a closed-loop system with respect to arbitrary values of the fractional orders λ and μ of the FO PID controller. The findings are presented on the (K_p, K_i), (K_p, K_d), and (K_i, K_d) planes. In order to meet nominal performance specifications, a sensitivity function weight was introduced and FO PID controllers were sought to meet the weighted sensitivity constraint. This led to a complete set of possible values of FO PID parameters that satisfy the given performance specifications. Following the nominal stability and performance, robust stability and performance were investigated. For a robust stability requirement, a multiplicative weight was selected to bound all multiplicative errors of a closed-loop system. Such FO PID controllers allow the closed-loop to remain stable for all the sets of perturbed plants. Nominal performance and robust stability are the prerequisite conditions for the robust performance of a closed-loop system. Though, in robust stability analysis, the closed-loop system was designed only to remain stable, it was required not only to remain stable for all the uncertain plants but also to satisfy given performance specifications in the robust performance analysis. A substantial contribution of this research is the establishment of a complete set of solutions for FO PID controllers, with respect to nominal stability and performance and robust stability and performance. The use of frequency response of a system makes it possible to apply the results presented in this dissertation even when a system transfer function is not known or unavailable, as long as the experimental frequency data of a system can be obtained.

TABLE OF CONTENTS

TABLE OF CONTENTS (continued)

TABLE OF CONTENTS (continued)

Chapter Page

LIST OF FIGURES

LIST OF FIGURES (continued)

Figure Page

LIST OF FIGURES (continued)

Figure Page

LIST OF TABLES

Table Page

CHAPTER 1
INTRODUCTION

1.1 Background and Motivation

Though its origin traces back to the late seventeenth century, fractional calculus had largely remained a topic of pure mathematics shared only by a small number of mathematicians and pure scientists for over three hundred years [1]. Fractional calculus is a form of calculus generalized by expanding its orders from integers to real numbers. Recently, numerous attempts have been made to apply the concept of the fractional calculus to the fields of physics and engineering including, for example, nonlinear control and fractional order controllers [2] and [3]. In controls, Axtell and Bise demonstrated the application of fractional calculus to control systems using both the *s*-domain and frequency-domain with the introduction of s^q operator [4]. Undiminishing popularity of proportional-integral-derivative (PID) controllers in the process control field brought about considerable interest in their non-integer counterpart, $PI^{\lambda}D^{\mu}$ controllers (where λ and μ are arbitrary real numbers) or so called fractional-order PID controllers.

In order to clearly differentiate the two kinds of PID controllers, hereinafter, conventional integer-order PID controllers are referred to as IO PID controllers, and non-integer order or fractional-order PID controllers are referred to as FO PID controllers. Strictly speaking, the term 'fractional order' is rather a misnomer because the orders of integration and differentiation can be any real numbers including not only fractions (rational numbers) but also irrational numbers. For that reason, it is more appropriate to use the term 'non-integer order.' Nonetheless, there has been much more research using 'fractional-order' than 'non-integer order' in automatic control as well as in mathematics and physics. Thus, in order to provide a consistent and strong connection between existing results found in the literature and the research presented here, the term 'fractional-order (FO)' will be used in the rest of this paper.

As can be appreciated from the relationship between integer numbers and real numbers, the best FO PID controllers were shown to outperform the best IO PID controllers in [5]. While IO mathematical models are easier to work with, real physical systems are often described more accurately and naturally through non-integer order models. In [6], a torsional system consisting of a rigid disk and a flexible shaft attached thereto was modeled using an FO transfer function.

The resulting frequency response shows that the mechanical resonance effect is represented more naturally with an FO model than an IO model.

In addition, a technique was provided for finding all IO PID controllers that stabilize a given plant transfer function of an arbitrary order in [7]. The stabilizing controllers that lie within the stability regions are plotted in three different planes of (K_p, K_i), (K_p, K_d) and (K_d, K_i). Furthermore, a graphical method was developed for finding all robustly stabilizing IO PID controllers for a closed-loop system in [8]. In particular, the methods in [7] and [8] used system frequency response to respective results.

Thus, it is the objective of this research to provide generalized methods for finding all FO PID controllers (which of course include IO PID controllers as well) for a given system of arbitrary order that satisfy stability, robustness, or performance requirements by combining two important topics, i.e., the fractional calculus and PID controllers. Especially, the methods presented here will bring the existing solutions that have been applicable only to IO PID controllers so far under one generalized complete solution. Moreover, the benefits of using an FO PID controller over an IO PID controller will be demonstrated by comparing the results found using FO PID controllers with those found using IO PID controllers.

1.2 Outline of the Dissertation

The rest of this paper is organized as follows. Fractional calculus is introduced in Chapter 2. Definitions, examples of calculations, and frequency domain response are included. Then, Chapter 3 provides a review of related literature, mainly on FO controllers, stability discussion of IO and FO PID controllers, and robust stability and performance of PID controllers including H_∞ control. Chapter 4 will provide a method for finding all stabilizing FO PID controllers in terms of the proportional gain K_p, integral gain K_i, and derivative gain K_d of FO PID controllers, along with specified gain and phase margin requirements. A weighted sensitivity constraint will be utilized to determine all stabilizing FO PID controllers that satisfy certain performance requirements in Chapter 5. In Chapter 6, all FO PID controllers will be determined not only to stabilize a given system but also to meet a robust stability constraint. Such FO PID controllers guarantee the stability of a closed-loop system in question for all the possible sets of perturbed plants. Following the investigation of the robust stability and nominal performance of a closed-loop system containing an FO PID controller, robust performance design of FO PID controllers

will be addressed in Chapter 7 so as to meet required performance specifications as well as robust stability constraint. Lastly, Chapter 8 will show the practical applicability of the technique proposed in Chapters 3 to 7 through the application to a DC motor system.

CHAPTER 2
INTRODUCTION TO FRACTIONAL CALCULUS

2.1 Introduction

As some readers may not be familiar with the concept of fractional calculus, it is beneficial to provide some background knowledge of the fractional calculus to help better understand the underlying principle of FO PID controllers. Thus, this chapter serves to provide a brief history, basic definitions, some examples, and the Laplace and Fourier transforms of the fractional calculus.

2.2 Inception of Fractional Calculus

Fractional calculus is believed to have its origin from correspondence between scholars in the late 17^{th} century. In particular, the letters between Gottfried Leibniz and de l'Hôpital on September 30, 1695 provided the notion of fractional calculus. In the letters, Leibniz had asked de l'Hôpital about the possibility of non-integer orders in derivatives, and de l'Hôpital responded with a specific order of $\frac{1}{2}$ (i.e. $\frac{1}{2}$th derivative). Based on such historic letters, September 30, 1695 is considered the birthday of fractional calculus, with Gottfried Leibniz being its father [1]. Laplace defined a fractional derivative in the form of an integral in 1812 and later S.F. Lacroix first discussed a derivative of fractional orders in his calculus text that included Laplace's work. It is Niels Abel who applied a fractional operation for the first time to solve an integral equation in the tautochrone problem in 1823 [9].

2.3 Definitions of Fractional Calculus

2.3.1 Definition by Riemann-Liouville

Joseph Liouville first defined a fractional derivative of arbitrary order using an infinite series. Because of the limitation on the values of the order in his earlier definition, he proposed a second definition of fractional derivative of $x^{(-\alpha)}$, where both x and α are positive. In the meantime, Bernhard Riemann presented arbitrary-order integration using Taylor series [9] and [10]. Fortunately, the two seemingly different definitions of the integration of arbitrary order

proposed by Liouville and Riemann, respectively, were incorporated into a single formula so called the Riemann-Liouville fractional integral formula [11]:

$$J_c^{\alpha} f(t) = \frac{1}{\Gamma(\alpha)} \int_c^t \frac{f(\tau)}{(t-\tau)^{1-\alpha}} d\tau \tag{1}$$

where J^{α} is fractional integral operator of order $\alpha \in \mathbb{R}^+$, $f(t)$ is a causal function of time that identically vanishes for t < 0, c is a lower limit of integration, and Γ is the Gamma function.

For example, if we integrate $f(t)$ with $\alpha = 1$, then

$$\begin{aligned} J_c^{\alpha} f(t) &= \frac{1}{\Gamma(\alpha)} \int_c^t \frac{f(\tau)}{(t-\tau)^{1-\alpha}} d\tau \Big|_{\alpha=1} \\ J_c^{1} f(t) &= \frac{1}{\Gamma(1)} \int_c^t \frac{f(\tau)}{(t-\tau)^{1-1}} d\tau \\ &= \int_c^t f(\tau) d\tau \end{aligned} \tag{2}$$

which matches the standard integration of $f(t)$.

Next, Riemann-Liouville fractional derivative of order α is derived from the fractional integral in (1) on the basis of the reverse relationship between integral and derivative. The fractional derivative formula of order $\alpha > 0$ is defined for a positive integer m such that $n-1 \le \alpha < n$ [10] and [11]:

$${}_a D_t^{\alpha} f(t) = {}_a D_t^{n} J_a^{n-\alpha} f(t) = \frac{d^n}{dt^n} \left[\frac{1}{\Gamma(n-\alpha)} \int_a^t \frac{f(\tau)}{(t-\tau)^{\alpha+1-n}} d\tau \right] \tag{3}$$

where D^n is the operator of the derivative of integer order n. D^n is only the left-inverse to the corresponding integral operator J^n ($D^n J^n = I$). D^{α} is the operator of the derivative of order $\alpha \in \mathbb{R}^+$ (which is defined as left-inverse to J^{α} for arbitrary order α).

2.3.2 Definition by Grunwald-Letnikov

Along with Riemann-Liouville formula, Grunwald-Letnikov is one of the most widely used formulae for fractional calculus, which was introduced by Anton Karl Grunwald and then was demonstrated by A. V. Letnikov. The Grunwald-Letnikov fractional derivative formula was given by:

$$ {}_aD^{\alpha} f(t) = \lim_{h \to 0} \frac{1}{h^{\alpha}} \sum_{m=0}^{\frac{t-a}{h}} (-1)^m \frac{\Gamma(\alpha+1)}{m!\Gamma(\alpha-m+1)} f(t-mh) \tag{4} $$

where a and t are the lower and upper limits of differentiation, respectively [10].

Likewise, the Grunwald-Letnikov definition of the fractional integral (5) was obtained from the Grunwald-Letnikov derivative formula (4) by taking negative α in the derivative formula (4). Thus, Grunwald-Letnikov fractional integral formula was given by:

$$ {}_aD^{-\alpha} f(t) = \lim_{h \to 0} h^{\alpha} \sum_{m=0}^{\frac{t-a}{h}} \frac{\Gamma(\alpha+m)}{m!\Gamma(\alpha)} f(t-mh) \tag{5} $$

As can be seen from (4) and (5), differentiation is defined for positive index (α) and integration is defined for negative index ($-\alpha$) for the differ-integral operator (D), which is why (4) and (5) are collectively called "Grunwald-Letnikov fractional differintegrals" [10]. Given the two different forms of definition, the Riemann-Liouville formula is appropriate for determining the analytical solution of rather simple functions such as x^a, e^x, $sin(x)$ etc., whereas, the Grunwald-Letnikov definition is preferred for numerical calculations [12].

2.3.3 Definition by Caputo

In addition to the Riemann-Liouville and Grunwald-Letnikov definitions, M. Caputo introduced a definition of the fractional derivative in 1967 [10]:

$$ {}_a^C D_t^{\alpha} f(t) = \frac{1}{\Gamma(n-\alpha)} \int_a^t \frac{f^{(n)}(\tau)}{(t-\alpha)^{\alpha+1-n}} d\tau \tag{6} $$

which is defined for the order $\alpha > 0$ (where $n-1 < \alpha \le n$ for a positive integer m). Although (6) proposed by Caputo is quite similar to (3) provided by Riemann-Liouville, the Caputo derivative (6) is preferred to the Riemann-Liouville derivative (3), in particular, in various engineering applications [12]. In addition to the above three definitions, Oldham and Spanier, K.S. Miller and B. Ross, Kolwankar and Gangal et al. had also introduced definitions and modifications thereof.

2.4 Examples of Fractional Calculus

The α^{st} fractional derivative of a function $f(t)$ given by Grunwald-Letnikov derivative is equated with a general expression of the α^{st} derivative of a function $f(t)$ in [10]:

$$\begin{aligned} D^{\alpha} f(t) &= \lim_{h \to 0} \frac{1}{h^{\alpha}} \sum_{m=0}^{\frac{t-a}{h}} (-1)^m \frac{\Gamma(\alpha+1)}{m!\Gamma(\alpha-m+1)} f(t-mh) \\ &= \lim_{h \to 0} \frac{1}{h^{\alpha}} \sum_{m=0}^{\alpha} (-1)^m \frac{\Gamma(\alpha+1)}{m!\Gamma(\alpha-m+1)} f(t-mh) \end{aligned} \tag{7}$$

By using the gamma function,

$$\frac{\Gamma(\alpha+1)}{\Gamma(m+1)\Gamma(\alpha-m+1)} = \frac{\alpha!}{m!(\alpha-m)!} = \binom{\alpha}{m} \tag{8}$$

equation (7) becomes equivalent to:

$$D^{\alpha} f(t) = \lim_{h \to 0} \frac{1}{h^{\alpha}} \sum_{m=0}^{\alpha} (-1)^m \binom{\alpha}{m} f(t-mh) \tag{9}$$

Example 1.

Let $f(t) = e^{at}$. Then, the α^{st} fractional derivative of the given function $f(t) = e^{at}$ can be determined as follows:

$$
\begin{aligned}
D^{\alpha} f(x) = D^{\alpha} e^{ax} &= \lim_{h\to 0} \frac{1}{h^{\alpha}} \sum_{n=0}^{\alpha} (-1)^n \binom{\alpha}{n} e^{a(x+(\alpha-n)h)} \\
&= e^{ax} \lim_{h\to 0} \frac{1}{h^{\alpha}} \sum_{n=0}^{\alpha} (-1)^n \binom{\alpha}{n} (e^{ah})^{\alpha-n} \\
&= e^{ax} \lim_{h\to 0} \frac{1}{h^{\alpha}} \sum_{n=0}^{\alpha} \binom{\alpha}{n} (e^{ah})^{\alpha-n} (-1)^n \\
&= e^{ax} \lim_{h\to 0} \frac{1}{h^{\alpha}} (e^{ah} - 1)^{\alpha} \\
&= e^{ax} \lim_{h\to 0} \frac{\alpha! a^{\alpha} \cdot e^{ah}}{\alpha! \cdot 1^{\alpha}} \\
&= a^{\alpha} e^{ax} \qquad (10)
\end{aligned}
$$

The binomial formula was utilized between the third and fourth lines and the l'Hopital's rule was applied between the fourth and fifth lines.

Example 2.

The above result (10) will be used in this example along with linearity and Euler's formula.

$$
\begin{aligned}
D^{\alpha} \cos x + jD^{\alpha} \sin x &= D^{\alpha} \left(\cos x + j \sin x \right) \\
&= D^{\alpha} e^{jx} = j^{\alpha} \cdot e^{jx} \\
&= e^{j\frac{\pi}{2}\alpha} \cdot e^{jx} = e^{j(x+\frac{\pi}{2}\alpha)} \\
&= \cos(x + \frac{\pi}{2}\alpha) + j \sin(x + \frac{\pi}{2}\alpha) \qquad (11)
\end{aligned}
$$

$$
\begin{aligned}
D^{\alpha} \cos x - jD^{\alpha} \sin x &= D^{\alpha} \left(\cos x - j \sin x \right) \\
&= D^{\alpha} e^{-jx} = (-j)^{\alpha} \cdot e^{-jx} \\
&= e^{j(-\frac{\pi}{2})\alpha} \cdot e^{-jx} = e^{-j(x+\frac{\pi}{2}\alpha)}
\end{aligned}
$$

$$= \cos(x + \frac{\pi}{2}\alpha) - j\sin(x + \frac{\pi}{2}\alpha) \tag{12}$$

Accordingly, from (11) and (12), $D^{\alpha}\cos x = \cos(x + \frac{\pi}{2}\alpha)$ and $D^{\alpha}\sin x = \sin(x + \frac{\pi}{2}\alpha)$.

2.5 Frequency Domain Response

The Laplace transform of the fractional derivative is given by:

$$L\{{}_0D_t^{\alpha} f(t)\} = s^{\alpha}F(s) - \sum_{k=0}^{n-1} s_0^k D_t^{\alpha-k-1} f(0) \tag{13}$$

for the order α such that $n-1 < \alpha < n$ [10] and [13]. With zero initial conditions, as is usual when deriving transfer functions, (13) can be simplified to:

$$L\{{}_0D_t^{\alpha} f(t)\} = s^{\alpha}F(s) \tag{14}$$

In light of the relationship between derivative and integral, $-\alpha$ is used in (13) and (14) for the Laplace transform of fractional integral. Thus, the Laplace transforms of fractional derivative/integral order α have a fractional Laplace operator s^{α} for derivative and $s^{-\alpha}$ for integral, or collectively, the fractional Laplace operator $s^{\pm\alpha}$. With (13) and (14), any system represented by a differential equation of fractional order can be treated in the same way as integer order systems to find, for example, the transfer function [13].

Likewise, the Fourier transform of fractional derivative can be found by replacing s^{α} with $(j\omega)^{\alpha}$ in (14) as:

$$F\{{}_0D_t^{\alpha} f(t)\} = (j\omega)^{\alpha}F(j\omega) \tag{15}$$

Therefore, it can be seen that the frequency-domain analysis of a fractional order system can be carried out in the same way as that of integer order systems through the use of standard tools for the classical integer order systems, such as Bode and Nyquist plots.

CHAPTER 3
LITERATURE REVIEW

3.1 Fractional-Order (FO) Controllers

As an application of fractional calculus in control, Tustin introduced fractional-order (FO) control using fractional-order D^{α} controller in 1958 [14]. However, the unfamiliar concept of fractional-order hindered widespread adoption of the FO control among engineers. Fortunately, for the past couple of decades, fractional calculus has gained significant attention in controls. In [10], application of fractional calculus to electrical circuits, electrochemistry, and system identification and control is described, in addition to mathematical point of view such as solutions to fractional differential equations. The French control team CRONE (Controle Robuste d'Ordre Non-Entier) has also been deeply involved in the application of FO controllers including suspension control [15] and flexible transmission [16] of vehicles through different generations of CRONE controllers. It is Podlubny who generalized the fractional-order (FO) PID controller, or the $PI^{\lambda}D^{\mu}$ controller, where λ and μ are arbitrary real numbers representing the orders of integrator and differentiator, respectively [17]. A simpler form of FO PID controller, or so called FO PID^{k} controller (where k is any real number), was used to suppress vibrations resulting from the nonlinearity of gear backlash in a torsional system [18]. In [19], FO PD, PI, and PID controllers are discussed by providing techniques of finding optimum values of the fractional orders λ and μ.

3.2 Stability of IO and FO PID Controllers

As in the case of IO PID controllers, the stability boundary of an FO PID controller is an important research topic and has received significant attention. In [20], the D-partition method proposed by J. Neimark in [21] and later by Y. I. Neimark in [22], which had been used for parameter space design of IO controllers, was used to find stability bounds of FO PI or PI^{λ} controllers for four cases. These cases include all combinations of an IO/FO plant and an IO/FO controller. However, only a first order IO plant or an FO plant with order α (where $0<\alpha<1$ $0<\alpha<1$) was considered.

In [23], the D-decomposition method was used for $PI^{\lambda}D^{\mu}$ controllers that stabilize a given FO system with a time delay. For the closed-loop FO characteristic equation, the boundaries of

the stability region described by real root boundaries (RRB), infinite root boundaries (IRB) and complex root boundaries (CRB) were determined using the D-decomposition method. In particular, RRB, IRB and CRB provide a general stability region in (K_p, K_i) plane for fixed values of K_d, λ and μ. Unfortunately, solutions in the (K_p, K_d) plane and the (K_i, K_d) plane were not considered. The (K_p, K_d) plane solution is important if a PD controller is considered. The (K_i, K_d) plane is important because for certain forms of PID controllers it allows a user to easily determine the values of K_p that will produce stabilizing controllers.

Thus, there exists a need for a more efficient and less complicated way of finding all IO or FO PID controllers that stabilize a given system with an IO or FO transfer function. In [7], the frequency response was used to find all stabilizing IO PID controllers for a given plant transfer function of arbitrary order. The stabilizing controllers that lie within the stability regions were plotted in three different planes: (K_p, K_i), (K_p, K_d) and (K_d, K_i). However, the results obtained as such were not applicable to more complicated FO controllers with extra degrees of freedom.

3.3 Robust Stability and Performance of IO and FO PID Controllers

For a control system design to be of practical importance, it must be robust to uncertainties in the system transfer function. As a consequence, the H_∞ design methodology is often used to guarantee robustness as well as performance of a system. In [24], a method of H_∞ optimal design was utilized for an FO PID controller to meet performance specifications and stability margins. A multivariable PID controller was designed to satisfy the H_∞ norm in H_∞ control problem in [25], and input and output robust stability of a predictive IO PID controller was discussed in [26]. Emami and Watkins proposed a graphical method for finding all IO PID controllers from the system frequency response that robustly stabilize a closed-system in [8]. The technique in [8] was applicable to single-input single-output (SISO) linear time-invariant (LTI) systems with time delays.

In relation to performance requirements, a technique was proposed for finding all IO PID controllers that stabilize a given system and simultaneously satisfy an H_∞ weighted sensitivity constraint in [27], in which the sensitivity function weight was introduced to meet performance specifications. In addition, methods were provided for determining all stabilizing IO PID controllers that satisfy an H_∞ sensitivity or robust performance constraint, respectively, in [28] and [29]. Unfortunately, the methods in [25], [26], [8], [27], [28], and [29] are limited only to IO

PID controllers, and the technique in [24] cannot be applied to H_∞ weighted sensitivity design of FO PID controllers.

With respect to FO PID, PI^{λ}, or PD^{μ} controllers, Monje et al. discussed a variety of tuning rules for finding optimum values of the fractional orders λ or μ of the integrator and differentiator of the FO PID controller in [19]. For robustness to noise, disturbances, and uncertainties, Monje et al. also provided optimization methods for finding an FO $PI^{\lambda}D^{\mu}$ controller with the introduction of five design specifications in [19].

CHAPTER 4
DETERMINATION OF ALL STABILIZING FO PID CONTROLLERS

4.1 Introduction

In this chapter, a method for finding all stabilizing FO PID controllers, or $PI^{\lambda}D^{\mu}$ controllers for a given plant transfer function of arbitrary order is presented. In particular, it is an objective of this chapter to provide a method for determining all the possible values of the PID parameters K_p, K_i, and K_d that stabilize a given system of arbitrary order, with respect to arbitrary values of the fractional orders (λ and μ) of the integral and derivative parts of the FO PID controller. In addition to finding all stabilizing FO PID controllers for a given plant transfer function, the method makes it possible to determine all the parameters of FO PID controllers that satisfy specified gain and phase margins as well. Furthermore, the method does not require knowledge of plant parameters nor complicated mathematical processes. The stability boundaries of such FO PID controllers are calculated in the frequency domain and are given in terms of the proportional gain K_p, integral gain K_i, and derivative gain K_d. The stabilizing FO PID controllers determined as such will be represented in the (K_p, K_i, K_d) parameter space. This chapter builds upon the work in [32]. A detailed mathematical derivation, results, and examples follow.

4.2 Stabilizing FO PID Controllers

4.2.1 Problem Formulation

Consider the following unity feedback control system, which is a single-input single-output (SISO) linear time-invariant (LTI) system, shown in Fig. 1.

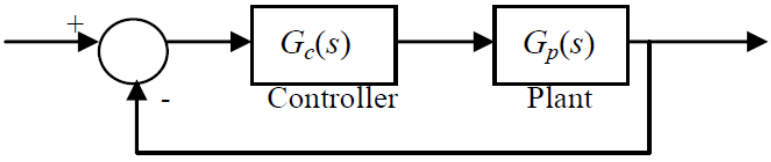

Fig. 1. A control system with negative unity feedback.

The plant transfer function is $G_p(s)$ and the transfer function of the FO PID controller $G_c(s)$ is given by

$$G_c(s) = K_p + \frac{K_i}{s^\lambda} + K_d s^\mu \tag{16}$$

where K_p, K_i, and K_d denote the proportional, integral and derivative gains, respectively, and λ and μ are arbitrary real numbers.

To determine all the stabilizing FO PID controllers for the given plant, K_p, K_i, and K_d values can be found such that the close-loop characteristic polynomial $\Delta(s)$ of the system shown in Fig. 1 is Hurwitz stable. By determining all the values of the parameters K_p, K_i, and K_d that put the closed-loop system poles on the $j\omega$ axis, which represents the marginal stability of the closed-loop system, all the stabilizing FO PID controllers can be found. For marginal stability, the characteristic equation $\Delta(s)$ is expressed in the frequency domain by replacing s with $j\omega$.

$$\Delta(j\omega) = 1 + G_p(j\omega)G_c(j\omega) = 0 \tag{17}$$

The plant transfer function $G_p(j\omega)$ can be decomposed into real and imaginary parts as follows:

$$G_p(j\omega) = R_p(\omega) + jI_p(\omega) \tag{18}$$

Then, the characteristic equation (17) becomes

$$\Delta(j\omega) = 1 + \left(R_p(\omega) + jI_p(\omega)\right)\left(K_p + \frac{K_i}{(j\omega)^\lambda} + K_d(j\omega)^\mu\right) = 0 \tag{19}$$

For (19), the following formula from fractional calculus is used:

$$j^\lambda = e^{j(\frac{\pi}{2})\lambda} = \cos\left(\frac{\pi}{2}\lambda\right) + j\sin\left(\frac{\pi}{2}\lambda\right) \tag{20}$$

Thus,

$$
\begin{aligned}
&K_p + \frac{K_i}{(j\omega)^{\lambda}} + K_d (j\omega)^{\mu} \\
&= K_p + \frac{K_i}{\omega^{\lambda}}\left(\cos\left(\frac{\pi}{2}\lambda\right) - j\sin\left(\frac{\pi}{2}\lambda\right)\right) + K_d\omega^{\mu}\left(\cos\left(\frac{\pi}{2}\mu\right) + j\sin\left(\frac{\pi}{2}\mu\right)\right)
\end{aligned} \tag{21}
$$

Expanding the characteristic equation in (19) and writing it in terms of its real and imaginary parts yields

$$
\Delta(j\omega) = R_{\Delta}(\omega) + jI_{\Delta}(\omega) = 0 \tag{22}
$$

where

$$
\begin{aligned}
R_{\Delta}(\omega) &= 1 + K_p R_p(\omega) \\
&+ \frac{1}{\omega^{\lambda}}\left(\cos\left(\frac{\pi}{2}\lambda\right) R_p(\omega) + \sin\left(\frac{\pi}{2}\lambda\right) I_p(\omega)\right) K_i \\
&+ \omega^{\mu}\left(\cos\left(\frac{\pi}{2}\mu\right) R_p(\omega) - \sin\left(\frac{\pi}{2}\mu\right) I_p(\omega)\right) K_d
\end{aligned} \tag{23}
$$

$$
\begin{aligned}
I_{\Delta}(\omega) &= K_p I_p(\omega) \\
&+ \frac{1}{\omega^{\lambda}}\left(\cos\left(\frac{\pi}{2}\lambda\right) I_p(\omega) - \sin\left(\frac{\pi}{2}\lambda\right) R_p(\omega)\right) K_i \\
&+ \omega^{\mu}\left(\cos\left(\frac{\pi}{2}\mu\right) I_p(\omega) + \sin\left(\frac{\pi}{2}\mu\right) R_p(\omega)\right) K_d
\end{aligned} \tag{24}
$$

Setting the real and imaginary parts equal to zero gives:

$$
\omega^{\lambda} R_p(\omega) K_p + X_{Ri} K_i + X_{Rd} K_d = -\omega^{\lambda} \tag{25}
$$

$$
\omega^{\lambda} I_p(\omega) K_p + X_{Ii} K_i + X_{Id} K_d = 0 \tag{26}
$$

where

$$
X_{Ri} = \cos\left(\frac{\pi}{2}\lambda\right) R_p(\omega) + \sin\left(\frac{\pi}{2}\lambda\right) I_p(\omega)
$$

$$X_{Rd} = \omega^{\lambda+\mu}\left(\cos\left(\frac{\pi}{2}\mu\right)R_p(\omega) - \sin\left(\frac{\pi}{2}\mu\right)I_p(\omega)\right)$$

$$X_{Ii} = -\sin\left(\frac{\pi}{2}\lambda\right)R_p(\omega) + \cos\left(\frac{\pi}{2}\lambda\right)I_p(\omega)$$

$$X_{Id} = \omega^{\lambda+\mu}\left(\sin\left(\frac{\pi}{2}\mu\right)R_p(\omega) + \cos\left(\frac{\pi}{2}\mu\right)I_p(\omega)\right)$$

4.2.2 Solution in (K_p, K_i) Plane

This is a three dimensional system in terms of the controller parameters K_p, K_i, and K_d. Hence, we will fix the value of K_d to find the stability region in the (K_p, K_i) plane. In order to deal with two unknowns K_p and K_i, (25) and (26) are rearranged as:

$$\begin{bmatrix} \omega^{\lambda}R_p(\omega) & X_{Ri} \\ \omega^{\lambda}I_p(\omega) & X_{Ii} \end{bmatrix}\begin{bmatrix} K_p \\ K_i \end{bmatrix} = \begin{bmatrix} -X_{Rd}K_d - \omega^{\lambda} \\ -X_{Id}K_d \end{bmatrix} \tag{27}$$

Solving (27) for $\omega \neq 0$ and $\lambda \neq 2n$ (where n is an integer), K_p and K_i are given by

$$K_p = -K_d\omega^{\mu}\frac{\sin\left(\frac{\pi}{2}(\lambda+\mu)\right)}{\sin\left(\frac{\pi}{2}\lambda\right)} - \frac{R_p(\omega) - \cot\left(\frac{\pi}{2}\lambda\right)I_p(\omega)}{\left|G_p(j\omega)\right|^2} \tag{28}$$

$$K_i = K_d\omega^{\lambda+\mu}\frac{\sin\left(\frac{\pi}{2}\mu\right)}{\sin\left(\frac{\pi}{2}\lambda\right)} - \frac{\omega^{\lambda}I_p(\omega)}{\sin\left(\frac{\pi}{2}\lambda\right)\left|G_p(j\omega)\right|^2} \tag{29}$$

where

$$\left|G_p(j\omega)\right|^2 = {R_p}^2(\omega) + {I_p}^2(\omega) \tag{30}$$

If $\omega = 0$, then (27) becomes

$$\begin{bmatrix} 0 & \cos\left(\frac{\pi}{2}\lambda\right)R_p(0)+\sin\left(\frac{\pi}{2}\lambda\right)I_p(0) \\ 0 & -\sin\left(\frac{\pi}{2}\lambda\right)R_p(0)+\cos\left(\frac{\pi}{2}\lambda\right)I_p(0) \end{bmatrix}\begin{bmatrix} K_p \\ K_i \end{bmatrix}=\begin{bmatrix} 0 \\ 0 \end{bmatrix} \tag{31}$$

Solving (31), we obtain that K_p is arbitrary and K_i=0, or K_p and K_i both are arbitrary with $R_p(0)=I_p(0)=0$, which indicates that $G_p(s)$ has a zero at the origin. In such a case, the zero of a plant transfer function at the origin would cancel the pole of the PID controller at the origin. This should be avoided as it would cause internal instability.

If λ=2n, then the solution exists for the following two cases:

i) For $\mu\neq 2n$ and any frequency ω_i that satisfies

$$K_d=\frac{I_p(\omega_i)}{\omega_i^{\mu}\sin\left(\frac{\pi}{2}\mu\right)\left|G_p(j\omega_i)\right|^2} \tag{32}$$

the solution for K_i is given in terms of K_p as

$$K_i=-\frac{\omega_i^{\lambda}}{\cos\left(\frac{\pi}{2}\lambda\right)}\left(K_p+\frac{R_p(\omega_i)+\cot\left(\frac{\pi}{2}\mu\right)I_p(\omega_i)}{\left|G_p(j\omega_i)\right|^2}\right) \tag{33}$$

ii) For μ=2n and any frequency ω_k that satisfies

$$I_p(\omega_k)=0 \tag{34}$$

the solution for K_i is given in terms of K_p for a fixed K_d value as

$$K_i = -\frac{{\omega_k}^{\lambda}}{\cos\left(\frac{\pi}{2}\lambda\right)}\left(K_p + {\omega_k}^{\mu}\cos\left(\frac{\pi}{2}\mu\right)K_d + \frac{1}{R_p(\omega_k)}\right) \tag{35}$$

Thus, all possible values of the parameters K_p and K_i of stabilizing FO PID controllers for a fixed K_d value can be found by plotting a two-dimensional graph using the above results, with K_p and K_i as two Cartesian axes. This procedure will be described in detail through an example given in Section 4.4. In addition, for λ=μ=1, which is a conventional IO PID controller, the above results reduce to those presented in [7].

4.2.3 Solution in (K_p, K_d) Plane

Next, in order to find the stability region in the (K_p, K_d) plane, we will fix the value of K_i. Then, (25) and (26) can be rewritten as:

$$\begin{bmatrix} \omega^{\lambda}R_p(\omega) & X_{Rd} \\ \omega^{\lambda}I_p(\omega) & X_{Id} \end{bmatrix}\begin{bmatrix} K_p \\ K_d \end{bmatrix} = \begin{bmatrix} -X_{Ri}K_i - \omega^{\lambda} \\ -X_{Ii}K_i \end{bmatrix} \tag{36}$$

Solving (36) for $\omega \neq 0$ and $\mu \neq 2n$ (where n is an integer), K_p and K_d are given by

$$K_p = -K_i\frac{\sin\left(\frac{\pi}{2}(\lambda+\mu)\right)}{\omega^{\lambda}\sin\left(\frac{\pi}{2}\mu\right)} - \frac{R_p(\omega) + \cot\left(\frac{\pi}{2}\mu\right)I_p(\omega)}{\left|G_p(j\omega)\right|^2} \tag{37}$$

$$K_d = K_i\frac{\sin\left(\frac{\pi}{2}\lambda\right)}{\omega^{\lambda+\mu}\sin\left(\frac{\pi}{2}\mu\right)} + \frac{I_p(\omega)}{\omega^{\mu}\sin\left(\frac{\pi}{2}\mu\right)\left|G_p(j\omega)\right|^2} \tag{38}$$

If ω=0, then K_p and K_d both are arbitrary with K_i=0 or $R_p(0) = I_p(0) = 0$, as is obvious from (36).

If $\mu = 2n$ and $\omega \neq 0$, then the solution exists for the following two cases:

i) For $\lambda \neq 2n$ and any frequency ω_i that satisfies

$$K_i = -\frac{\omega^{\lambda} I_p(\omega_i)}{\sin\left(\frac{\pi}{2}\lambda\right)\left|G_p(j\omega_i)\right|^2} \tag{39}$$

the solution for K_d is given in terms of K_p as

$$K_d = -\frac{1}{\omega_i^{\mu}\cos\left(\frac{\pi}{2}\mu\right)}\left(K_p + \frac{R_p(\omega_i) - \cot\left(\frac{\pi}{2}\lambda\right) I_p(\omega_i)}{\left|G_p(j\omega_i)\right|^2}\right) \tag{40}$$

ii) For $\lambda = 2n$ and any frequency ω_k that satisfies

$$I_p(\omega_k) = 0 \tag{41}$$

the solution for K_d is given in terms of K_p for a fixed K_i value as

$$K_d = -\frac{1}{\omega_k^{\mu}\cos\left(\frac{\pi}{2}\mu\right)}\left(K_p + \frac{\cos\left(\frac{\pi}{2}\lambda\right)}{\omega_k^{\lambda}} K_i + \frac{1}{R_p(\omega_k)}\right) \tag{42}$$

Therefore, all the possible values of the parameters K_p and K_d of stabilizing FO PID controllers for a fixed K_i value can be determined by plotting a two-dimensional graph using the above results, with K_p and K_d as two Cartesian axes. Again, this procedure will be described in detail through an example given in Section 4.4. For $\lambda = \mu = 1$, which is a conventional IO PID controller, the above results reduce to those presented in [7].

4.2.4 Solution in (K_i, K_d) Plane

Lastly, we will fix the value of K_p in order to determine the stability region in the (K_i, K_d) plane. Then, (25) and (26) can be rewritten as:

$$\begin{bmatrix} X_{Ri} & X_{Rd} \\ X_{Ii} & X_{Id} \end{bmatrix} \begin{bmatrix} K_i \\ K_d \end{bmatrix} = \begin{bmatrix} -\omega^{\lambda} R_p(\omega) K_p - \omega^{\lambda} \\ -\omega^{\lambda} I_p(\omega) K_p \end{bmatrix} \tag{43}$$

Solving (43) for $\omega \neq 0$ and $\lambda+\mu \neq 2n$ (where n is an integer), K_i and K_d are given by

$$K_i = -K_p \frac{\omega^{\lambda} \sin\left(\frac{\pi}{2}\mu\right)}{\sin\left(\frac{\pi}{2}(\lambda+\mu)\right)} - \frac{\omega^{\lambda}\left(\sin\left(\frac{\pi}{2}\mu\right) R_p(\omega) + \cos\left(\frac{\pi}{2}\mu\right) I_p(\omega)\right)}{\sin\left(\frac{\pi}{2}(\lambda+\mu)\right)\left|G_p(j\omega)\right|^2} \tag{44}$$

$$K_d = -\left(\frac{K_p}{\omega^{\mu}}\right) \frac{\sin\left(\frac{\pi}{2}\lambda\right)}{\sin\left(\frac{\pi}{2}(\lambda+\mu)\right)} - \frac{\left(\sin\left(\frac{\pi}{2}\lambda\right) R_p(\omega) - \cos\left(\frac{\pi}{2}\lambda\right) I_p(\omega)\right)}{\omega^{\mu}\sin\left(\frac{\pi}{2}(\lambda+\mu)\right)\left|G_p(j\omega)\right|^2} \tag{45}$$

If $\omega=0$, then K_i and K_d both are arbitrary with $R_p(0) = I_p(0) = 0$, or $K_i=0$ and K_d is arbitrary.

If $\lambda+\mu=2n$ (where n is an integer), the solution exists for the following two cases:

i) For $\lambda \neq 2n$ and any frequency ω_i that satisfies

$$K_p = \frac{\cot\left(\frac{\pi}{2}\lambda\right) I_p(\omega_i) - R_p(\omega_i)}{\left|G_p(j\omega_i)\right|^2} \tag{46}$$

the solution for K_d is given in terms of K_i as

$$K_d = \frac{\sin\left(\frac{\pi}{2}\lambda\right)R_p(\omega_i) - \cos\left(\frac{\pi}{2}\lambda\right)I_p(\omega_i)}{\omega_i^{\lambda+\mu}\left(\sin\left(\frac{\pi}{2}\mu\right)R_p(\omega_i) + \cos\left(\frac{\pi}{2}\mu\right)I_p(\omega_i)\right)}\left(K_i + \frac{\omega^{\lambda}I_p(\omega_i)}{\sin\left(\frac{\pi}{2}\lambda\right)\left|G_p(j\omega_i)\right|^2}\right) \tag{47}$$

ii) For $\lambda=2n$ and any frequency ω_k that satisfies

$$I_p(\omega_k) = 0 \tag{48}$$

the solution for K_d is given in terms of K_i for a fixed K_p value as

$$K_d = -\frac{1}{\omega_k{}^{\mu}\cos\left(\frac{\pi}{2}\mu\right)}\left(\frac{\cos\left(\frac{\pi}{2}\lambda\right)}{\omega_k{}^{\lambda}}K_i + K_p + \frac{1}{R_p(\omega_k)}\right) \tag{49}$$

Similarly, all the possible values of the parameters K_i and K_d of stabilizing FO PID controllers for a fixed K_p value can be found by plotting a two-dimensional graph using the above results, with K_i and K_d as two Cartesian axes. This procedure will be described in detail through an example given in Section 4.4. For $\lambda=\mu=1$, which is a conventional IO PID controller, the above results reduce to those presented in [7].

4.3 Stabilizing FO PID Controllers with Specified Gain and Phase Margins

4.3.1 Problem Formulation

Often times, it is desirable to find a controller that satisfies certain gain margin (GM) and phase margin (PM). To this end, a gain and phase margin test function $C_{gp} = ge^{-j\phi}$ is inserted in the feedforward path of Fig. 1 [30], where g and ϕ are specified gain and phase margins, respectively. Thus, the characteristic equation of the closed-loop system is given in the frequency domain by:

$$\Delta_{gp}(j\omega) = 1 + G_p(j\omega)C_{gp}G_c(j\omega) \tag{50}$$

The transfer functions for the plant and the FO PID controller are given in (16) and (18) as before. Accordingly, the characteristic equation (50) becomes

$$\Delta_{gp}(j\omega) = 1 + \left(K_p + \frac{K_i}{(j\omega)^{\lambda}} + K_d (j\omega)^{\mu} \right) g \left(\cos\phi - j \sin\phi \right) \left(R_p(\omega) + j I_p(\omega) \right) \tag{51}$$

To determine all the stabilizing FO PID controllers that satisfy specified gain and phase margins g and ϕ with the given plant, K_p, K_i and K_d values can be found such that the close-loop characteristic polynomial $\Delta_{gp}(s)$ of the system is Hurwitz stable. By determining all the values of the parameters K_p, K_i and K_d that give marginal stability to the closed-loop system, all the stabilizing FO PID controllers can be determined. For marginal stability, the characteristic equation in the frequency domain is set to zero as:

$$\Delta_{gp}(j\omega) = 0 \tag{52}$$

Expanding the characteristic equation (51) and writing it in terms of its real and imaginary parts yields

$$\Delta_{gp}(j\omega) = R_{\Delta}(\omega) + j I_{\Delta}(\omega) = 0 \tag{53}$$

where

$$\begin{aligned} R_{\Delta}(\omega) = {} & 1 + g \left(\cos\phi R_p(\omega) + \sin\phi I_p(\omega) \right) K_p \\ & + \frac{g}{\omega^{\lambda}} [\cos\phi \left(\cos\left(\frac{\pi}{2} \lambda \right) R_p(\omega) + \sin\left(\frac{\pi}{2} \lambda \right) I_p(\omega) \right) \\ & + \sin\phi \left(\cos\left(\frac{\pi}{2} \lambda \right) I_p(\omega) - \sin\left(\frac{\pi}{2} \lambda \right) R_p(\omega) \right)] K_i \\ & + g \omega^{\mu} [\cos\phi \left(\cos\left(\frac{\pi}{2} \mu \right) R_p(\omega) - \sin\left(\frac{\pi}{2} \mu \right) I_p(\omega) \right) \\ & + \sin\phi \left(\cos\left(\frac{\pi}{2} \mu \right) I_p(\omega) + \sin\left(\frac{\pi}{2} \mu \right) R_p(\omega) \right)] K_d \end{aligned} \tag{54}$$

$$
\begin{aligned}
I_{\Delta}(\omega) = {} & g\left(\cos\phi I_p(\omega) - \sin\phi R_p(\omega)\right)K_p \\
& + \frac{g}{\omega^{\lambda}}[\cos\phi\left(\cos\left(\frac{\pi}{2}\lambda\right)I_p(\omega) - \sin\left(\frac{\pi}{2}\lambda\right)R_p(\omega)\right) \\
& \quad - \sin\phi\left(\cos\left(\frac{\pi}{2}\lambda\right)R_p(\omega) + \sin\left(\frac{\pi}{2}\lambda\right)I_p(\omega)\right)]K_i \\
& + g\omega^{\mu}[\cos\phi\left(\cos\left(\frac{\pi}{2}\mu\right)I_p(\omega) + \sin\left(\frac{\pi}{2}\mu\right)R_p(\omega)\right) \\
& \quad - \sin\phi\left(\cos\left(\frac{\pi}{2}\mu\right)R_p(\omega) - \sin\left(\frac{\pi}{2}\mu\right)I_p(\omega)\right)]K_d
\end{aligned}
\tag{55}
$$

Setting the real and imaginary parts (54) and (55) equal to zero and further simplifying them through the trigonometric identities gives:

$$
\frac{\omega^{\lambda}}{g} + X_{Rp}K_p + X_{Ri}K_i + X_{Rd}K_d = 0 \tag{56}
$$

$$
X_{Ip}K_p + X_{Ii}K_i + X_{Id}K_d = 0 \tag{57}
$$

Where

$$
X_{Rp} = \omega^{\alpha}\left(\cos\phi R_p(\omega) + \sin\phi I_p(\omega)\right)
$$

$$
X_{Ri} = \cos\left(\phi + \frac{\pi}{2}\lambda\right)R_p(\omega) + \sin\left(\phi + \frac{\pi}{2}\lambda\right)I_p(\omega)
$$

$$
X_{Rd} = \omega^{\lambda+\mu}\left(\cos\left(\phi - \frac{\pi}{2}\mu\right)R_p(\omega) + \sin\left(\phi - \frac{\pi}{2}\mu\right)I_p(\omega)\right)
$$

$$
X_{Ip} = \omega^{\alpha}\left(\cos\phi I_p(\omega) - \sin\phi R_p(\omega)\right)
$$

$$
X_{Ii} = \cos\left(\phi + \frac{\pi}{2}\lambda\right)I_p(\omega) - \sin\left(\phi + \frac{\pi}{2}\lambda\right)R_p(\omega)
$$

$$
X_{Id} = \omega^{\lambda+\mu}\left(\cos\left(\phi - \frac{\pi}{2}\mu\right)I_p(\omega) - \sin\left(\phi - \frac{\pi}{2}\mu\right)R_p(\omega)\right)
$$

With the similar procedure to that of Section 4.2, all the values of the parameters K_p, K_i, and K_d can be determined in pairs with a third parameter fixed. The results are given in the following Subsections.

4.3.2 Solution in (K_p, K_i) Plane

Once again, as this is a three dimensional system in terms of the controller parameters K_p, K_i, and K_d, we first fix the K_d value to find the solutions of K_p and K_i. For $\omega \neq 0$ and $\lambda \neq 2n$ (where n is an integer), K_p and K_i are given as follows:

$$K_p = -K_d \omega^{\mu} \frac{\sin\left(\frac{\pi}{2}(\lambda+\mu)\right)}{\sin\left(\frac{\pi}{2}\lambda\right)} - \frac{\sin\left(\phi+\frac{\pi}{2}\lambda\right)R_p(\omega) - \cos\left(\phi+\frac{\pi}{2}\lambda\right)I_p(\omega)}{g\sin\left(\frac{\pi}{2}\lambda\right)\left|G_p(j\omega)\right|^2} \tag{58}$$

$$K_i = K_d \omega^{\lambda+\mu} \frac{\sin\left(\frac{\pi}{2}\mu\right)}{\sin\left(\frac{\pi}{2}\lambda\right)} + \frac{\omega^{\lambda}\left(\sin\phi R_p(\omega) - \cos\phi I_p(\omega)\right)}{g\sin\left(\frac{\pi}{2}\lambda\right)\left|G_p(j\omega)\right|^2} \tag{59}$$

As in Subsection 4.2.2, if $\omega=0$, we find that K_p is arbitrary and $K_i=0$, or K_p and K_i both are arbitrary with $R_p(0) = I_p(0) = 0$, in which case $G_p(s)$ has a zero at the origin.

If $\lambda=2n$, then the solution exists for the following two cases:

i) For $\mu \neq 2n$ and any frequency ω_i that satisfies

$$K_d = \frac{\cos\phi I_p(\omega_i) - \sin\phi R_p(\omega_i)}{g\omega_i^{\mu}\sin\left(\frac{\pi}{2}\mu\right)\left|G_p(j\omega_i)\right|^2} \tag{60}$$

the solution for K_i is given in terms of K_p as

$$K_i = -\frac{\omega_i^{\lambda}}{\cos\left(\frac{\pi}{2}\lambda\right)}\left(K_p + \frac{\cos\left(\phi-\frac{\pi}{2}\mu\right)I_p(\omega_i) - \sin\left(\phi-\frac{\pi}{2}\mu\right)R_p(\omega_i)}{g\sin\left(\frac{\pi}{2}\mu\right)\left|G_p(j\omega_i)\right|^2}\right) \tag{61}$$

ii) For μ=2n and any frequency ω_k that satisfies

$$I_p(\omega_k) = R_p(\omega_k)\tan\phi \tag{62}$$

the solution for K_i is given in terms of K_p for a fixed K_d value as

$$K_i = -\frac{\omega_k{}^{\lambda}}{\cos\left(\frac{\pi}{2}\lambda\right)}\left(K_p + \omega_k{}^{\mu}\cos\left(\frac{\pi}{2}\mu\right)K_d + \frac{\cos\phi}{gR_p(\omega_k)}\right) \tag{63}$$

For g=1 and $\phi = 0$, which is a nominal case for an FO PID controller, the above results (58) to (63) reduce to (28) to (35) in Subsection 4.2.2.

4.3.3 Solution in (K_p, K_d) Plane

Next, K_p and K_d are determined in pair for $\omega \neq 0$ and $\mu \neq 2n$ (where n is an integer) for a fixed K_i value by

$$K_p = -K_i\frac{\sin\left(\frac{\pi}{2}(\lambda+\mu)\right)}{\omega^{\lambda}\sin\left(\frac{\pi}{2}\mu\right)} - \frac{\cos\left(\phi-\frac{\pi}{2}\mu\right)I_p(\omega) - \sin\left(\phi-\frac{\pi}{2}\mu\right)R_p(\omega)}{g\sin\left(\frac{\pi}{2}\mu\right)\left|G_p(j\omega)\right|^2} \tag{64}$$

$$K_d = K_i\frac{\sin\left(\frac{\pi}{2}\lambda\right)}{\omega^{\lambda+\mu}\sin\left(\frac{\pi}{2}\mu\right)} + \frac{\cos\phi I_p(\omega) - \sin\phi R_p(\omega)}{g\omega^{\mu}\sin\left(\frac{\pi}{2}\mu\right)\left|G_p(j\omega)\right|^2} \tag{65}$$

If ω=0, then K_p and K_d both are arbitrary with K_i=0 or $R_p(0) = I_p(0) = 0$, as in Subsection 4.2.3.

If μ =2n and $\omega \neq 0$, then the solution exists for the following two cases:

i) For $\lambda \neq 2n$ and any frequency ω_i that satisfies

$$K_i = -\frac{\omega_i^{\lambda}\left(\cos\phi I_p(\omega_i) - \sin\phi R_p(\omega_i)\right)}{g\sin\left(\frac{\pi}{2}\lambda\right)\left|G_p(j\omega_i)\right|^2} \tag{66}$$

the solution for K_d is given in terms of K_p as

$$K_d = -\frac{1}{\omega_i^{\mu}\cos\left(\frac{\pi}{2}\mu\right)}\left(K_p + \frac{\sin\left(\phi+\frac{\pi}{2}\lambda\right)R_p(\omega_i) - \cos\left(\phi+\frac{\pi}{2}\lambda\right)I_p(\omega_i)}{g\sin\left(\frac{\pi}{2}\lambda\right)\left|G_p(j\omega_i)\right|^2}\right) \tag{67}$$

ii) For $\lambda=2n$ and any frequency ω_k that satisfies

$$I_p(\omega_k) = R_p(\omega_k)\tan\phi \tag{68}$$

the solution for K_d is given in terms of K_p for a fixed K_i value as

$$K_d = -\frac{1}{\omega_k{}^{\mu}\cos\left(\frac{\pi}{2}\mu\right)}\left(K_p + \frac{\cos\left(\frac{\pi}{2}\lambda\right)}{\omega_k{}^{\lambda}}K_i + \frac{\cos\phi}{gR_p(\omega_k)}\right) \tag{69}$$

Again, the above results match the ones in Subsection 4.2.3 for a nominal case of g=1 and ϕ=0.

4.3.4 Solution in (K_i, K_d) Plane

Lastly, K_i and K_d are given with a fixed value K_p for $\omega\neq0$ and $\lambda+\mu\neq2n$ (where n is an integer) by

$$K_i = -K_p\omega^{\lambda}\frac{\sin\left(\frac{\pi}{2}\mu\right)}{\sin\left(\frac{\pi}{2}(\lambda+\mu)\right)} - \frac{\omega^{\lambda}\left(\cos\left(\phi-\frac{\pi}{2}\mu\right)I_p(\omega) - \sin\left(\phi-\frac{\pi}{2}\mu\right)R_p(\omega)\right)}{g\sin\left(\frac{\pi}{2}(\lambda+\mu)\right)\left|G_p(j\omega)\right|^2} \tag{70}$$

$$K_d = -\left(\frac{K_p}{\omega^\mu}\right)\frac{\sin\left(\frac{\pi}{2}\lambda\right)}{\sin\left(\frac{\pi}{2}(\lambda+\mu)\right)} - \frac{\left(\sin\left(\phi+\frac{\pi}{2}\lambda\right)R_p(\omega)-\cos\left(\phi+\frac{\pi}{2}\lambda\right)I_p(\omega)\right)}{g\omega^\mu \sin\left(\frac{\pi}{2}(\lambda+\mu)\right)\left|G_p(j\omega)\right|^2} \tag{71}$$

If ω=0, then K_i and K_d both are arbitrary with $R_p(0)=I_p(0)=0$, or K_i=0 and K_d is arbitrary, as in Subsection 4.2.4.

If $\lambda+\mu=2n$ (where n is an integer), the solution exists for the following two cases:

i) For $\lambda\neq 2n$ and any frequency ω_i that satisfies

$$K_p = \frac{\cos\left(\phi+\frac{\pi}{2}\lambda\right)I_p(\omega_i)-\sin\left(\phi+\frac{\pi}{2}\lambda\right)R_p(\omega_i)}{g\sin\left(\frac{\pi}{2}\lambda\right)\left|G_p(j\omega_i)\right|^2} \tag{72}$$

the solution for K_d is given in terms of K_i as

$$\begin{aligned} K_d = {} & \frac{\sin\left(\phi+\frac{\pi}{2}\lambda\right)R_p(\omega_i)-\cos\left(\phi+\frac{\pi}{2}\lambda\right)I_p(\omega_i)}{\omega_i^{\lambda+\mu}\left(\cos\left(\phi-\frac{\pi}{2}\mu\right)I_p(\omega_i)-\sin\left(\phi-\frac{\pi}{2}\mu\right)R_p(\omega_i)\right)} \\ & \times\left(K_i+\frac{\omega_i^\lambda\left(\cos\phi I_p(\omega_i)-\sin\phi R_p(\omega_i)\right)}{g\sin\left(\frac{\pi}{2}\lambda\right)\left|G_p(j\omega_i)\right|^2}\right) \end{aligned} \tag{73}$$

ii) For λ=2n and any frequency ω_k that satisfies

$$I_p(\omega_k) = R_p(\omega_k)\tan\phi \tag{74}$$

the solution for K_d is given in terms of K_i for a fixed K_p value as

$$K_d = -\frac{1}{\omega_k{}^{\mu}\cos\left(\frac{\pi}{2}\mu\right)}\left(\frac{\cos\left(\frac{\pi}{2}\lambda\right)}{\omega_k{}^{\lambda}}K_i + K_p + \frac{\cos\phi}{gR_p(\omega_k)}\right) \tag{75}$$

Thus, (70) to (75) can be used to determine all the values of the parameters K_i and K_d of stabilizing FO PID controllers that guarantee specified gain and phase margins g and ϕ, respectively, for a given plant.

4.4 Example

4.4.1 Problem Formulation

Consider the following plant with a second order transfer function having a time delay of 0.8 seconds

$$G_p(s) = \frac{4s+1}{s^2+0.4s+6}e^{-0.8s} \tag{76}$$

The objective here is to find all values of the parameters K_p, K_i, and K_d of FO PID controllers that stabilize the plant transfer function (76) and to compare them with IO PID controllers. There are a plurality of tuning rules for finding optimum values of the fractional orders λ and μ of an FO PID controller described by (16), such as those proposed by Monje et al. in [19]. However, since the goal of this research is to provide a method for finding all the possible values of the parameters K_p, K_i, and K_d of FO PID controllers that stabilize a plant transfer function and simultaneously satisfy specified gain and phase margins at any values of λ and μ, non-optimum values of λ=1.0 and μ=0.5 are selected for the controller transfer function in (16) for this example. Thus, the FO PID controller used is given by

$$G_c(s) = K_p + \frac{K_i}{s} + K_d s^{0.5} \tag{77}$$

4.4.2 Stabilizing (K_p, K_i, K_d) Parameter Space with Varying K_d

In order to find all the values of the parameters K_p, K_i, and K_d of the FO PID controller (77) that stabilize the plant transfer function (76), (28) and (29) were used. Fig. 2 shows the stabilizing (K_p, K_i, K_d) parameter space of the FO PID controller and that of the IO PID controller with varying K_d values. In particular, even though (28) and (29) may be used with one fixed value of K_d, a three-dimensional plot like Fig. 2 can be obtained by varying the values of K_d over a certain range. As can be seen, the FO PID controller provides a much larger stabilizing parameter region than the IO PID controller.

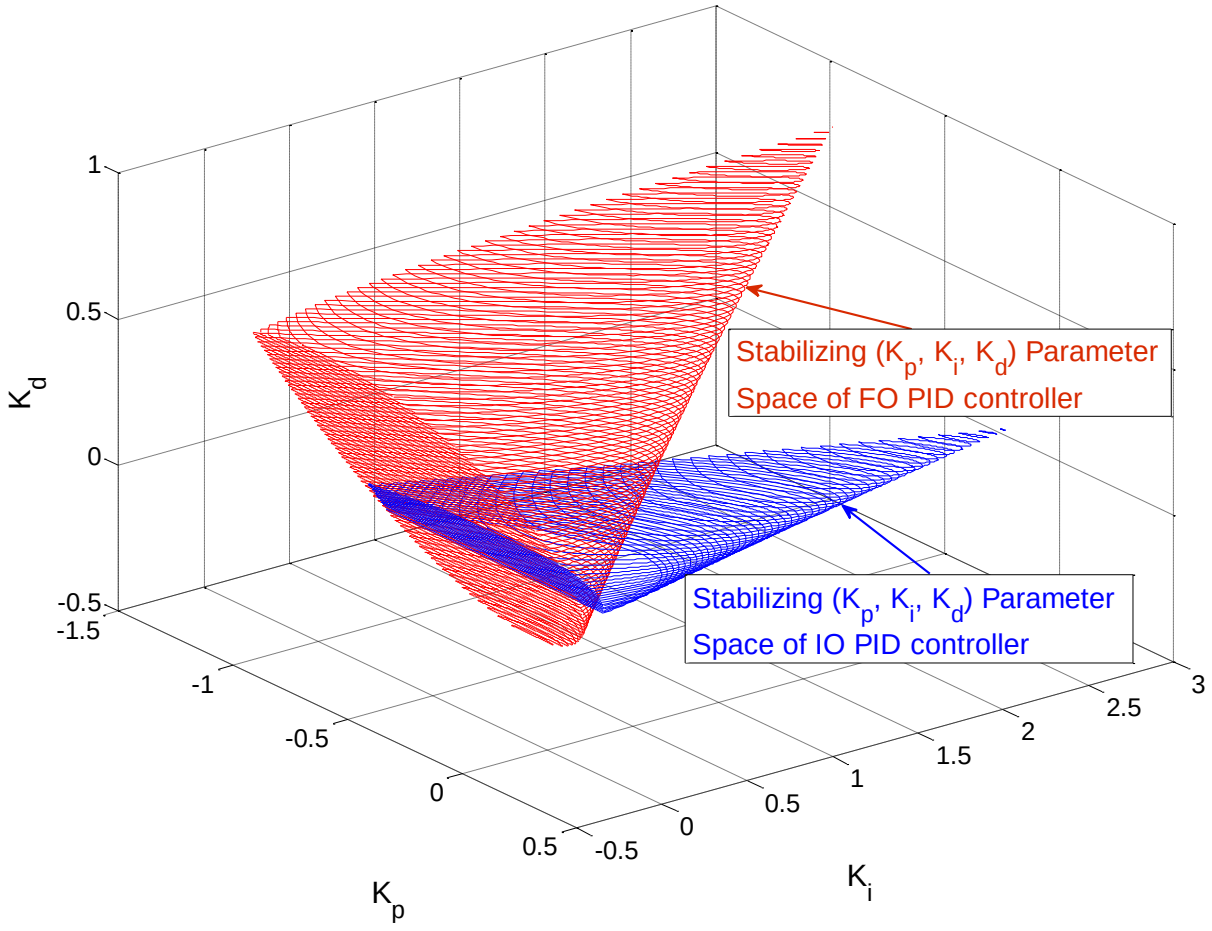

Fig. 2. Stabilizing (K_p, K_i, K_d) parameter spaces of the FO and IO PID controllers with varying K_d values.

4.4.3 Stabilizing (K_p, K_d, K_i) Parameter Space with a Phase Margin of 30 °

In this case, (64) and (65) were used to determine the parameter space region of the FO PID controller (77) that stabilizes the plant transfer function (76)) and simultaneously guarantees a minimum phase margin (PM) of 30°. The regions in the FO PID controller (77) parameter space that stabilize the closed-loop system and meet the PM=30° requirement are shown in Fig. 3 in red and blue, respectively. As both conditions must be satisfied, Fig. 4 shows the intersection of the two regions from Fig. 3, that is, the region of all stabilizing FO PID controllers (77) that guarantee a PM of at least 30°.

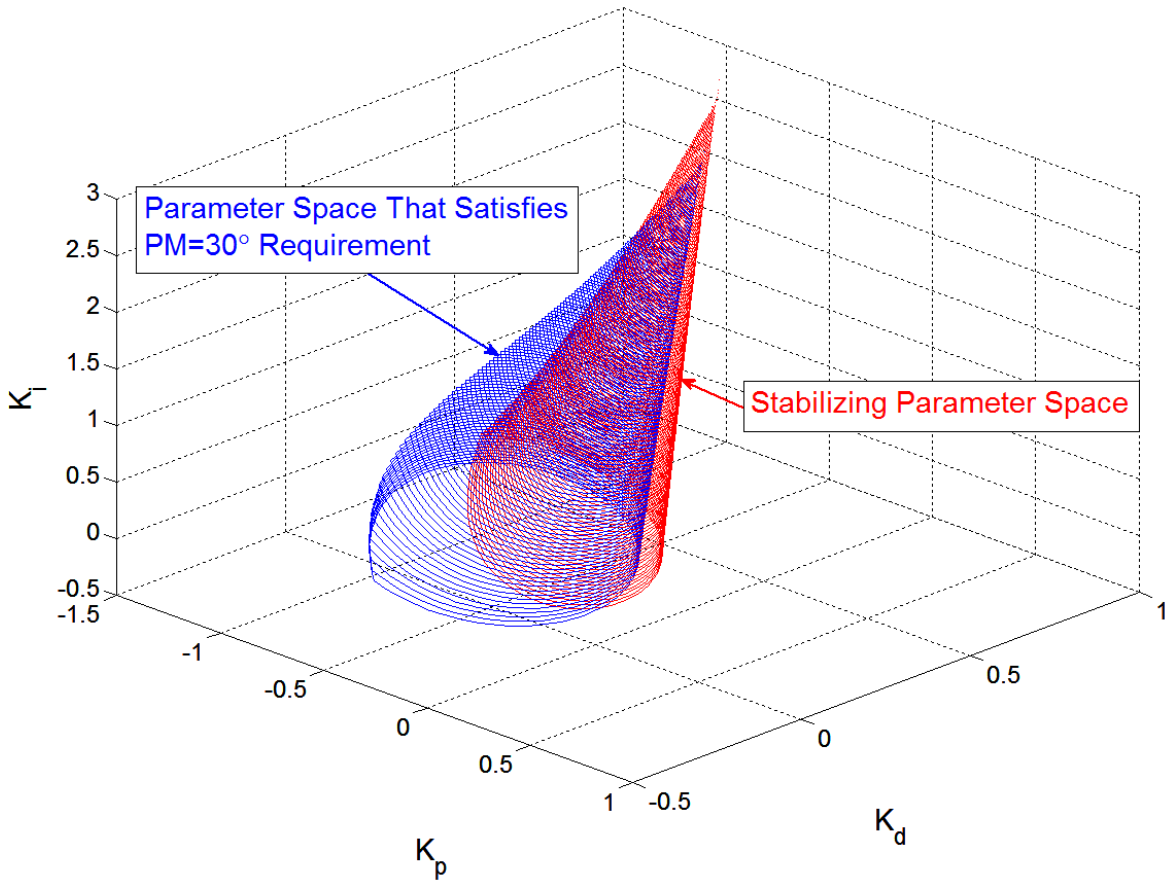

Fig. 3. Stabilizing (K_p, K_d, K_i) parameter spaces of the FO PID controller with varying K_i values.

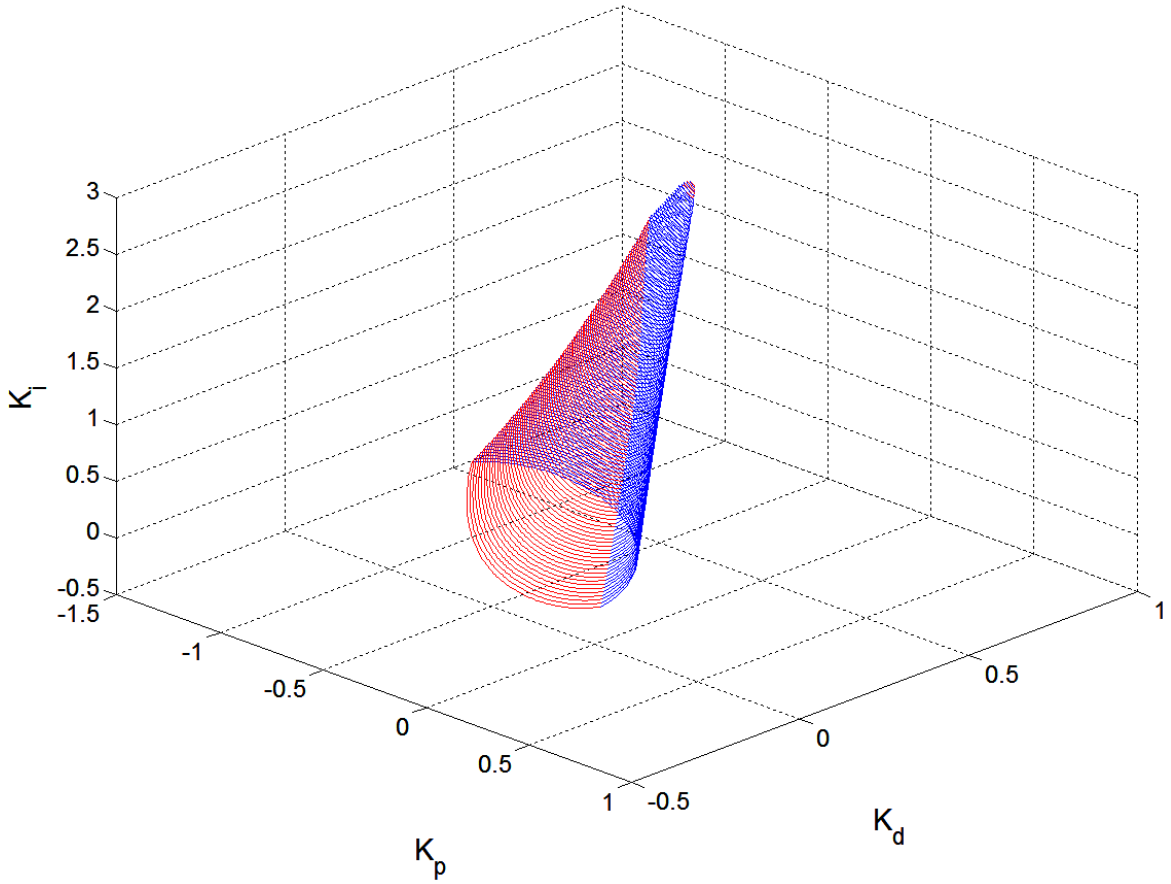

Fig. 4. Stabilizing (K_p, K_d, K_i) parameter space of the FO PID controller for a PM of 30°.

Likewise, the regions in the IO PID controller parameter space that stabilize the closed-loop system and meet the PM=30° requirement are shown in Fig. 5 in red and blue, respectively. As both conditions must be satisfied, Fig. 6 shows the intersection of the two regions from Fig. 5, that is, the region of all stabilizing IO PID controllers that guarantee a PM of at least 30°.

As can be seen from Figs. 4 and 6, the FO PID controller again provides a much larger stabilizing parameter region with a PM of 30° than the IO PID controller.

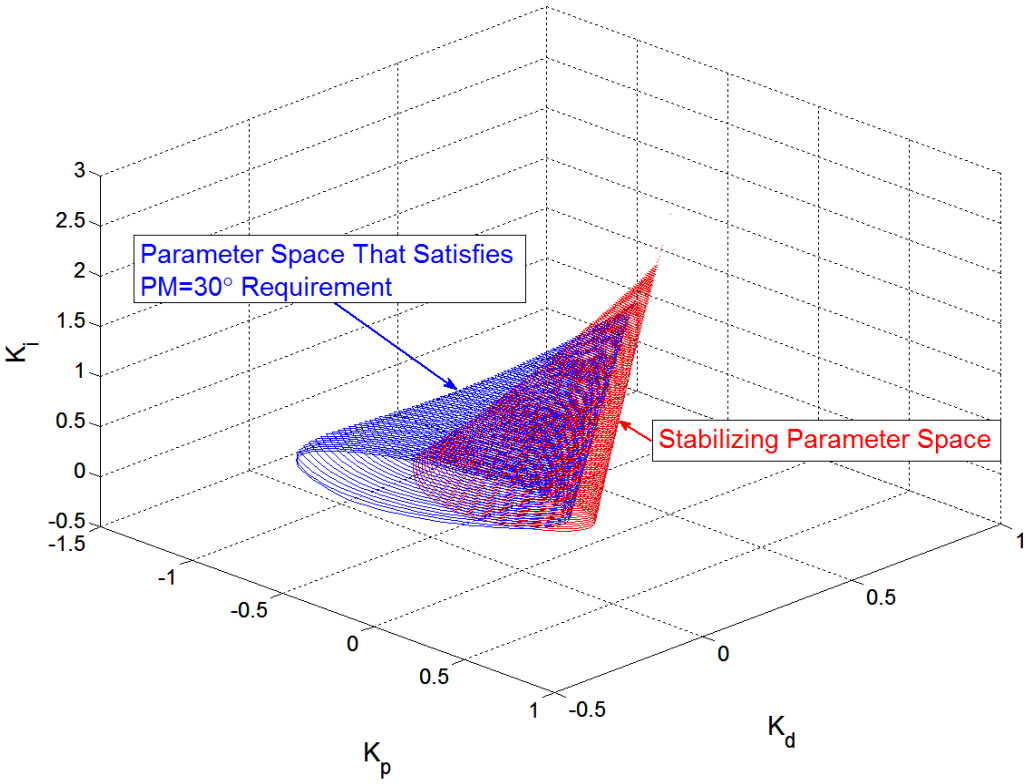

Fig. 5. Stabilizing (K_p, K_d, K_i) parameter spaces for the IO PID controller with varying K_i values.

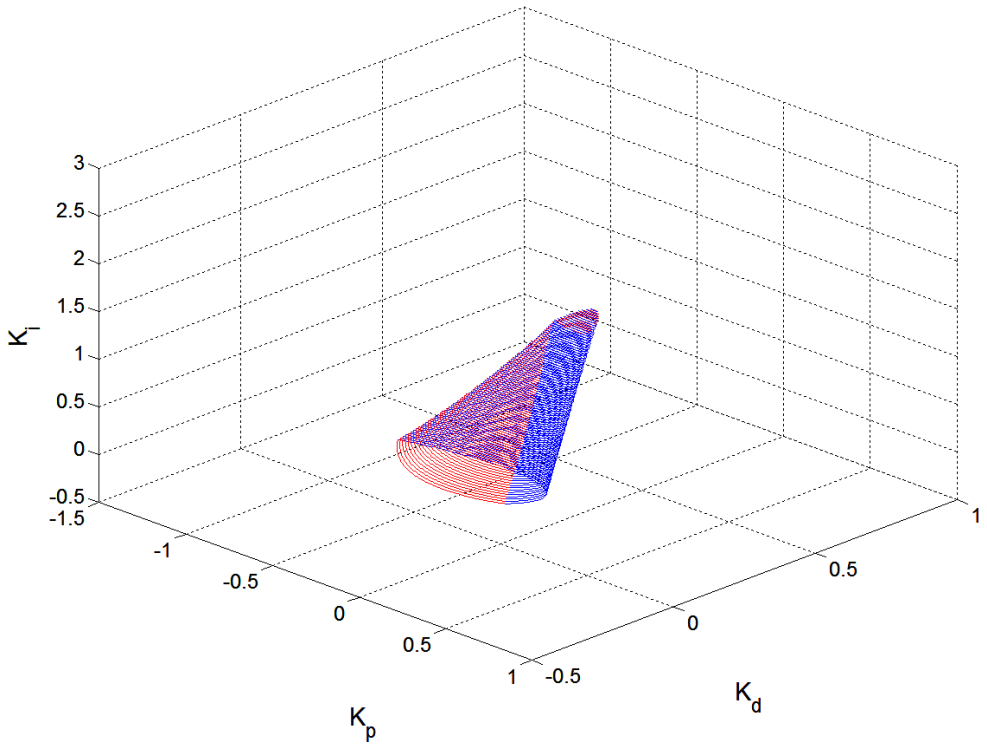

Fig. 6. Stabilizing (K_p, K_d, K_i) parameter space of the IO PID controller for a PM of 30°.

4.4.4 Stabilizing (K_i, K_d, K_p) Parameter Space with Varying K_p

Lastly, (44) and (45) were used to determine the stabilizing (K_i, K_d, K_p) parameter space of the FO PID controller with varying K_p values, which is shown in Fig. 7 along with that of the IO PID controller. Not surprisingly, if Fig. 7 is rotated appropriately, it perfectly matches Fig. 2, thereby confirming that the stabilizing (K_p, K_i, K_d) parameter space determined using (28) and (29) by sweeping K_d values is congruent to the stabilizing (K_i, K_d, K_p) parameter space determined using (44) and (45) by sweeping K_p values. Of course, both of these regions would be congruent to the stabilizing (K_p, K_d, K_i) parameter space determined using (37) and (38) by sweeping K_i values. Again as can be expected from the relationship between integer and real numbers, the FO PID controller provides a much larger stabilizing parameter region than the IO PID controller.

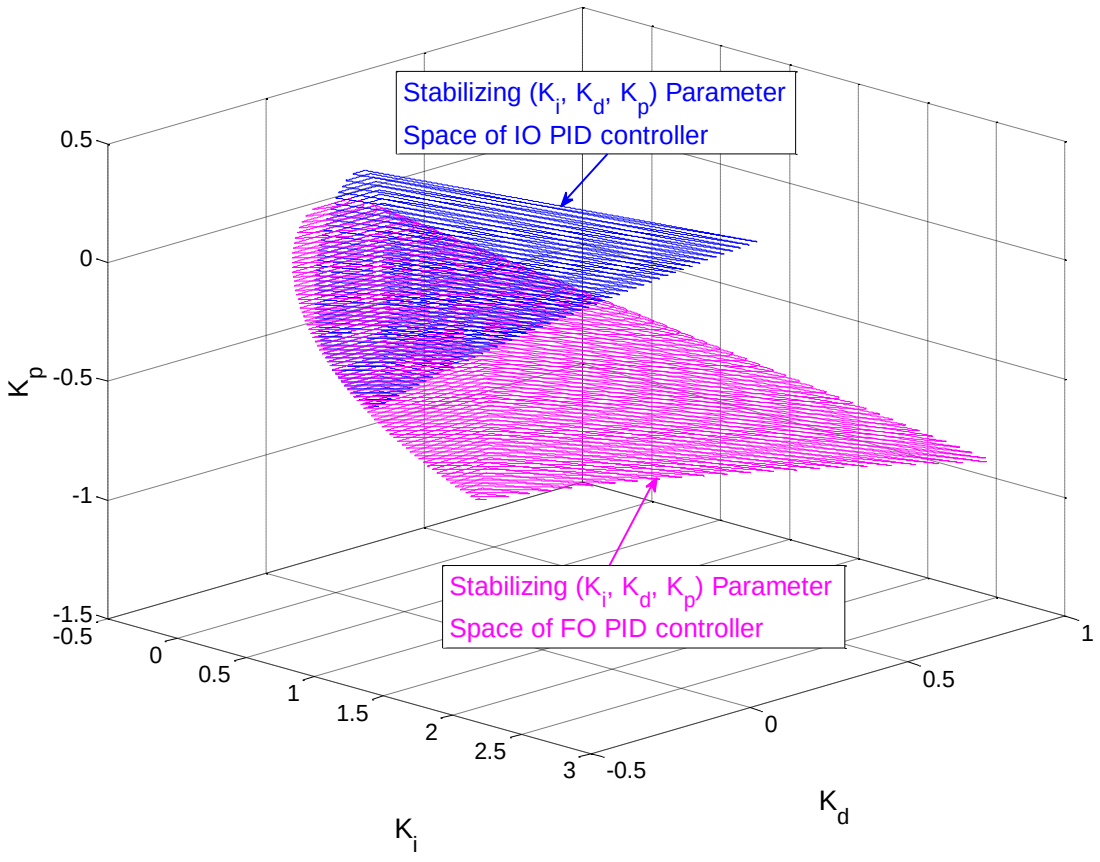

Fig. 7. Stabilizing (K_i, K_d, K_p) parameter spaces of the FO and IO PID controllers with varying K_p values.

4.5 Conclusion

As described in Sections 4.2, 4.3, and 4.4, a method for determining all stabilizing $PI^{\lambda}D^{\mu}$ or so called FO PID controllers for a given system is presented. In particular, the method makes it possible to determine all the values of the parameters K_p, K_i, and K_d of FO PID controllers that not only stabilize a plant transfer function but also satisfy specified gain and phase margins. Since the method is fundamentally based on the frequency response of a system, this method can be applied even when the system parameters such as a plant transfer function are not known. In addition, the results shown in Section 4.4 are promising because for this example an FO PID controller provides a much wider stabilizing parameter space than an IO PID controller, which in turn gives more flexibility in designing a controller. This is not surprising as an IO PID controller is a special case of an FO PID controller.

CHAPTER 5
STABILIZING FO PID CONTROLLERS WITH A WEIGHTED SENSITIVITY CONSTRAINT

5.1 Introduction

It is the objective of this chapter to present a method for finding all the values of the parameters K_p, K_i and K_d of FO PID controllers that not only stabilize a given system of arbitrary order but also meet an H_∞ weighted sensitivity condition. In particular, the method provides all the possible values of the parameters of PID controllers with respect to arbitrary values of the fractional orders (λ and μ) of an FO PID controller. This chapter builds upon the work in [33]. Such a method will surely complement the tuning rules for finding the values of the fractional order λ or μ of an FO PID controller, such as those proposed in [19].

To this end, a single-input single-output (SISO) linear time-invariant (LTI) system is considered. As the derivation of this method is based on the frequency response, the method does not necessarily require a system transfer function or complicated mathematics. All the parameters of such FO PID controllers are calculated in the frequency domain and are given in terms of the proportional gain K_p, integral gain K_i, and derivative gain K_d. A detailed mathematical derivation, results, and examples follow.

5.2 FO PID Controller Design with an H_∞ Weighted Sensitivity Constraint

5.2.1 Problem Formulation

Consider the closed-loop system shown in Fig. 8:

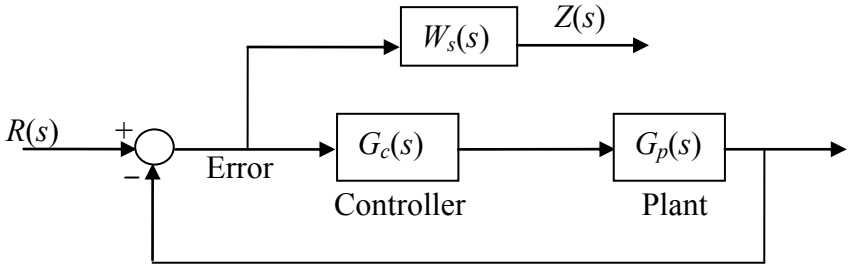

Fig. 8. A closed-loop system with sensitivity function weight.

The plant transfer function is $G_p(s)$ and the transfer function of the $PI^{\lambda}D^{\mu}$ or FO PID controller $G_c(s)$ is given by

$$G_c(s) = K_p + \frac{K_i}{s^{\lambda}} + K_d s^{\mu} \tag{78}$$

where K_p, K_i and K_d denote the proportional, integral, and derivative gains, respectively, and λ and μ are arbitrary positive real numbers. $W_s(s)$ is the sensitivity function weight, $R(s)$ is the exogenous input signal, and $Z(s)$ is the exogenous output signal representing the weighted error. The sensitivity function weight, $W_s(s)$, is selected to meet performance specifications, such as a settling time, percent overshoot, etc. [31].

FO PID controllers that stabilize the given system $G_p(s)$ and meet the weighted sensitivity condition at the same time can be determined by finding all the parameters K_p, K_i and K_d of such FO PID controllers. In [32], all the values of K_p, K_i and K_d of the FO PID controllers that stabilize the closed-loop system shown in Fig. 8 were determined. Thus, the weighted sensitivity condition will be considered next.

Based on performance requirements, FO PID controllers are sought to meet the following weighted sensitivity constraint:

$$\left|S(j\omega)\right| \le \frac{\gamma}{\left|W_s(j\omega)\right|}, \qquad \forall \omega \tag{79}$$

Or equivalently, using the H_∞ norm,

$$\left\|W_s(j\omega)S(j\omega)\right\|_\infty \le \gamma \tag{80}$$

Where $S(j\omega) = \dfrac{1}{1+G_p(j\omega)G_C(j\omega)}$ is the frequency domain expression of the sensitivity function $S(s) = \dfrac{1}{1+G_p(s)G_C(s)}$ and γ is a positive scalar that defines an upper bound of the magnitude of $S(j\omega)$ in conjunction with $W_s(j\omega)$. The plant transfer function $G_p(s)$ and the

sensitivity function weight $W_s(s)$ can be expressed in real and imaginary parts in the frequency domain as:

$$G_p(j\omega) = R_p(\omega) + jI_p(\omega) \tag{81}$$

$$W_s(j\omega) = R_s(\omega) + jI_s(\omega) \tag{82}$$

Likewise, the FO PID controller transfer function (78) can be written in frequency domain as:

$$G_c(j\omega) = K_p + \frac{K_i}{(j\omega)^\lambda} + K_d(j\omega)^\mu \tag{83}$$

The bound in (80) can be written as:

$$\left\| W_s(j\omega)S(j\omega) \right| e^{j\angle W_s(j\omega)S(j\omega)} \Big| \le \gamma, \quad \forall\omega \tag{84}$$

which is equivalent to:

$$W_s(j\omega)S(j\omega)e^{j\angle\theta_s} \le \gamma, \quad \forall\omega \tag{85}$$

for some $\theta_s \in [0, 2\pi)$, where $\theta_s = -\angle W_s(j\omega)S(j\omega)$. Thus, (85) tells us that all the FO PID controllers that meet the condition (80) must lie within the intersecting region defined by the controllers that satisfy (85) for all $\theta_s \in [0, 2\pi)$. From (85), it can be seen that

$$W_s(j\omega)S(j\omega)e^{j\angle\theta_S} = \gamma \tag{86}$$

constitutes the boundary condition such that any FO PID controller within such boundary will satisfy (85), for all $\theta_s \in [0, 2\pi)$. Accordingly, (86) leads to

$$1 + G_p(j\omega)G_c(j\omega) - \frac{1}{\gamma}W_s(j\omega)e^{j\angle\theta_s} = 0 \tag{87}$$

By substituting (81), (82), and (83), and using $e^{j\theta_s} = \cos\theta_s + j\sin\theta_s$, the boundary condition (87) becomes:

$$1+\left(R_p(\omega)+jI_p(\omega)\right)\left(K_p+\frac{K_i}{(j\omega)^{\lambda}}+K_d(j\omega)^{\mu}\right)-\frac{1}{\gamma}\left(R_s(\omega)+jI_s(\omega)\right)\left(\cos\theta_S+j\sin\theta_S\right)=0 \qquad (88)$$

It can be easily seen that if $\lambda=\mu=1$, (88) reduces to the case of the conventional IO PID controller in [27] and if γ approaches infinity, (88) reduces the case of the closed-loop stability of the FO PID controller in [32].

Expanding (88) into real and imaginary parts gives:

$$X_{Rp}K_p + X_{Ri}K_i + X_{Rd}K_d = Y_R \qquad (89)$$

$$X_{Ip}K_p + X_{Ii}K_i + X_{Id}K_d = Y_I \qquad (90)$$

where

$$X_{Rp} = \omega^{\lambda}R_p(\omega)$$

$$X_{Ri} = \cos(\frac{\pi}{2}\lambda)R_p(\omega) + \sin(\frac{\pi}{2}\lambda)I_p(\omega)$$

$$X_{Rd} = \omega^{\lambda+\mu}\left(\cos(\frac{\pi}{2}\mu)R_p(\omega) - \sin(\frac{\pi}{2}\mu)I_p(\omega)\right)$$

$$X_{Ip} = \omega^{\lambda}I_p(\omega)$$

$$X_{Ii} = -\sin(\frac{\pi}{2}\lambda)R_p(\omega) + \cos(\frac{\pi}{2}\lambda)I_p(\omega)$$

$$X_{Id} = \omega^{\lambda+\mu}\left(\sin(\frac{\pi}{2}\mu)R_p(\omega) + \cos(\frac{\pi}{2}\mu)I_p(\omega)\right)$$

$$Y_R = -\omega^{\lambda} + \frac{\omega^{\lambda}}{\gamma}\left(R_S(\omega)\cos\theta_S - I_S(\omega)\sin\theta_S\right)$$

$$Y_I = \frac{\omega^{\lambda}}{\gamma}\left(R_S(\omega)\sin\theta_S + I_S(\omega)\cos\theta_S\right)$$

5.2.2 Solution in (K_p, K_i) Plane

As this is a three dimensional system in terms of the controller parameters K_p, K_i and K_d, we will fix the value of K_d to find the solution to (89) and (90) of the boundary condition (87). In matrix form, (89) and (90) are rearranged to deal with two unknowns K_p and K_i as:

$$\begin{bmatrix} X_{Rp} & X_{Ri} \\ X_{Ip} & X_{Ii} \end{bmatrix} \begin{bmatrix} K_p \\ K_i \end{bmatrix} = \begin{bmatrix} Y_R - X_{Rd}K_d \\ Y_I - X_{Id}K_d \end{bmatrix} \tag{91}$$

Solving (91) for $\omega \neq 0$ and $\lambda \neq 2n$ (where n is an integer), K_p and K_i are given by

$$\begin{aligned} K_p = -K_d\omega^{\mu}\frac{\sin\left(\frac{\pi}{2}(\lambda+\mu)\right)}{\sin(\frac{\pi}{2}\lambda)} - \frac{R_p(\omega)-\cot(\frac{\pi}{2}\lambda)I_p(\omega)}{\left|G_p(j\omega)\right|^2} \\ + \frac{\begin{pmatrix} \cos(\frac{\pi}{2}\lambda+\theta_S)\left(R_p(\omega)I_S(\omega)-I_p(\omega)R_S(\omega)\right)+ \\ \sin(\frac{\pi}{2}\lambda+\theta_S)\left(R_p(\omega)R_S(\omega)+I_p(\omega)I_S(\omega)\right) \end{pmatrix}}{\gamma\sin(\frac{\pi}{2}\lambda)\left|G_p(j\omega)\right|^2} \end{aligned} \tag{92}$$

$$\begin{aligned} K_i = K_d\omega^{\lambda+\mu}\frac{\sin(\frac{\pi}{2}\mu)}{\sin(\frac{\pi}{2}\lambda)} - \frac{\omega^{\lambda}I_p(\omega)}{\sin(\frac{\pi}{2}\lambda)\left|G_p(j\omega)\right|^2} \\ - \omega^{\lambda}\frac{\begin{pmatrix} \cos\theta_S\left(R_p(\omega)I_S(\omega)-I_p(\omega)R_S(\omega)\right)+ \\ \sin\theta_S\left(R_p(\omega)R_S(\omega)+I_p(\omega)I_S(\omega)\right) \end{pmatrix}}{\gamma\sin(\frac{\pi}{2}\lambda)\left|G_p(j\omega)\right|^2} \end{aligned} \tag{93}$$

where

$$\left|G_p(j\omega)\right|^2 = R_p{}^2(\omega) + I_p{}^2(\omega) \tag{94}$$

If ω=0, then K_i=0 is implied to define a valid FO PID controller as in (78), which in turn leads to a PD$^{\mu}$ controller. Such a case will be addressed in the following Subsection 5.2.3 with the (K_p, K_d) plane. Thus, $\omega \neq 0$ is assumed in the (K_p, K_i) plane.

If λ=2n, then the solution exists for the following two cases:

i) For $\mu \neq 2n$ and any frequency ω_i that satisfies

$$K_d = \frac{I_p(\omega_i) + \frac{1}{\gamma}\begin{pmatrix} R_p(\omega_i)\left(R_p(\omega_i)\sin\theta_S + I_S(\omega_i)\cos\theta_S\right) \\ -I_p(\omega_i)\left(R_S(\omega_i)\cos\theta_S - I_S(\omega_i)\sin\theta_S\right) \end{pmatrix}}{\omega_i^{\mu}\sin(\frac{\pi}{2}\mu)\left|G_p(j\omega_i)\right|^2} \tag{95}$$

the solution for K_i is given in terms of K_p as

$$K_i = -\frac{\omega_i^{\lambda}}{\cos(\frac{\pi}{2}\lambda)}\left(K_p + \frac{R_p(\omega_i) + \cot(\frac{\pi}{2}\mu)I_p(\omega_i)}{\left|G_p(j\omega_i)\right|^2}\right) + \frac{\omega_i^{\lambda}\left(R_S(\omega_i)\sin\theta_S + I_S(\omega_i)\cos\theta_S\right)}{\gamma\cos(\frac{\pi}{2}\lambda)I_p(\omega_i)} + \frac{\begin{pmatrix} R_p(\omega_i) + \\ \cot(\frac{\pi}{2}\mu)I_p(\omega_i) \end{pmatrix}\begin{pmatrix} R_p(\omega_i)\left(R_S(\omega_i)\sin\theta_S + I_S(\omega_i)\cos\theta_S\right) \\ -I_p(\omega_i)\left(R_S(\omega_i)\cos\theta_S - I_S(\omega_i)\sin\theta_S\right) \end{pmatrix}}{\gamma\cos(\frac{\pi}{2}\lambda)I_p(\omega_i)\left|G_p(j\omega_i)\right|^2} \tag{96}$$

ii) For μ=2n and any frequency ω_k that satisfies

$$I_p(\omega_k) = -\frac{R_S(\omega_k)\sin\theta_S + I_S(\omega_k)\cos\theta_S}{\gamma - \left(R_S(\omega_k)\cos\theta_S - I_S(\omega_k)\sin\theta_S\right)}R_p(\omega_k) \tag{97}$$

the solution for K_i is given in terms of K_p for a fixed K_d value as

$$K_i = -\frac{\omega_k^{\lambda}}{\cos(\frac{\pi}{2}\lambda)}\left(K_p + \omega_k^{\mu}\cos(\frac{\pi}{2}\mu)K_d + \frac{1}{R_p(\omega_k)}\right) + \frac{\omega_k^{\lambda}\left(R_S(\omega_k)\cos\theta_S - I_S(\omega_k)\sin\theta_S\right)}{\gamma\cos(\frac{\pi}{2}\lambda)R_p(\omega_k)} \tag{98}$$

Thus, all the possible values of K_p and K_i of stabilizing FO PID controllers for a fixed K_d value that meet the weighted sensitivity condition (80) can be plotted in a two-dimensional graph using the above results with K_p and K_i as two Cartesian axes. If $\lambda = \mu = 1$, which is a conventional IO PID controller, the above results reduce to those presented in [27].

5.2.3 Solution in (K_p, K_d) Plane

Likewise, we fix the value of K_i to find the solution in the (K_p, K_d) plane. Accordingly, (89) and (90) are rearranged as:

$$\begin{bmatrix} X_{Rp} & X_{Rd} \\ X_{Ip} & X_{Id} \end{bmatrix} \begin{bmatrix} K_p \\ K_d \end{bmatrix} = \begin{bmatrix} Y_R - X_{Ri} K_i \\ Y_I - X_{Ii} K_i \end{bmatrix} \tag{99}$$

Solving (99) for $\omega \neq 0$ and $\mu \neq 2n$ (where n is an integer), K_p and K_d are given by

$$\begin{aligned} K_p = -K_i \frac{\sin\left(\frac{\pi}{2}(\lambda+\mu)\right)}{\omega^{\lambda}\sin(\frac{\pi}{2}\mu)} - \frac{R_p(\omega) + \cot(\frac{\pi}{2}\mu) I_p(\omega)}{\left|G_p(j\omega)\right|^2} \\ + \frac{\begin{pmatrix} \cos(\frac{\pi}{2}\mu - \theta_S)\left(-R_p(\omega)I_S(\omega) + I_p(\omega)R_S(\omega)\right) + \\ \sin(\frac{\pi}{2}\mu - \theta_S)\left(R_p(\omega)R_S(\omega) + I_p(\omega)I_S(\omega)\right) \end{pmatrix}}{\gamma \sin(\frac{\pi}{2}\mu)\left|G_p(j\omega)\right|^2} \end{aligned} \tag{100}$$

$$\begin{aligned} K_d = K_i \frac{\sin(\frac{\pi}{2}\lambda)}{\omega^{\lambda+\mu}\sin(\frac{\pi}{2}\mu)} + \frac{I_p(\omega)}{\omega^{\mu}\sin(\frac{\pi}{2}\mu)\cdot\left|G_p(j\omega)\right|^2} \\ + \frac{\begin{pmatrix} \cos\theta_S\left(R_p(\omega)I_S(\omega) - I_p(\omega)R_S(\omega)\right) + \\ \sin\theta_S\left(R_p(\omega)R_S(\omega) + I_p(\omega)I_S(\omega)\right) \end{pmatrix}}{\gamma\omega^{\mu}\sin(\frac{\pi}{2}\mu)\left|G_p(j\omega)\right|^2} \end{aligned} \tag{101}$$

If ω=0, then K_i=0 as discussed above in Subsection 5.2.2, leading to the following two cases:

i) If $I_p(0) = -\dfrac{R_S(0)\sin\theta_S + I_S(0)\cos\theta_S}{\gamma - \left(R_S(0)\cos\theta_S - I_S(0)\sin\theta_S\right)} R_p(0)$,

$$K_p = \frac{1}{R_p(0)}\left(-1 + \frac{1}{\gamma}\left(R_S(0)\cos\theta_S - I_S(0)\sin\theta_S\right)\right) \tag{102}$$

and K_d is arbitrary.

ii) Otherwise, no solution exists for K_p but K_d is arbitrary.

If μ =2n and $\omega\neq 0$, then the solution exists for the following two cases:

i) For $\lambda\neq 2n$ and any frequency ω_i that satisfies

$$K_i = -\frac{\omega^{\lambda} I_p(\omega_i)}{\sin(\frac{\pi}{2}\lambda)\left|G_p(j\omega_i)\right|^2} - \omega^{\lambda}\frac{\begin{pmatrix} R_p(\omega_i)\left(R_S(\omega_i)\sin\theta_S + I_S(\omega_i)\cos\theta_S\right) \\ -I_p(\omega_i)\left(R_S(\omega_i)\cos\theta_S - I_S(\omega_i)\sin\theta_S\right)\end{pmatrix}}{\gamma\sin(\frac{\pi}{2}\lambda)\left|G_p(j\omega_i)\right|^2} \tag{103}$$

the solution for K_d is given in terms of K_p as

$$\begin{aligned} K_d = &-\frac{1}{\omega_i^{\mu}\cos(\frac{\pi}{2}\mu)}\left(K_p + \frac{R_p(\omega_i) - \cot(\frac{\pi}{2}\lambda)I_p(\omega_i)}{\left|G_p(j\omega_i)\right|^2}\right) + \frac{\left(R_S(\omega_i)\sin\theta_S + I_S(\omega_i)\cos\theta_S\right)}{\gamma\omega_i^{\mu}\cos(\frac{\pi}{2}\mu)I_p(\omega_i)} \\ &+ \frac{\begin{pmatrix} R_p(\omega_i) - \\ \cot(\frac{\pi}{2}\lambda)I_p(\omega_i)\end{pmatrix}\begin{pmatrix} R_p(\omega_i)\left(R_S(\omega_i)\sin\theta_S + I_S(\omega_i)\cos\theta_S\right) \\ -I_p(\omega_i)\left(R_S(\omega_i)\cos\theta_S - I_S(\omega_i)\sin\theta_S\right)\end{pmatrix}}{\gamma\omega_i^{\mu}\cos(\frac{\pi}{2}\mu)I_p(\omega_i)\left|G_p(j\omega_i)\right|^2} \end{aligned} \tag{104}$$

ii) For λ=2n and any frequency ω_k that satisfies

$$I_p(\omega_k) = -\frac{R_S(\omega_k)\sin\theta_S + I_S(\omega_k)\cos\theta_S}{\gamma - \left(R_S(\omega_k)\cos\theta_S - I_S(\omega_k)\sin\theta_S\right)} R_p(\omega_k) \tag{105}$$

the solution for K_d is given in terms of K_p for a fixed K_i value as

$$K_d = -\frac{1}{\omega_k{}^{\mu}\cos(\frac{\pi}{2}\mu)}\left(K_p + \frac{\cos(\frac{\pi}{2}\lambda)}{\omega_k{}^{\lambda}}K_i + \frac{1}{R_p(\omega_k)}\right) + \frac{R_S(\omega_k)\cos\theta_S - I_S(\omega_k)\sin\theta_S}{\gamma\omega_k{}^{\mu}\cos(\frac{\pi}{2}\mu)R_p(\omega_k)} \tag{106}$$

Again, all the possible values of K_p and K_d of stabilizing FO PID controllers that satisfy the weighted sensitivity constraint (80) for a fixed K_i value can be plotted in a two-dimensional graph using the above results with K_p and K_d as two Cartesian axes. If $\lambda = \mu = 1$, which is a conventional IO PID controller, the above results reduce to those presented in [27].

5.2.4 Solution in (K_i, K_d) Plane

Lastly, the (K_i, K_d) plane solution will be determined by fixing the value of K_p. To this end, (89) and (90) are arranged as:

$$\begin{bmatrix} X_{Ri} & X_{Rd} \\ X_{Ii} & X_{Id} \end{bmatrix}\begin{bmatrix} K_i \\ K_d \end{bmatrix} = \begin{bmatrix} Y_R - X_{Rp}K_p \\ Y_I - X_{Ip}K_p \end{bmatrix} \tag{107}$$

Solving (107) for $\omega \neq 0$ and $\lambda+\mu \neq 2n$ (where n is an integer), K_i and K_d are given by

$$\begin{aligned} K_i = -K_p\omega^{\lambda}\frac{\sin(\frac{\pi}{2}\mu)}{\sin(\frac{\pi}{2}(\lambda+\mu))} - \frac{\omega^{\lambda}\left(\sin(\frac{\pi}{2}\mu)R_p(\omega) + \cos(\frac{\pi}{2}\mu)I_p(\omega)\right)}{\sin(\frac{\pi}{2}(\lambda+\mu))\left|G_p(j\omega)\right|^2} \\ + \omega^{\lambda}\frac{\begin{pmatrix}\cos(\frac{\pi}{2}\mu-\theta_S)\left(-R_p(\omega)I_S(\omega) + I_p(\omega)R_S(\omega)\right) + \\ \sin(\frac{\pi}{2}\mu-\theta_S)\left(R_p(\omega)R_S(\omega) + I_p(\omega)I_S(\omega)\right)\end{pmatrix}}{\gamma\sin(\frac{\pi}{2}(\lambda+\mu))\left|G_p(j\omega)\right|^2} \end{aligned} \tag{108}$$

$$K_d = -\left(\frac{K_p}{\omega^\mu}\right)\frac{\sin(\frac{\pi}{2}\lambda)}{\sin(\frac{\pi}{2}(\lambda+\mu))} - \frac{\left(\sin(\frac{\pi}{2}\lambda)R_p(\omega) - \cos(\frac{\pi}{2}\lambda)I_p(\omega)\right)}{\omega^\mu \sin(\frac{\pi}{2}(\lambda+\mu))\left|G_p(j\omega)\right|^2} + \frac{\left(\begin{array}{l}\cos(\frac{\pi}{2}\lambda+\theta_S)\left(R_p(\omega)I_S(\omega) - I_p(\omega)R_S(\omega)\right)+ \\ \sin(\frac{\pi}{2}\lambda+\theta_S)\left(R_p(\omega)R_S(\omega) + I_p(\omega)I_S(\omega)\right)\end{array}\right)}{\gamma\omega^\mu \sin(\frac{\pi}{2}(\lambda+\mu))\left|G_p(j\omega)\right|^2} \tag{109}$$

In the (K_i, K_d) plane, again $\omega \neq 0$ is assumed without loss of generality as discussed above. If $\lambda+\mu=2n$ (where n is an integer), the solution exists for the following two cases:

i) For $\lambda \neq 2n$ and any frequency ω_i that satisfies

$$K_p = \frac{\cot(\frac{\pi}{2}\lambda)I_p(\omega_i) - R_p(\omega_i)}{\left|G_p(j\omega_i)\right|^2} + \frac{\left(\begin{array}{l}\cos(\frac{\pi}{2}\lambda+\theta_S)\left(R_p(\omega_i)I_S(\omega_i) - I_p(\omega_i)R_S(\omega_i)\right)+ \\ \sin(\frac{\pi}{2}\lambda+\theta_S)\left(R_p(\omega_i)R_S(\omega_i) + I_p(\omega_i)I_S(\omega_i)\right)\end{array}\right)}{\gamma\sin(\frac{\pi}{2}\lambda)\left|G_p(j\omega_i)\right|^2} \tag{110}$$

the solution for K_d is given in terms of K_i as

$$K_d = \frac{\sin(\frac{\pi}{2}\lambda)R_p(\omega_i) - \cos(\frac{\pi}{2}\lambda)I_p(\omega_i)}{\omega_i^{\lambda+\mu}\left(\sin(\frac{\pi}{2}\mu)R_p(\omega_i) + \cos(\frac{\pi}{2}\mu)I_p(\omega_i)\right)}\left(K_i + \frac{\omega^\lambda I_p(\omega_i)}{\sin(\frac{\pi}{2}\lambda)\left|G_p(j\omega_i)\right|^2}\right) + \frac{\left(R_S(\omega_i)\sin\theta_S + I_S(\omega_i)\cos\theta_S\right)}{\gamma\omega_i^\mu\left(\sin(\frac{\pi}{2}\mu)R_p(\omega_i) + \cos(\frac{\pi}{2}\mu)I_p(\omega_i)\right)} - \frac{I_p(\omega_i)\left(\begin{array}{l}\cos(\frac{\pi}{2}\lambda+\theta_S)\left(R_p(\omega_i)I_S(\omega_i) - I_p(\omega_i)R_S(\omega_i)\right)+ \\ \sin(\frac{\pi}{2}\lambda+\theta_S)\left(R_p(\omega_i)R_S(\omega_i) + I_p(\omega_i)I_S(\omega_i)\right)\end{array}\right)}{\gamma\omega_i^\mu\sin(\frac{\pi}{2}\lambda)\left|G_p(j\omega_i)\right|^2\left(\sin(\frac{\pi}{2}\mu)R_p(\omega_i) + \cos(\frac{\pi}{2}\mu)I_p(\omega_i)\right)} \tag{111}$$

ii) For $\lambda=2n$ and any frequency ω_k that satisfies

$$I_p(\omega_k) = -\frac{R_S(\omega_k)\sin\theta_S + I_S(\omega_k)\cos\theta_S}{\gamma - \left(R_S(\omega_k)\cos\theta_S - I_S(\omega_k)\sin\theta_S\right)} R_p(\omega_k) \tag{112}$$

the solution for K_d is given in terms of K_i for a fixed K_p value as

$$K_d = -\frac{1}{\omega_k{}^{\mu}\cos(\frac{\pi}{2}\mu)}\left(\frac{\cos(\frac{\pi}{2}\lambda)}{\omega_k{}^{\lambda}}K_i + K_p + \frac{1}{R_p(\omega_k)}\right) + \frac{R_S(\omega_k)\cos\theta_S - I_S(\omega_k)\sin\theta_S}{\gamma\omega_k{}^{\mu}\cos(\frac{\pi}{2}\mu)R_p(\omega_k)} \tag{113}$$

Likewise, all the values of K_i and K_d of stabilizing FO PID controllers that satisfy the weighted sensitivity condition (80) for a fixed K_p value can be found in the (K_i, K_d) plane using the above results with K_i and K_d as two Cartesian axes. For $\lambda = \mu = 1$, the above results reduce to those presented in [27].

It should be noted that all the results in this section are expressed in the frequency domain. As a consequence, the controller parameters K_p, K_i, and K_d of the FO PID controllers that not only stabilize a given system but also meet an H_∞ weighted sensitivity condition can be determined directly from an experimental frequency response when the system transfer function or system parameters are unknown.

5.3 Example

5.3.1 Problem Formulation

Now, a numerical example will be given to illustrate the application and effectiveness of the results derived in Section 5.2. In order to present a comparable and tangible example, I will use the liquid level system in [19], which was modeled by a first-order transfer function as

$$G_p(s) = \frac{3.13}{433.33s + 1}e^{-50s} \tag{114}$$

with a time delay of 50 seconds.

The objective of this example is to find all the possible values of the parameters K_p, K_i and K_d of FO PID controllers that stabilize the given system (114) and simultaneously satisfy the weighted sensitivity condition (80) where $\gamma = 1$. Then the results will be compared with those of an IO PID controller for better understanding of advantages in using FO PID controllers. There are a plurality of tuning rules for finding optimum values of the fractional orders λ and μ of FO PID controllers. So, the values λ=0.8968 and μ=0.4773 in [19] will be used for the FO PID controller in (78) to show how effective and useful the method presented here is to find the values of the parameters K_p, K_i, and K_d of FO PID controllers. Thus, the FO PID controller used is given by

$$G_c(s) = K_p + \frac{K_i}{s^{0.8968}} + K_d s^{0.4773} \tag{115}$$

In addition, let the closed-loop system shown in Fig. 8 be required to meet performance specifications of a settling time of 1000 seconds, a percent overshoot of 15%, and a steady-state error less than or equal to 0.05. For such performance requirements, the method described in [31] leads to the following sensitivity function weight $W_s(s)$:

$$W_S(s) = \frac{0.69224(s + 0.007904)}{(s + 0.0002736)} \tag{116}$$

5.3.2 Weighted Sensitivity Region in (K_p, K_i) Plane

In order to find the weighted sensitivity region in the (K_p, K_i) plane for the plant transfer function (114) and the FO PID controller transfer function (115), (92) and (93) were used with a fixed value K_d=4.3867 which is again from [19], when $\gamma = 1$. In detail, all the possible values of the parameters K_p and K_i of FO PID controllers that satisfy the weighted sensitivity condition defined by (80) can be determined by finding an intersecting region of all the solutions to (92) and (93) for $\theta_S \in [0, 2\pi)$ in a given range of frequency ω. Such an intersecting region lies on or within the boundary set by (86) for $\theta_S \in [0, 2\pi)$, thereby constituting the solution for meeting the

weighted sensitivity constraint (80). The corresponding stability region can be obtained by taking $\gamma = \infty$ in (92) and (93), which is the same as that disclosed in [32].

In Fig. 9, the weighted sensitivity region and the stability boundary of the FO PID controller are plotted in the (K_p, K_i) plane for K_d=4.3867. For comparison, those of the IO PID controller are shown in Fig. 10. As can be seen from Figs. 2 and 3, even though the FO and IO PID controllers both provide a fairly large stability region, the FO PID controller provides a much larger weighted sensitivity region than the IO PID controller for K_d=4.3867. These weighted sensitivity regions represent all the possible values of K_p and K_i for K_d=4.3867 that stabilize the plant transfer function (114) and meet the weighted sensitivity condition (80).

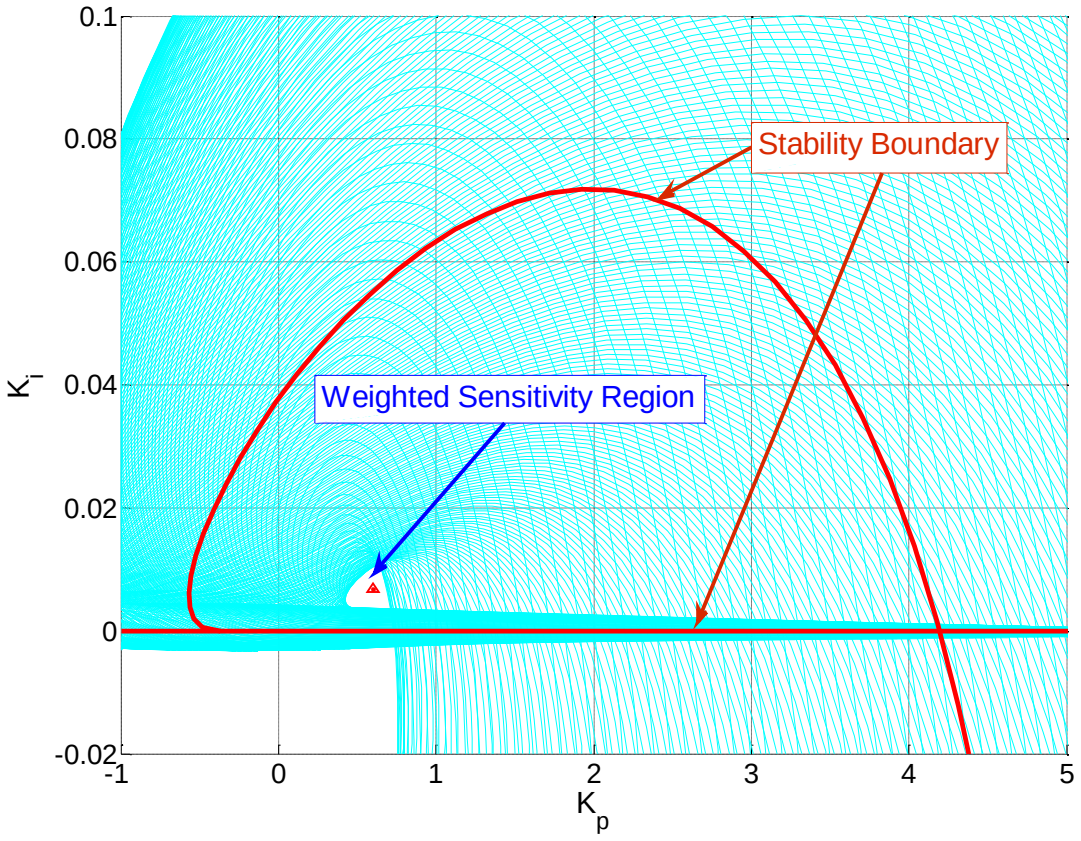

Fig. 9. Stability boundary and weighted sensitivity region in (K_p, K_i) plane for the FO PID controller in (115) with K_d=4.3867.

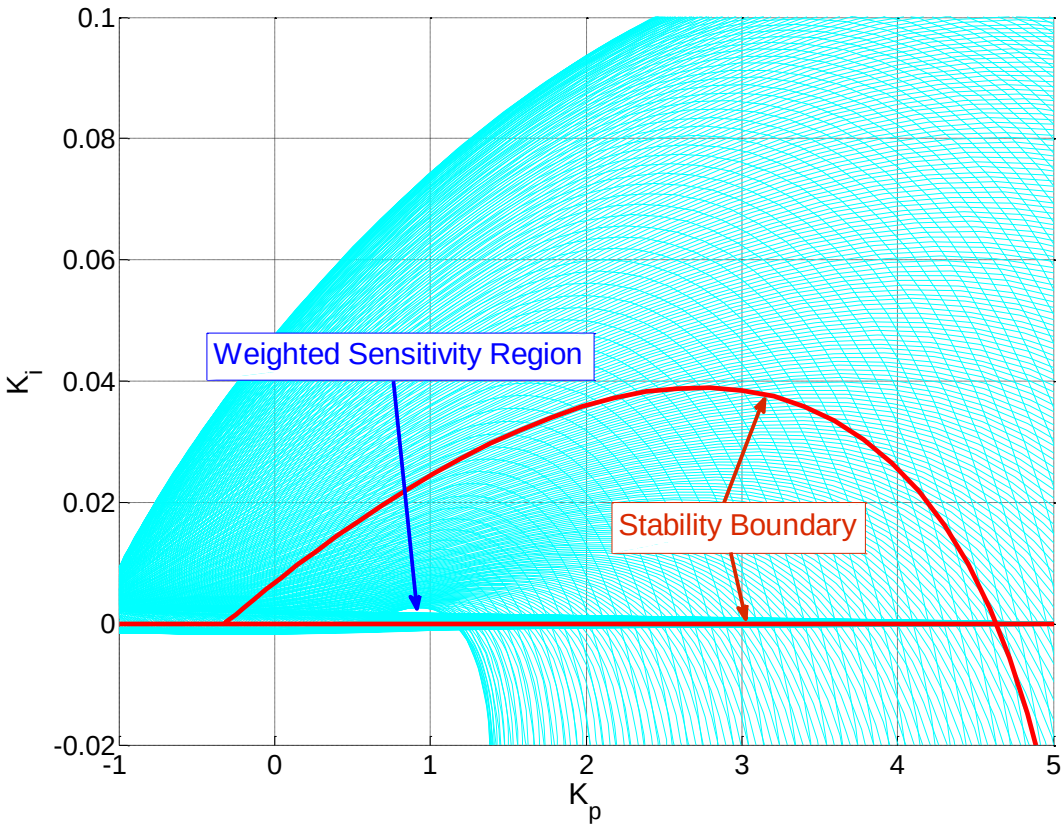

Fig. 10. Stability boundary and weighted sensitivity region in (K_p, K_i) plane for the IO PID controller with K_d=4.3867.

To verify that FO PID controllers lying in such intersecting region truly meet the weighted sensitivity condition (80) and the performance specifications, an arbitrary controller was chosen from the weighted sensitivity region of the FO PID controller in Fig. 9, which is K_p= 0.5982 and K_i=0.0068, as marked on the plot. Therefore, the chosen FO PID controller is

$$G_{cFO}(s) = 0.5982 + \frac{0.0068}{s^{0.8968}} + 4.3867 s^{0.4773} \tag{117}$$

Fig. 11 shows $\left|W_S(j\omega)S(j\omega)\right|$ with the FO PID controller in (117) and illustrates that $\left\|W_S(j\omega)S(j\omega)\right\|_\infty$ is equal to 0.973, which is of course less than $\gamma = 1$. Fig. 12 illustrates the corresponding closed-loop step response with the FO PID controller (117). The closed-loop system shows a percent overshoot of P.O=5.42%, a 2% settling time of t_s=871 seconds, and a

steady-state error of 0.002, all of which meet the performance requirements (t_s=1000 seconds, P.O=15%, and a steady-state error less than or equal to 0.05). To plot the closed-loop step response with the FO PID controller (117), the FO PID controller transfer function was approximated using the fractional power pole (FPP) and fractional power zero (FPZ) methods given in [34] and [35], respectively.

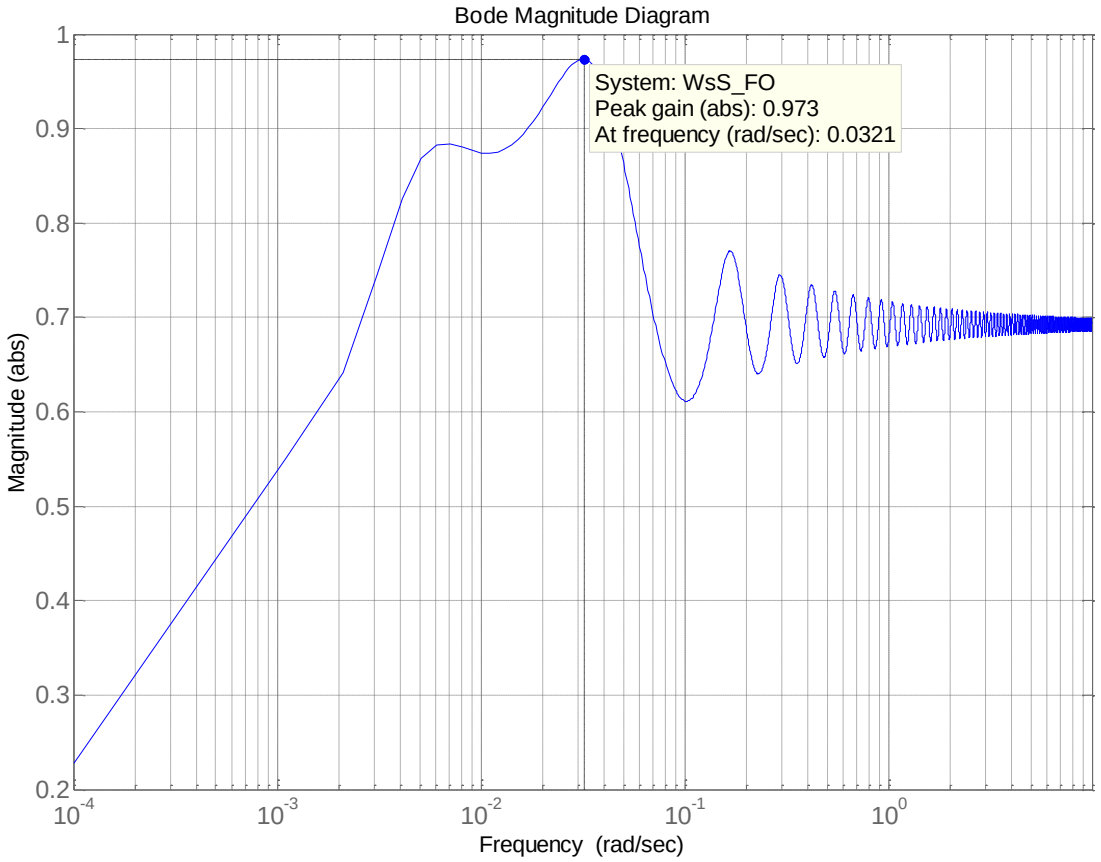

Fig. 11. $\left|W_S(j\omega)S(j\omega)\right|$ with the FO PID controller in (117).

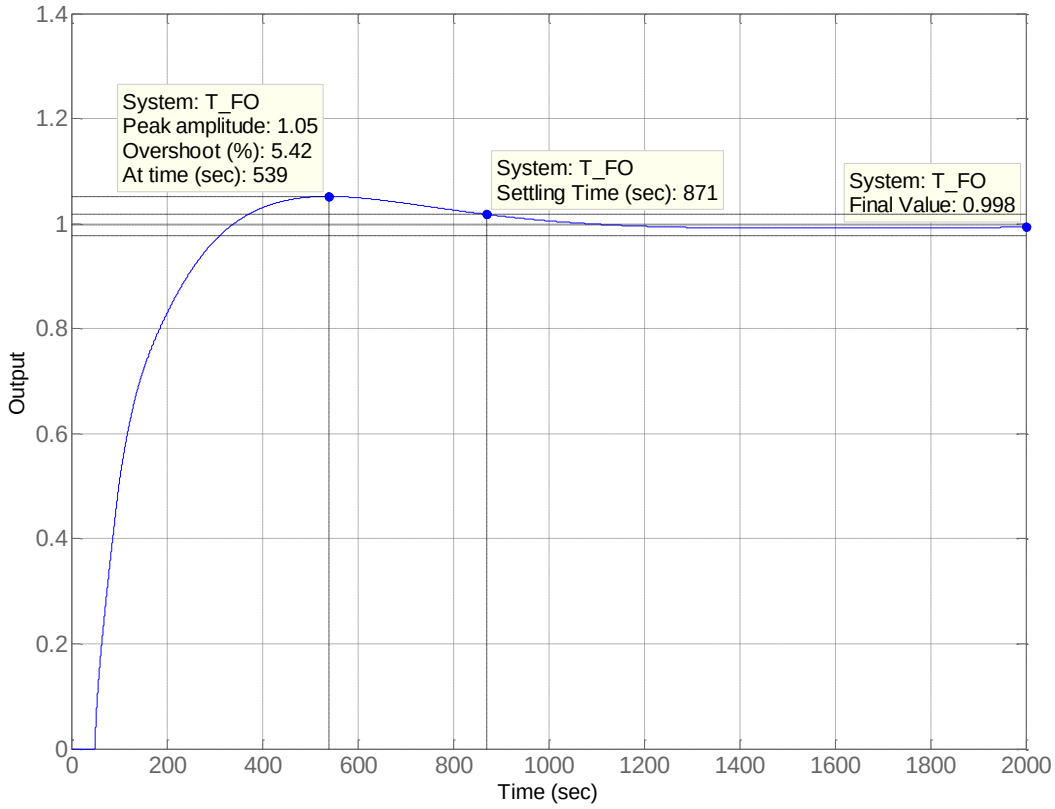

Fig. 12. Closed-loop step response with the FO PID controller in (117).

5.3.3 Weighted Sensitivity Region in (K_p, K_d) Plane

Similarly, the stability boundary and the weighted sensitivity region in the (K_p, K_d) plane for the system transfer function (114) and the FO PID controller transfer function (115) with a fixed value K_i=0.01, which is again from [19], were determined by using (100) and (101). As discussed previously, an intersecting region of all solutions to (100) and (101) when γ=1 for $\theta_S \in [0, 2\pi)$ in a range of frequency ω is the weighted sensitivity region and the corresponding stability region is obtained by setting $\gamma = \infty$ in (100) and (101). For comparison, those of the IO PID controller were also determined.

Fig. 13 shows the stability boundaries of the FO PID controller (115) and that of the IO PID controllers for K_i=0.01, respectively. Fig. 14 and Fig. 15 show the weighted sensitivity regions of the FO PID controller (115) and that of the IO PID controller in the (K_p, K_d) plane for K_i=0.01, respectively.

As can be seen from Fig. 13, the IO PID controller provides a noticeably larger stability region than the FO PID controller (115) for K_i=0.01 in the (K_p, K_d) plane. However, whereas the

FO PID controller (115) provides a fairly large weighted sensitivity region in the (K_p, K_d) plane for K_i=0.01, the IO PID controller does not provide any weighted sensitivity region. The IO PID controller could be a better choice if we considered a stability region only; however, the FO PID controller is definitely a better choice in light of satisfying the performance specifications described early. In particular, the IO PID controller is not a plausible choice in this specific example with the weighted sensitivity constraint.

While one weighted sensitivity region was determined in the (K_p, K_d) plane for a value of K_i in the example, it is possible to find all the weighted sensitivity regions by varying K_i values.

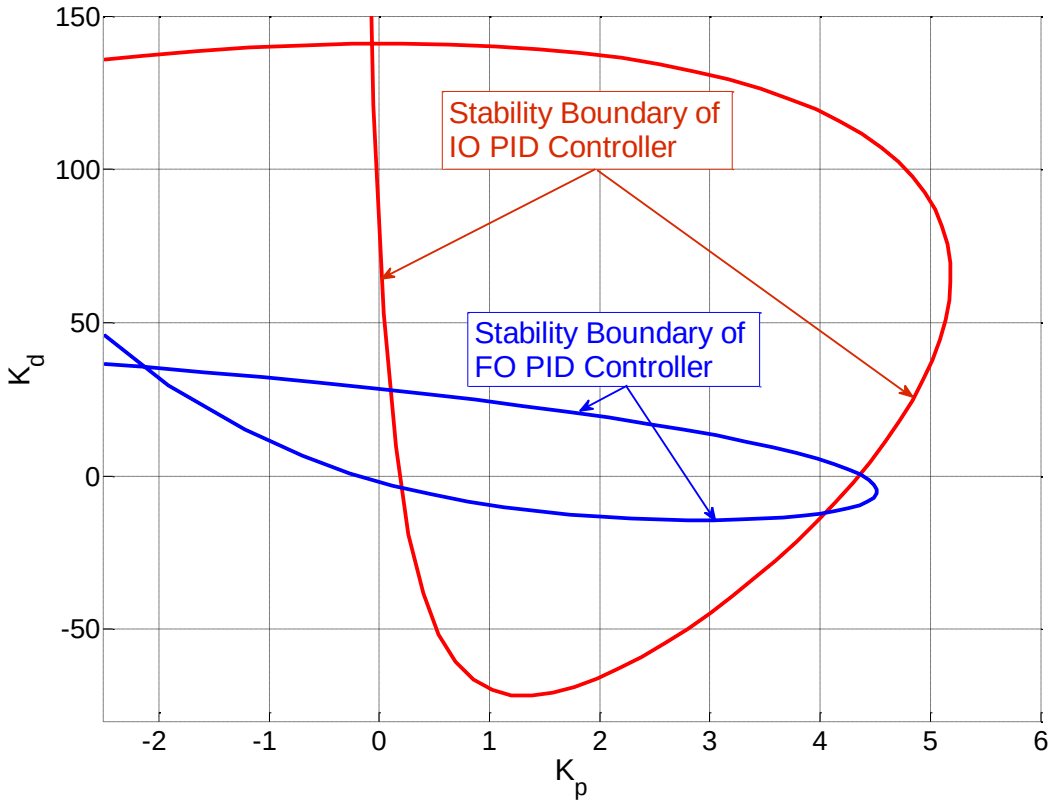

Fig. 13. Stability boundaries of the FO and IO PID controllers in (K_p, K_d) plane for K_i=0.01.

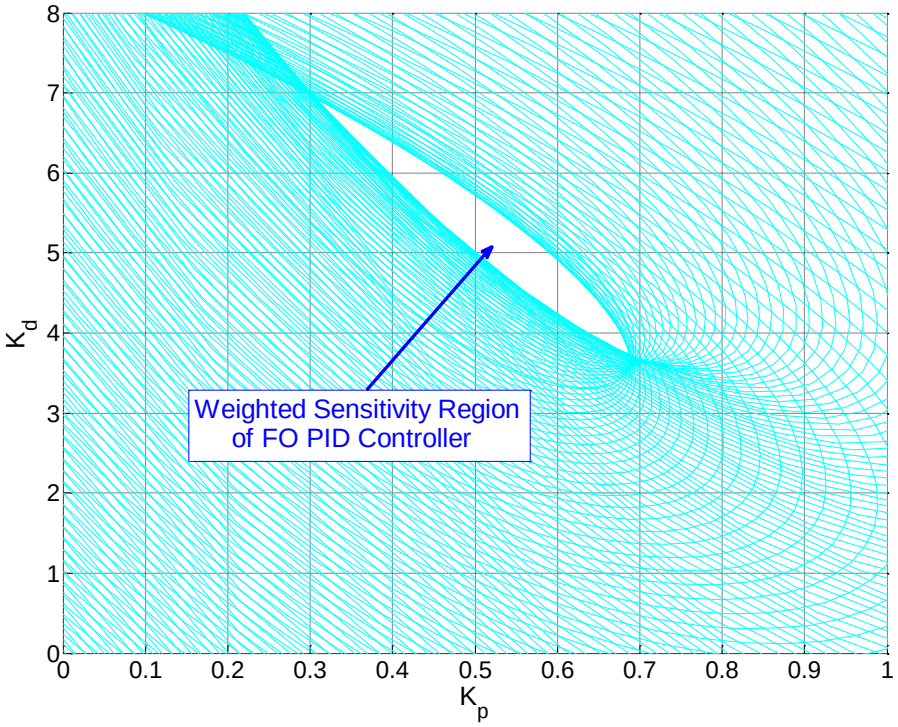

Fig. 14. Weighted sensitivity region in (K_p, K_d) plane for the FO PID controller with K_i=0.01.

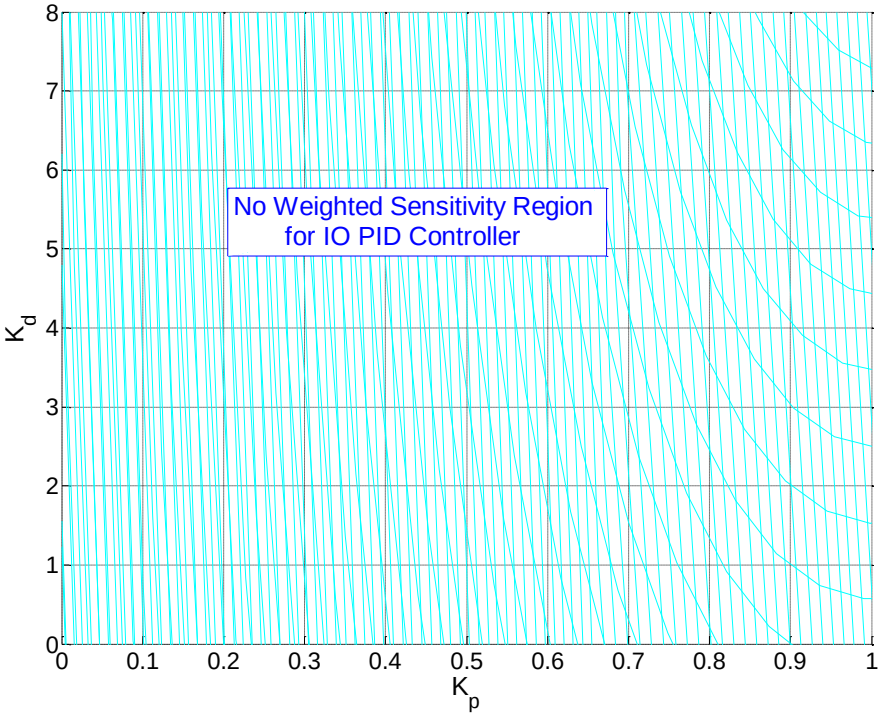

Fig. 15. Weighted sensitivity region in (K_p, K_d) plane for the IO PID controller with K_i=0.01.

5.4 Conclusion

As described in Sections 5.2 and 5.3, a method is presented for determining all the values of the parameters of FO PID controllers, which include IO PID controllers as well, that not only stabilize a given system but also meet an H_∞ weighted sensitivity condition. In particular, since the presented method includes existing solutions applicable to IO PID controllers and provides a complete set of solutions to so called FO PID controllers, it serves as a complete and generalized solution to determining all parameters of stabilizing PID controllers with a weighted sensitivity constraint. The method complements tuning rules for finding optimum values of the fractional orders λ and μ such as those proposed in [19].

Furthermore, as the results have been derived using frequency response of a system, this method can be applied even when a system transfer function is not known as long as the frequency response data of the system is obtainable. Furthermore, the results shown in Section 5.3 clearly indicate that even in cases where no IO PID controllers satisfy a given H_∞ weighted sensitivity condition, FO PID controllers may provide a fairly wide range of solutions.

CHAPTER 6
ROBUSTLY STABILIZING FO PID CONTROLLERS

6.1 Introduction

This chapter is directed to the robust stability of a control system. A method is presented for finding all PID controllers (both IO and FO PID controllers) that stabilize a system of arbitrary order with a time delay and simultaneously meet a robust stability condition. In particular, the method is designed to determine all the values of the parameters K_p, K_i, and K_d of FO PID controllers that robustly stabilize the closed-loop system. For a robust stability requirement, a multiplicative weight is selected to bound all multiplicative errors of the closed-loop system. Especially, such FO PID controllers remain stable for all the possible sets of perturbed plants. This chapter builds upon the work in [36]. This technique can be used even when the transfer function of a system is not available, as long as the system frequency response can be obtained.

A single-input single-output (SISO) linear time-invariant (LTI) system shown in Fig. 16 is considered. As the derivation of this method relies on the frequency response only, the method does not necessarily require a system transfer function. A detailed mathematical derivation, results, and examples follow.

6.2 FO PID Controller Design for Robust Stability

6.2.1 Problem Formulation

Consider the closed-loop system shown in Fig. 16,

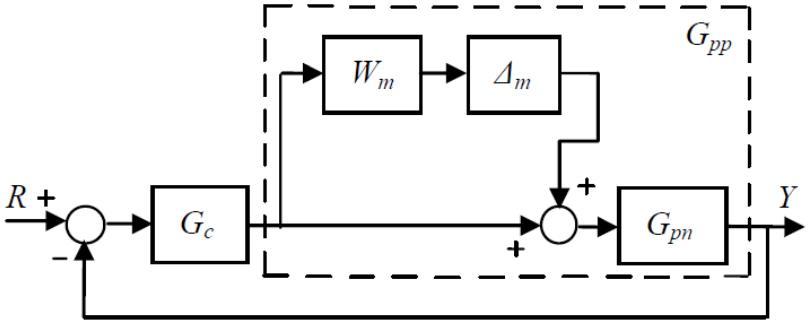

Fig. 16. A closed-loop system with multiplicative uncertainty.

where $G_{pn}(s)$ is the nominal plant and $G_{pp}(s)$ is the perturbed plant. The FO PID controller, $G_c(s)$, is given by

$$G_c(s) = K_p + \frac{K_i}{s^\lambda} + K_d s^\mu \tag{118}$$

where K_p, K_i and K_d denote the proportional, integral, and derivative gains, respectively, and λ and μ are arbitrary positive real numbers. $W_m(s)$ is the multiplicative weight (or multiplicative weighting function) and $\Delta_m(s)$ represents normalized uncertain perturbation such that $\|\Delta_m(j\omega)\|_\infty \le 1$. Signal $R(s)$ is the reference input, and $Y(s)$ is the output. The multiplicative weight, $W_m(s)$, is selected to bound all multiplicative errors of the closed-loop system, as described in [31].

In this chapter, FO PID controllers that stabilize the closed-loop system and simultaneously meet a robust stability condition will be determined by finding all the parameters K_p, K_i and K_d of such FO PID controllers for $\|\Delta_m(j\omega)\|_\infty \le 1$. Possible values of K_p, K_i and K_d of the FO PID controllers that stabilize the closed-loop system shown in Fig. 16 were found in [32].

The closed-loop system in Fig. 16 is robustly stable if the nominal system is stable and if

$$|T(j\omega)| \le \frac{\gamma}{|W_m(j\omega)|}, \quad \forall \omega \tag{119}$$

where $\gamma = 1$ [31].

This can be written equivalently as,

$$\|W_m(j\omega)T(j\omega)\|_\infty \le \gamma \tag{120}$$

where $T(j\omega) = \dfrac{G_{pn}(j\omega)G_c(j\omega)}{1+G_{pn}(j\omega)G_c(j\omega)}$ is the frequency domain representation of the complementary sensitivity function $T(s) = \dfrac{G_{pn}(s)G_c(s)}{1+G_{pn}(s)G_c(s)}$ and γ is a positive scalar that defines the upper bound of the magnitude of $T(j\omega)$ in conjunction with $W_m(j\omega)$.

In the frequency domain, the nominal plant transfer function $G_{pn}(s)$ and the multiplicative weight $W_m(s)$ can be expressed in terms of their real and imaginary parts as:

$$G_{pn}(j\omega) = R_p(\omega) + jI_p(\omega) \tag{121}$$

$$W_m(j\omega) = R_m(\omega) + jI_m(\omega) \tag{122}$$

Similarly, the FO PID controller transfer function (118) can be expressed in frequency domain as:

$$G_c(j\omega) = K_p + \frac{K_i}{(j\omega)^\lambda} + K_d(j\omega)^\mu \tag{123}$$

The constraint in (119) and (120) can be written as:

$$\left\| W_m(j\omega)T(j\omega) \right| e^{j\angle W_m(j\omega)T(j\omega)} \Big| \le \gamma, \quad \forall \omega \tag{124}$$

which is equivalent to:

$$W_m(j\omega)T(j\omega)e^{j\theta_m} \le \gamma, \quad \forall \omega \tag{125}$$

for some $\theta_m \in [0, 2\pi)$, where $\theta_m = -\angle W_m(j\omega)T(j\omega)$. Thus, (125) tells us that all the FO PID controllers that meet the condition (120) must lie in the intersection defined by the controllers that satisfy (125) for all $\theta_m \in [0, 2\pi)$. From (125), it is clear that

$$W_m(j\omega)T(j\omega)e^{j\theta_m} = \gamma \tag{126}$$

constitutes the boundary condition such that any FO PID controller within such boundary will satisfy (125), for all $\theta_m \in [0, 2\pi)$. Accordingly, (126) can be written as

$$1 + G_{pn}(j\omega)G_c(j\omega) - \frac{1}{\gamma}W_m(j\omega)G_{pn}(j\omega)G_c(j\omega)e^{j\theta_m} = 0 \tag{127}$$

By substituting (121), (122), and (123), and using $e^{j\theta_m} = \cos\theta_m + j\sin\theta_m$, the boundary condition (127) becomes:

$$\begin{aligned} &1+\left(R_p(\omega)+jI_p(\omega)\right)\left(K_p+\frac{K_i}{(j\omega)^{\lambda}}+K_d(j\omega)^{\mu}\right) \\ &-\frac{1}{\gamma}\left(R_m(\omega)+jI_m(\omega)\right)\left(R_p(\omega)+jI_p(\omega)\right)\left(K_p+\frac{K_i}{(j\omega)^{\lambda}}+K_d(j\omega)^{\mu}\right)\left(\cos\theta_m+j\sin\theta_m\right)=0 \end{aligned} \tag{128}$$

It can be easily seen that if $\lambda=\mu=1$, (128) reduces to the case of the IO PID controller in [8] and if γ goes to infinity, (128) reduces to the case of the closed-loop stability of the FO PID controller in [32].

Expanding (128) into real and imaginary parts gives:

$$X_{Rp}K_p + X_{Ri}K_i + X_{Rd}K_d = Y_R \tag{129}$$

$$X_{Ip}K_p + X_{Ii}K_i + X_{Id}K_d = Y_I \tag{130}$$

where

$$X_{Rp} = \omega^{\lambda}\left(R_p(\omega)+\frac{1}{\gamma}\begin{pmatrix}R_p(\omega)\left(-R_m(\omega)\cos\theta_m+I_m(\omega)\sin\theta_m\right)\\+I_p(\omega)\left(R_m(\omega)\sin\theta_m+I_m(\omega)\cos\theta_m\right)\end{pmatrix}\right),$$

$$X_{Ri} = \cos\left(\frac{\pi}{2}\lambda\right)R_p(\omega)+\sin\left(\frac{\pi}{2}\lambda\right)I_p(\omega)+\frac{1}{\gamma}\begin{pmatrix}\cos\left(\frac{\pi}{2}\lambda-\theta_m\right)\left(-R_p(\omega)R_m(\omega)+I_p(\omega)I_m(\omega)\right)\\-\sin\left(\frac{\pi}{2}\lambda-\theta_m\right)\left(R_p(\omega)I_m(\omega)+I_p(\omega)R_m(\omega)\right)\end{pmatrix},$$

$$\begin{aligned} X_{Rd} =& \omega^{\lambda+\mu}\left(\cos\left(\frac{\pi}{2}\mu\right)R_p(\omega)-\sin\left(\frac{\pi}{2}\mu\right)I_p(\omega)\right) \\ &+\frac{\omega^{\lambda+\mu}}{\gamma}\begin{pmatrix}\cos\left(\frac{\pi}{2}\mu+\theta_m\right)\left(-R_p(\omega)R_m(\omega)+I_p(\omega)I_m(\omega)\right)\\+\sin\left(\frac{\pi}{2}\mu+\theta_m\right)\left(R_p(\omega)I_m(\omega)+I_p(\omega)R_m(\omega)\right)\end{pmatrix}, \end{aligned}$$

$$X_{Ip} = \omega^{\lambda}\left(I_p(\omega) - \frac{1}{\gamma}\begin{pmatrix} R_p(\omega)\left(R_m(\omega)\sin\theta_m + I_m(\omega)\cos\theta_m\right) \\ +I_p(\omega)\left(R_m(\omega)\cos\theta_m - I_m(\omega)\sin\theta_m\right) \end{pmatrix}\right),$$

$$X_{Ii} = \cos\left(\frac{\pi}{2}\lambda\right) I_p(\omega) - \sin\left(\frac{\pi}{2}\lambda\right) R_p(\omega) - \frac{1}{\gamma}\begin{pmatrix} \sin\left(\frac{\pi}{2}\lambda - \theta_m\right)\left(-R_p(\omega)R_m(\omega) + I_p(\omega)I_m(\omega)\right) \\ +\cos\left(\frac{\pi}{2}\lambda - \theta_m\right)\left(R_p(\omega)I_m(\omega) + I_p(\omega)R_m(\omega)\right) \end{pmatrix},$$

$$X_{Id} = \omega^{\lambda+\mu}\left(\cos\left(\frac{\pi}{2}\mu\right) I_p(\omega) + \sin\left(\frac{\pi}{2}\mu\right) R_p(\omega)\right)$$
$$-\frac{\omega^{\lambda+\mu}}{\gamma}\begin{pmatrix} \sin\left(\frac{\pi}{2}\mu + \theta_m\right)\left(R_p(\omega)R_m(\omega) - I_p(\omega)I_m(\omega)\right) \\ +\cos\left(\frac{\pi}{2}\mu + \theta_m\right)\left(R_p(\omega)I_m(\omega) + I_p(\omega)R_m(\omega)\right) \end{pmatrix},$$

$Y_R = -\omega^{\lambda}$, and $Y_I = 0$.

6.2.2 Solution in (K_p, K_i) Plane

As this is a three dimensional system in terms of the controller parameters K_p, K_i and K_d, the value of K_d will be fixed to find the solution to (129) and (130) in the (K_p, K_i) plane. In matrix form, (129) and (130) can be written in terms of the two unknowns K_p and K_i as:

$$\begin{bmatrix} X_{Rp} & X_{Ri} \\ X_{Ip} & X_{Ii} \end{bmatrix}\begin{bmatrix} K_p \\ K_i \end{bmatrix} = \begin{bmatrix} Y_R - X_{Rd}K_d \\ Y_I - X_{Id}K_d \end{bmatrix} \tag{131}$$

Solving (131) for non-singular case, K_p and K_i are given by

$$K_p = -K_d\omega^{\mu}\frac{\sin\left(\frac{\pi}{2}(\lambda+\mu)\right)}{\sin\left(\frac{\pi}{2}\lambda\right)} - \frac{\left(\begin{array}{l} R_p(\omega)\sin\left(\frac{\pi}{2}\lambda\right) - I_p(\omega)\cos\left(\frac{\pi}{2}\lambda\right) + \\ \frac{1}{\gamma}\left(\begin{array}{l} \cos\left(\frac{\pi}{2}\lambda-\theta_m\right)\left(R_p(\omega)I_m(\omega)+I_p(\omega)R_m(\omega)\right) \\ -\sin\left(\frac{\pi}{2}\lambda-\theta_m\right)\left(R_p(\omega)R_m(\omega)-I_p(\omega)I_m(\omega)\right) \end{array}\right) \end{array}\right)}{D_1} \tag{132}$$

$$K_i = K_d\omega^{\lambda+\mu}\frac{\sin\left(\frac{\pi}{2}\mu\right)}{\sin\left(\frac{\pi}{2}\lambda\right)} - \frac{\omega^{\lambda}\left(\frac{1}{\gamma}\left(\begin{array}{l} \cos\theta_m\left(R_p(\omega)I_m(\omega)+I_p(\omega)R_m(\omega)\right) \\ +\sin\theta_m\left(R_p(\omega)R_m(\omega)-I_p(\omega)I_m(\omega)\right) \end{array}\right) - I_p(\omega)\right)}{D_1} \tag{133}$$

where

$$D_1 = \sin\left(\frac{\pi}{2}\lambda\right)\left|G_p(j\omega)\right|^2\left(\frac{1}{\gamma^2}\left|W_m(j\omega)\right|^2 + 1 - \frac{2}{\gamma}\left(R_m(\omega)\cos\theta_m - I_m(\omega)\sin\theta_m\right)\right),$$

$\left|G_p(j\omega)\right|^2 = {R_p}^2(\omega) + {I_p}^2(\omega)$, and $\left|W_m(j\omega)\right|^2 = {R_m}^2(\omega) + {I_m}^2(\omega)$.

If ω=0, then (131) becomes

$$\begin{bmatrix} 0 & X_{Ri} \\ 0 & X_{Ii} \end{bmatrix}\begin{bmatrix} K_p \\ K_i \end{bmatrix} = \begin{bmatrix} 0 \\ 0 \end{bmatrix} \tag{134}$$

Solving (134), we determine that either K_p is arbitrary and K_i=0, or K_p and K_i both are arbitrary if $R_p(0) = I_p(0) = 0$, which indicates that $G_{pn}(s)$ has a zero at the origin. In such a case, the zero of a plant transfer function at the origin cancels the pole of the PID controller at the origin, thereby causing internal instability.

Thus, all the possible values of K_p and K_i of stabilizing FO PID controllers for a fixed K_d value that meet the robust stability condition (120) can be plotted in a two-dimensional graph using the above results with K_p and K_i as two Cartesian axes. If λ=μ=1, which is a conventional

IO PID controller, the above results reduce to those presented in [8].

6.2.3 Solution in (K_p, K_d) Plane

Likewise, value of K_i will be fixed to determine the solution in the (K_p, K_d) plane. Accordingly, (129) and (130) are rearranged as:

$$\begin{bmatrix} X_{Rp} & X_{Rd} \\ X_{Ip} & X_{Id} \end{bmatrix} \begin{bmatrix} K_p \\ K_d \end{bmatrix} = \begin{bmatrix} Y_R - X_{Ri}K_i \\ Y_I - X_{Ii}K_i \end{bmatrix} \tag{135}$$

Solving (135) for non-singular case, K_p and K_d are given by

$$K_p = -K_i \frac{\sin\left(\frac{\pi}{2}(\lambda+\mu)\right)}{\omega^{\lambda}\sin\left(\frac{\pi}{2}\mu\right)} - \frac{\left(\begin{array}{l} R_p(\omega)\sin\left(\frac{\pi}{2}\mu\right) + I_p(\omega)\cos\left(\frac{\pi}{2}\mu\right) - \\ \frac{1}{\gamma}\left(\begin{array}{l} \cos\left(\theta_m + \frac{\pi}{2}\mu\right)\left(R_p(\omega)I_m(\omega) + I_p(\omega)R_m(\omega)\right) \\ +\sin\left(\theta_m + \frac{\pi}{2}\mu\right)\left(R_p(\omega)R_m(\omega) - I_p(\omega)I_m(\omega)\right) \end{array}\right) \end{array}\right)}{D_2} \tag{136}$$

$$K_d = K_i \frac{\sin\left(\frac{\pi}{2}\lambda\right)}{\omega^{\lambda+\mu}\sin\left(\frac{\pi}{2}\mu\right)} + \frac{\left(\begin{array}{l} I_p(\omega) - \frac{1}{\gamma}\left(\begin{array}{l} \cos\theta_m\left(R_p(\omega)I_m(\omega) + I_p(\omega)R_m(\omega)\right) \\ +\sin\theta_m\left(R_p(\omega)R_m(\omega) - I_p(\omega)I_m(\omega)\right) \end{array}\right) \end{array}\right)}{\omega^{\mu}D_2} \tag{137}$$

where $D_2 = \sin\left(\frac{\pi}{2}\mu\right)\left|G_p(j\omega)\right|^2\left(\frac{1}{\gamma^2}\left|W_m(j\omega)\right|^2 + 1 - \frac{2}{\gamma}\left(R_m(\omega)\cos\theta_m - I_m(\omega)\sin\theta_m\right)\right)$.

If ω=0, then K_p and K_d both are arbitrary with K_i=0 or $R_p(0) = I_p(0) = 0$, as is obvious from (135).

Again, possible values of K_p and K_d of FO PID controllers that stabilize the closed-loop

system in Fig. 16 and simultaneously satisfy the robust stability condition (120) for a fixed K_i value can be plotted in a two-dimensional graph using the above results with K_p and K_d as two Cartesian axes. If $\lambda=\mu=1$, which is a conventional IO PID controller, the above results reduce to those presented in [8].

6.2.4 Solution in (K_i, K_d) Plane

Lastly, the (K_i, K_d) plane solution will be determined by fixing the value of K_p. Thus, (129) and (130) can be written as:

$$\begin{bmatrix} X_{Ri} & X_{Rd} \\ X_{Ii} & X_{Id} \end{bmatrix} \begin{bmatrix} K_i \\ K_d \end{bmatrix} = \begin{bmatrix} Y_R - X_{Rp}K_p \\ Y_I - X_{Ip}K_p \end{bmatrix} \tag{138}$$

Solving (138) for non-singular case, K_i and K_d are given by

$$K_i = -K_p\omega^\lambda \frac{\sin\left(\frac{\pi}{2}\mu\right)}{\sin\left(\frac{\pi}{2}(\lambda+\mu)\right)} + \frac{\omega^\lambda \left(\begin{array}{l} -\left(R_p(\omega)\sin\left(\frac{\pi}{2}\mu\right) + I_p(\omega)\cos\left(\frac{\pi}{2}\mu\right)\right) + \\ \frac{1}{\gamma}\left(\begin{array}{l} \cos\left(\theta_m + \frac{\pi}{2}\mu\right)\left(R_p(\omega)I_m(\omega) + I_p(\omega)R_m(\omega)\right) \\ +\sin\left(\theta_m + \frac{\pi}{2}\mu\right)\left(R_p(\omega)R_m(\omega) - I_p(\omega)I_m(\omega)\right) \end{array}\right) \end{array}\right)}{D_3} \tag{139}$$

$$K_d = -\left(\frac{K_p}{\omega^\mu}\right)\frac{\sin\left(\frac{\pi}{2}\lambda\right)}{\sin\left(\frac{\pi}{2}(\lambda+\mu)\right)} - \frac{\omega^\lambda \left(\begin{array}{l} R_p(\omega)\sin\left(\frac{\pi}{2}\lambda\right) - I_p(\omega)\cos\left(\frac{\pi}{2}\lambda\right) \\ \frac{1}{\gamma}\left(\begin{array}{l} \cos\left(\theta_m - \frac{\pi}{2}\lambda\right)\left(R_p(\omega)I_m(\omega) + I_p(\omega)R_m(\omega)\right) \\ +\sin\left(\theta_m - \frac{\pi}{2}\lambda\right)\left(R_p(\omega)R_m(\omega) - I_p(\omega)I_m(\omega)\right) \end{array}\right) \end{array}\right)}{\omega^\mu D_3} \tag{140}$$

where $D_3 = \sin\left(\frac{\pi}{2}(\lambda+\mu)\right)\left|G_p(j\omega)\right|^2\left(\frac{1}{\gamma^2}\left|W_m(j\omega)\right|^2 + 1 - \frac{2}{\gamma}\left(R_m(\omega)\cos\theta_m - I_m(\omega)\sin\theta_m\right)\right)$.

If ω=0, then K_i and K_d both are arbitrary if $R_p(0) = I_p(0) = 0$, or K_i=0 and K_d is arbitrary.

Likewise, all the values of K_i and K_d of stabilizing FO PID controllers that satisfy the robust stability condition (120) for a fixed K_p value can be found in the (K_i, K_d) plane using the above results with K_i and K_d as two Cartesian axes. For λ=μ=1, the above results reduce to those presented in [8].

It should be noted that all the results in this section were derived in the frequency domain. As a consequence, the controller parameters K_p, K_i, and K_d of FO PID controllers that stabilize a given system and simultaneously meet a robust stability condition can be determined directly from an experimental frequency response when either the system transfer function or system parameters are unknown.

6.3 Example

6.3.1 Problem Formulation

Now, a numerical example will be given to illustrate the application and effectiveness of the results derived in Section 6.2. In order to clearly show the advantage of using FO PID controllers over IO PID controllers, we will use the example in [8], in which all IO PID controllers that stabilized a closed-system and satisfied the robust stability condition were found. In the example of [8], a feedback loop comprises a DC motor and an unknown communication delay of between 0.05 and 0.15 seconds. The nominal model of the DC motor was given by

$$G_{pn}(s) = \frac{65.5}{s(s+34.6)}e^{-\tau s} \tag{141}$$

Where τ, representing a time delay, was selected to be the mean of the unknown communication delay, or 0.1 second.

The objective of this example is to find all the values of the parameters K_p, K_i and K_d of the FO PID controller that stabilizes the closed-loop system shown in Fig. 16 with the nominal plant (141) and simultaneously satisfy the robust stability condition (120) where γ=1. As

discussed above, there are a multitude of tuning rules for finding the values of the fractional orders λ and μ of the FO PID controllers. A non-optimal FO PID controller was chosen to have λ=1.32 and μ=0.65. Thus, the FO PID controller used is given by

$$G_{cFO}(s) = K_p + \frac{K_i}{s^{1.32}} + K_d s^{0.65} \tag{142}$$

In [8], the multiplicative weight, $W_m(s)$, was chosen as

$$W_m(s) = \frac{s}{0.357s + 20} \tag{143}$$

to bound the multiplicative errors.

6.3.2 Robust Stability Region in (K_p, K_i) Plane

In order to find the robust stability region in the (K_p, K_i) plane for the closed-loop system with the nominal plant transfer function (141) and the FO PID controller transfer function (142), (132) and (133) were used with a fixed value K_d=0.4 and γ=1. In detail, all the possible values of the parameters K_p and K_i of FO PID controllers that satisfy the robust stability condition defined by (120) can be determined by finding an intersection of all the solutions to (132) and (133) for $\theta_m \in [0, 2\pi)$ in a given range of frequency ω. Such intersection lies on or within the boundary set by (126) for $\theta_m \in [0, 2\pi)$, thereby constituting a true solution to the robust stability constraint (120). The corresponding nominal stability boundary can be calculated by taking γ=∞ in (132) and (133), which is the same as that disclosed in [32].

Fig. 17 shows the nominal stability boundary of the FO PID controller (142) and that of the IO PID controllers for K_d=0.4, respectively. Fig. 18 and Fig. 19 show the robust stability region of the FO PID controller (142) and that of the IO PID controller in the (K_p, K_i) plane for K_d=0.4, respectively.

As can be seen from Fig. 17, both the IO and FO PID controllers provide a large nominal stability region in the (K_p, K_i) plane for K_d=0.4. However, whereas the FO PID controller (142) provides a large robust stability region in the (K_p, K_i) plane for K_d=0.4, the IO PID controller

does not provide any weighted sensitivity region, as shown in Figs. 18 and 19 respectively. In more detail, the robust stability region represents all the possible values of K_p and K_i of the FO PID for K_d=0.4 that stabilizes the closed-loop system with the nominal plant transfer function (141) and simultaneously satisfy the robust stability condition (120). Accordingly, the IO PID controller is not a plausible choice in this specific example with the uncertainty of a time delay.

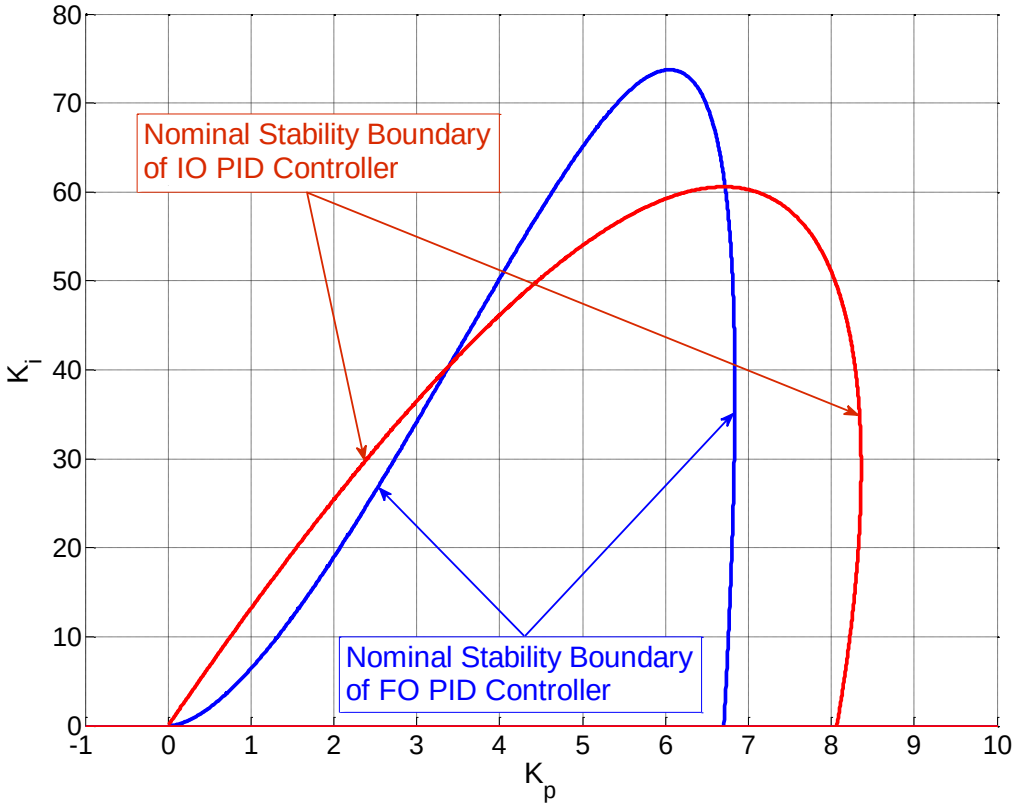

Fig. 17. Nominal stability boundaries of the FO and IO PID controllers in (K_p, K_i) plane for K_d=0.4.

To verify that the FO PID controllers lying in such intersection truly meet the robust stability constraint (120), an arbitrary controller was chosen from the robust stability region of the FO PID controller in Fig. 18, which is K_p= 2.8053 and K_i=11.4035, as marked on the plot. Therefore, the chosen FO PID controller is

$$G_{cFO}(s) = 2.8053 + \frac{11.4035}{s^{1.32}} + 0.4s^{0.65} \tag{144}$$

Fig. 20 shows $\left|W_m(j\omega)T(j\omega)\right|$ with the FO PID controller (144) and illustrates that $\left\|W_m(j\omega)T(j\omega)\right\|_\infty$ is equal to 0.699, which is of course less than γ=1.

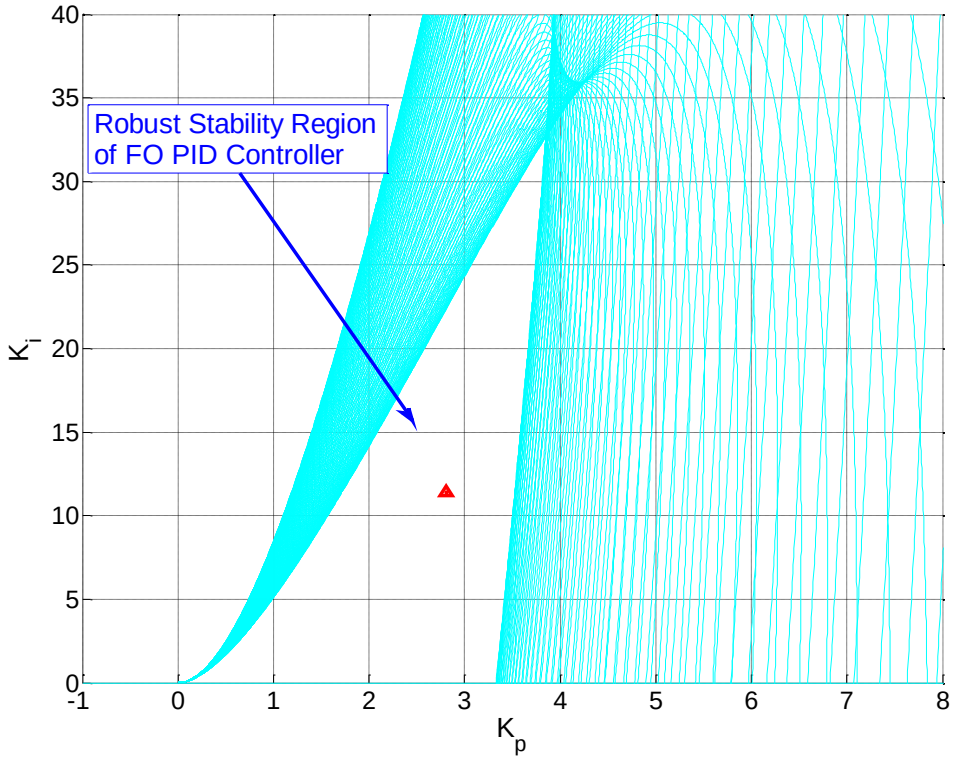

Fig. 18. Robust stability region in (K_p, K_i) plane for the FO PID controller with K_d=0.4.

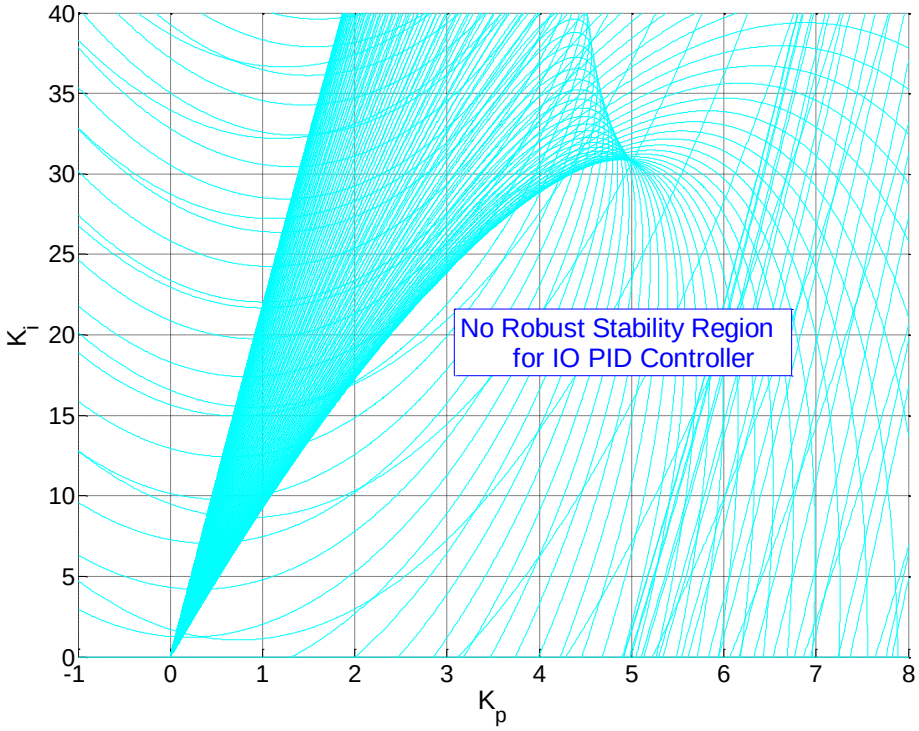

Fig. 19. Robust stability region in (K_p, K_i) plane for the IO PID controller with K_d=0.4.

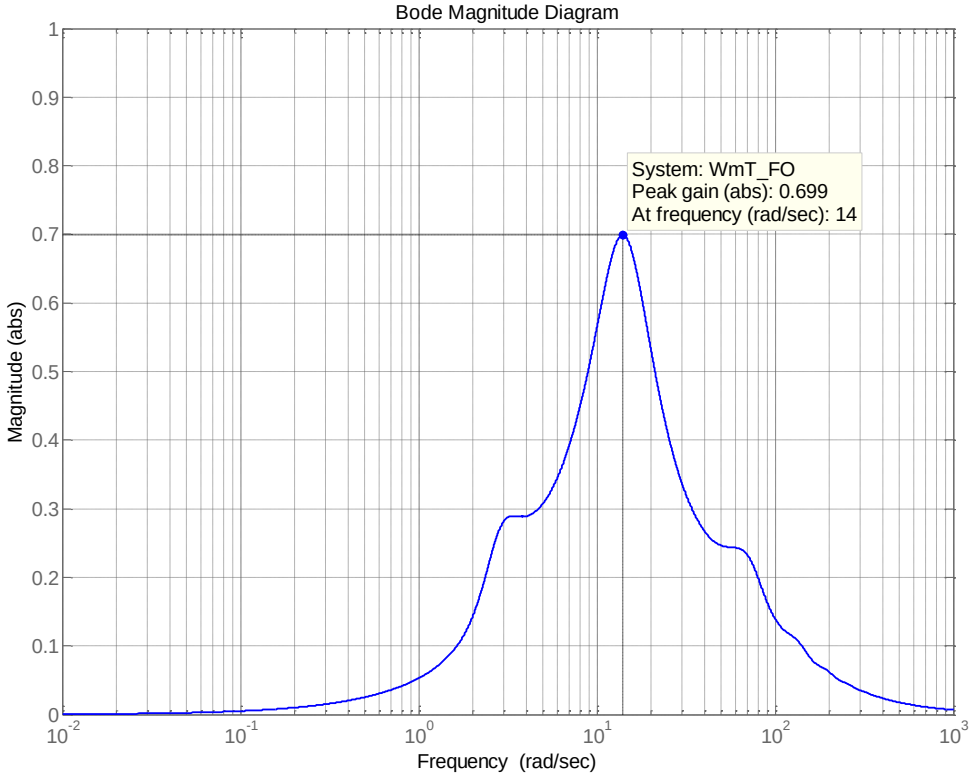

Fig. 20. $\left|W_m(j\omega)T(j\omega)\right|$ with the FO PID controller (144).

6.3.3 Robust Stability Region in (K_p, K_d) Plane

Similarly, the nominal stability boundary and the robust stability region in the (K_p, K_d) plane for the closed-loop system with the nominal plant (141) and the FO PID controller (142) were determined for a fixed value K_i=22 using (136) and (137). As discussed earlier, an intersecting region of all solutions to (136) and (137) when γ=1 for $\theta_m \in [0, 2\pi)$ in a given range of frequency ω is the robust stability region and the corresponding nominal stability boundary is obtained by setting γ=∞ in (136) and (137).

In Fig. 21, the robust stability region and the nominal stability boundary of the FO PID controller (142) are plotted in the (K_p, K_d) plane for K_i=22. For comparison, those of the IO PID controller are shown in Fig. 22. As can be seen from Figs. 21 and 22, even though the FO PID controller and the IO PID controller both provide a large nominal stability region, the FO PID controller provides a much larger robust stability region than the IO PID controller for K_i=22. While the robust stability region was determined in the (K_p, K_d) plane for one fixed value of K_i in the example, it is possible to find the entire robust stability region by varying K_i values over a certain range.

Again, in order to verify that FO PID controllers lying in such intersecting region meet the robust stability condition (120), an arbitrary controller was chosen from the robust stability region of the FO PID controller in Fig. 21, which is K_p= 3.3070 and K_d=0.3457, as marked on the plot. Therefore, the chosen FO PID controller is

$$G_{cFO}(s) = 3.3070 + \frac{22}{s^{1.32}} + 0.3457 s^{0.65} \tag{145}$$

Fig. 23 shows $\left|W_m(j\omega)T(j\omega)\right|$ with the FO PID controller (145) and illustrates that $\left\|W_m(j\omega)T(j\omega)\right\|_\infty$ is equal to 0.745, which is less than γ=1.

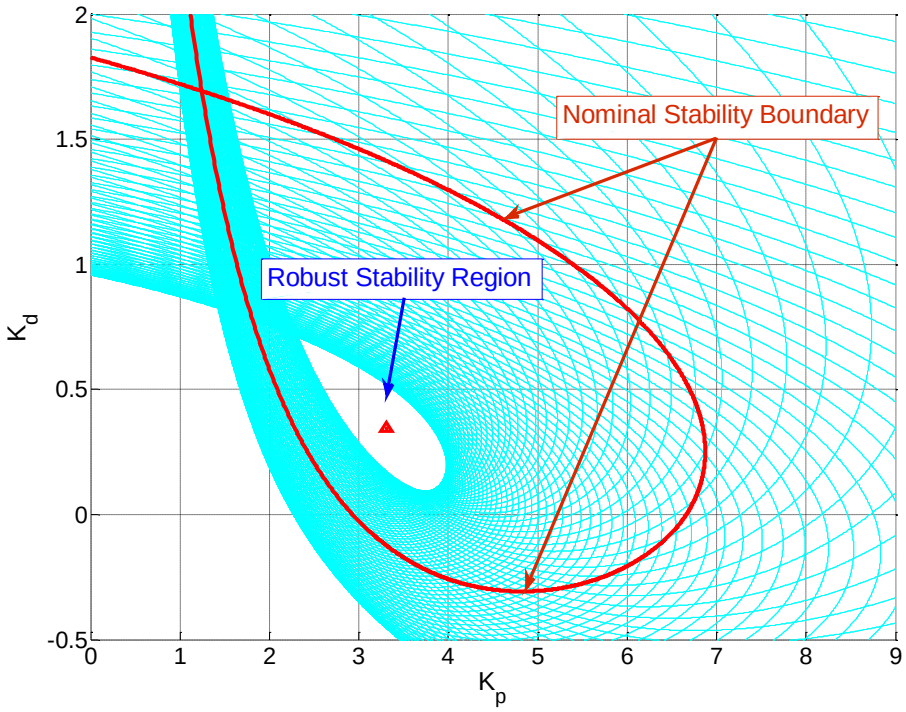

Fig. 21. Nominal stability boundary and robust stability region in (K_p, K_d) plane for the FO PID controller with K_i=22.

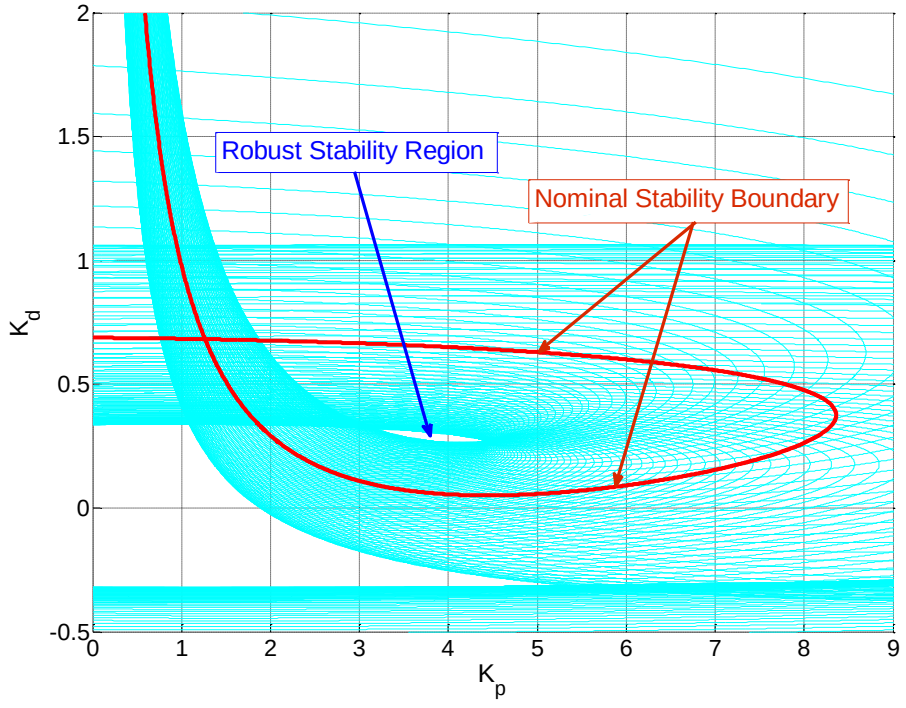

Fig. 22. Nominal stability boundary and robust stability region in (K_p, K_d) plane for the IO PID controller with K_i=22.

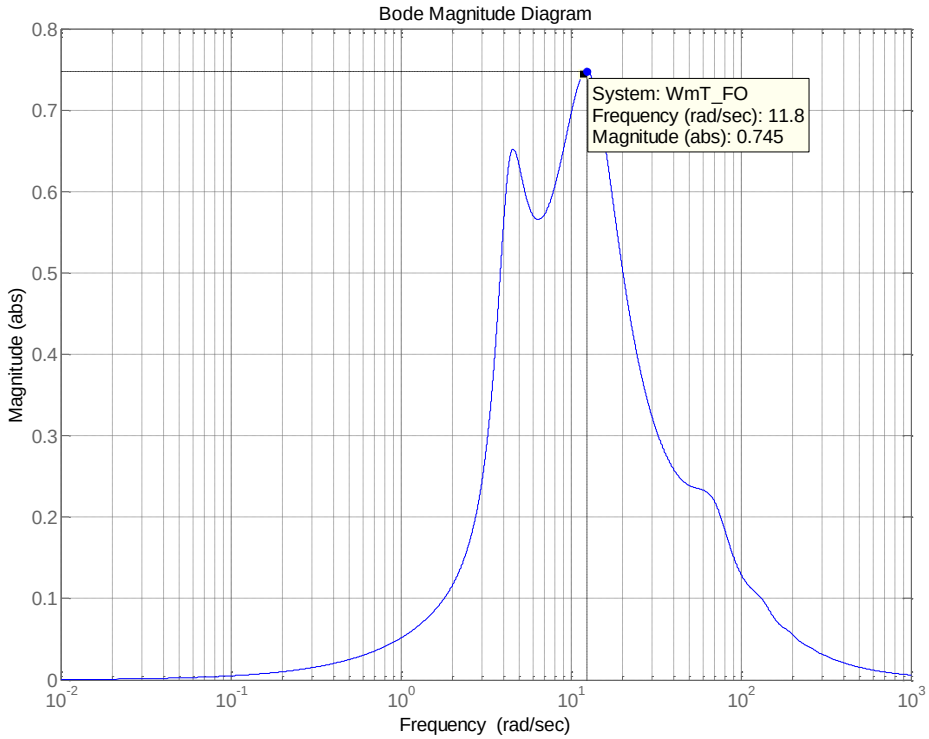

Fig. 23. $\left|W_m(j\omega)T(j\omega)\right|$ with the FO PID controller (145).

6.4 Conclusion

As described and illustrated in Sections 6.2 and 6.3, a method is presented for finding all the values of the parameters of FO PID controllers that stabilize a given system and meet a robust stability condition. In addition, the method presented here can be used alone as well as in combination with other tuning rules for finding the values of the fractional orders λ and μ of FO PID controllers. Furthermore, as the derivation has completely relied upon the frequency response of a system, this method can be used even when a system transfer function is not known as long as the frequency response data of the system can be acquired. Moreover, the results shown in Section 6.3 clearly show that FO PID controllers could provide a fairly wide range of solutions even if there would be no solution to IO PID controllers that satisfy a robust stability condition.

CHAPTER 7
FO PID CONTROLLER DESIGN FOR ROBUST PERFORMANCE

7.1 Introduction

Following the investigation of the robust stability and nominal performance of a control system, robust performance of a closed-loop system with an FO PID controller will be explored next. This chapter presents a method for finding all FO PID controllers that stabilize a given system of arbitrary order with a time delay and simultaneously meet a robust performance constraint. In particular, it is an object of this chapter to provide a method for determining all the possible values of the parameters K_p, K_i and K_d of stabilizing FO PID controllers that satisfy robust performance requirements. This chapter builds upon the work in [37]. For robust performance of a closed-loop system, the nominal performance requirement and robust stability constraint must be satisfied first, thereby leading to a problem of a combination of robust stability and weighted sensitivity.

To this end, a single-input single-output (SISO) linear time-invariant (LTI) system will be considered. As in the previous topics, the method presented here does not necessarily require a system transfer function because the procedure is completely based on the frequency response of the system. A detailed mathematical derivation, results, and examples follow.

7.2 FO PID Controller Design for Robust Performance

7.2.1 Problem Formulation

Consider the closed-loop system shown in Fig. 24,

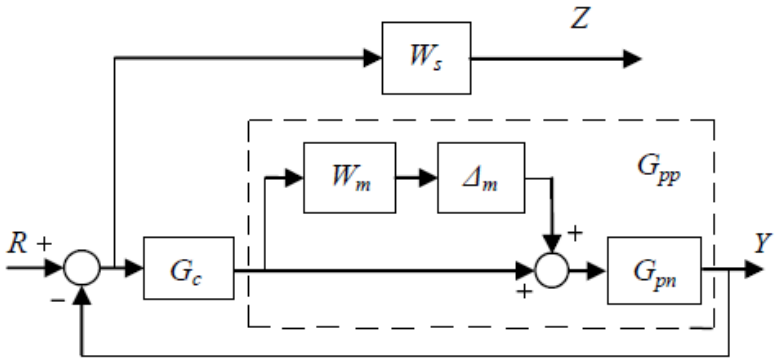

Fig. 24. A closed-loop system with multiplicative uncertainty.

where $G_{pn}(s)$ is the nominal plant and $G_{pp}(s)$ is the perturbed plant. The FO PID controller, $G_c(s)$, is given by

$$G_c(s) = K_p + \frac{K_i}{s^{\lambda}} + K_d s^{\mu} \tag{146}$$

where K_p, K_i and K_d denote the proportional, integral, and derivative gains, respectively, and λ and μ are arbitrary positive real numbers. $W_m(s)$ is the multiplicative weight and $\Delta_m(s)$ represents the normalized uncertain perturbation such that $\|\Delta_m(j\omega)\|_{\infty} \le 1$. $W_s(s)$ is the sensitivity function weight and $R(s)$ is the input signal. $Y(s)$ is the closed-loop system output and $Z(s)$ is the output signal representing the weighted error. The multiplicative weight, $W_m(s)$, is selected to bound all multiplicative errors of the closed-loop system and the sensitivity function weight, $W_s(s)$, is selected to meet performance specifications, such as a settling time, percent overshoot, et cetera, as described in [31].

In this paper, FO PID controllers that stabilize the nominal closed-loop system shown in Fig. 24 and meet a robust performance constraint at the same time can be determined by finding all the parameters K_p, K_i and K_d of such FO PID controllers. All the values of K_p, K_i and K_d of the FO PID controllers that stabilize the nominal closed-loop system were determined in [32].

The robust performance constraint for a SISO system is given in [31] by:

$$\left|W_s(j\omega)S(j\omega)\right| + \left|W_m(j\omega)T(j\omega)\right| \le \gamma, \quad \forall \omega \tag{147}$$

where $S(j\omega) = \dfrac{1}{1 + G_{pn}(j\omega)G_C(j\omega)}$ is the sensitivity function, $T(s) = \dfrac{G_{pn}(j\omega)G_c(j\omega)}{1 + G_{pn}(j\omega)G_c(j\omega)}$ is the complementary sensitivity function, and $\gamma = 1$ [31]. In the frequency domain, the nominal plant transfer function $G_{pn}(s)$, the multiplicative weight $W_m(s)$, and the sensitivity function weight $W_s(s)$ can be expressed in terms of their real and imaginary parts as:

$$G_{pn}(j\omega) = R_p(\omega) + jI_p(\omega) \tag{148}$$

$$W_m(j\omega) = R_m(\omega) + jI_m(\omega) \tag{149}$$

$$W_s(j\omega) = R_s(\omega) + jI_s(\omega) \tag{150}$$

Likewise, the FO PID controller transfer function (146) can be written in the frequency domain as:

$$G_c(j\omega) = K_p + \frac{K_i}{(j\omega)^{\lambda}} + K_d(j\omega)^{\mu} \tag{151}$$

The robust performance constraint in (147) can be written with magnitude and phase as:

$$\left\|W_s(j\omega)S(j\omega)\right| e^{j\angle W_s(j\omega)S(j\omega)}\Big| + \left\|W_m(j\omega)T(j\omega)\right| e^{j\angle W_m(j\omega)T(j\omega)}\Big| \le \gamma, \quad \forall\omega \tag{152}$$

which is equivalent to:

$$W_s(j\omega)S(j\omega)e^{j\angle\theta_s} + W_m(j\omega)T(j\omega)e^{j\theta_m} \le \gamma, \quad \forall\omega \tag{153}$$

for some $\theta_s \in [0, 2\pi)$, where $\theta_s = -\angle W_s(j\omega)S(j\omega)$ and $\theta_m \in [0, 2\pi)$, where $\theta_m = -\angle W_m(j\omega)T(j\omega)$. Thus, (153) indicates that all the FO PID controllers that meet the condition (147) must lie within the intersection defined by the controller parameters that satisfy (153) for all $\theta_s \in [0, 2\pi)$ and $\theta_m \in [0, 2\pi)$. From (153), the boundary equation for the robust performance condition is given by

$$W_s(j\omega)S(j\omega)e^{j\angle\theta_s} + W_m(j\omega)T(j\omega)e^{j\theta_m} = \gamma, \quad \forall\omega \tag{154}$$

Accordingly, expanding (154) leads to

$$1 + G_{pn}(j\omega)G_c(j\omega) - \frac{1}{\gamma}W_s(j\omega)e^{j\angle\theta_s} - \frac{1}{\gamma}W_m(j\omega)G_{pn}(j\omega)G_c(j\omega)e^{j\theta_m} = 0 \tag{155}$$

By substituting (148) through (151) and using $e^{j\theta_m} = \cos\theta_m + j\sin\theta_m$ and $e^{j\theta_s} = \cos\theta_s + j\sin\theta_s$, the boundary condition (155) becomes:

$$1+\left(R_p(\omega)+jI_p(\omega)\right)\left(K_p+\frac{K_i}{(j\omega)^{\lambda}}+K_d(j\omega)^{\mu}\right)-\frac{1}{\gamma}\left(R_s(\omega)+jI_s(\omega)\right)\left(\cos\theta_s+j\sin\theta_s\right)$$
$$-\frac{1}{\gamma}\left(R_m(\omega)+jI_m(\omega)\right)\left(R_p(\omega)+jI_p(\omega)\right)\times\left(K_p+\frac{K_i}{(j\omega)^{\lambda}}+K_d(j\omega)^{\mu}\right)\left(\cos\theta_m+j\sin\theta_m\right)=0 \quad (156)$$

It can be easily seen that if λ=μ=1, (156) reduces to the case of the conventional IO PID controller in [29] and if γ approaches infinity, (156) reduces to the case of the nominal closed-loop stability of the FO PID controller in [32].

Expanding (156) into real and imaginary parts and setting them equal to zero gives:

$$X_{Rp}K_p+X_{Ri}K_i+X_{Rd}K_d=Y_R \quad (157)$$

$$X_{Ip}K_p+X_{Ii}K_i+X_{Id}K_d=Y_I \quad (158)$$

where

$$X_{Rp}=\omega^{\lambda}\left(R_p(\omega)+\frac{1}{\gamma}\left(R_p(\omega)\left(-R_m(\omega)\cos\theta_m+I_m(\omega)\sin\theta_m\right)+I_p(\omega)\left(R_m(\omega)\sin\theta_m+I_m(\omega)\cos\theta_m\right)\right)\right)$$

$$X_{Ri}=\cos\left(\frac{\pi}{2}\lambda\right)R_p(\omega)+\sin\left(\frac{\pi}{2}\lambda\right)I_p(\omega)+\frac{1}{\gamma}\begin{pmatrix}\cos\left(\frac{\pi}{2}\lambda-\theta_m\right)\left(-R_p(\omega)R_m(\omega)+I_p(\omega)I_m(\omega)\right)\\-\sin\left(\frac{\pi}{2}\lambda-\theta_m\right)\left(R_p(\omega)I_m(\omega)+I_p(\omega)R_m(\omega)\right)\end{pmatrix},$$

$$X_{Rd}=\omega^{\lambda+\mu}\left(\cos\left(\frac{\pi}{2}\mu\right)R_p(\omega)-\sin\left(\frac{\pi}{2}\mu\right)I_p(\omega)\right)$$
$$+\frac{\omega^{\lambda+\mu}}{\gamma}\left(\cos\left(\frac{\pi}{2}\mu+\theta_m\right)\left(-R_p(\omega)R_m(\omega)+I_p(\omega)I_m(\omega)\right)+\sin\left(\frac{\pi}{2}\mu+\theta_m\right)\left(R_p(\omega)I_m(\omega)+I_p(\omega)R_m(\omega)\right)\right),$$

$$X_{Ip}=\omega^{\lambda}\left(I_p(\omega)-\frac{1}{\gamma}\left(R_p(\omega)\left(R_m(\omega)\sin\theta_m+I_m(\omega)\cos\theta_m\right)+I_p(\omega)\left(R_m(\omega)\cos\theta_m-I_m(\omega)\sin\theta_m\right)\right)\right),$$

$$X_{Ii}=\cos\left(\frac{\pi}{2}\lambda\right)I_p(\omega)-\sin\left(\frac{\pi}{2}\lambda\right)R_p(\omega)-\frac{1}{\gamma}\begin{pmatrix}\sin\left(\frac{\pi}{2}\lambda-\theta_m\right)\left(-R_p(\omega)R_m(\omega)+I_p(\omega)I_m(\omega)\right)\\+\cos\left(\frac{\pi}{2}\lambda-\theta_m\right)\left(R_p(\omega)I_m(\omega)+I_p(\omega)R_m(\omega)\right)\end{pmatrix},$$

$$X_{Id} = \omega^{\lambda+\mu}\left(\cos\left(\frac{\pi}{2}\mu\right)I_p(\omega) + \sin\left(\frac{\pi}{2}\mu\right)R_p(\omega)\right)$$
$$-\frac{\omega^{\lambda+\mu}}{\gamma}\left(\sin\left(\frac{\pi}{2}\mu+\theta_m\right)\left(R_p(\omega)R_m(\omega)-I_p(\omega)I_m(\omega)\right)+\cos\left(\frac{\pi}{2}\mu+\theta_m\right)\left(R_p(\omega)I_m(\omega)+I_p(\omega)R_m(\omega)\right)\right),$$

$$Y_R = -\omega^{\lambda} + \frac{\omega^{\lambda}}{\gamma}\left(R_s(\omega)\cos\theta_s - I_s(\omega)\sin\theta_s\right), \text{ and}$$

$$Y_I = \frac{\omega^{\lambda}}{\gamma}\left(R_s(\omega)\sin\theta_s + I_s(\omega)\cos\theta_s\right).$$

As this is a three dimensional system in terms of the controller parameters K_p, K_i and K_d, one of the three parameters will be fixed to find the solution for the other two parameters in (157) and (158).

7.2.2 Solution in (K_p, K_i) Plane

In order to find the solution in the (K_p, K_i) plane, the value of K_d will be fixed. In matrix form, (157) and (158) are rearranged to deal with the two unknowns K_p and K_i as:

$$\begin{bmatrix} X_{Rp} & X_{Ri} \\ X_{Ip} & X_{Ii} \end{bmatrix}\begin{bmatrix} K_p \\ K_i \end{bmatrix} = \begin{bmatrix} Y_R - X_{Rd}K_d \\ Y_I - X_{Id}K_d \end{bmatrix} \tag{159}$$

Solving (159) for the non-singular case, K_p and K_i are given by

$$K_p = -K_d\omega^{\mu}\frac{\sin\left(\frac{\pi}{2}(\lambda+\mu)\right)}{\sin(\frac{\pi}{2}\lambda)} - \frac{R_p(\omega)\sin(\frac{\pi}{2}\lambda) - I_p(\omega)\cos(\frac{\pi}{2}\lambda)}{D\sin(\frac{\pi}{2}\lambda)}$$
$$-\frac{\left(A_1\cos(\frac{\pi}{2}\lambda-\theta_m) - A_2\sin(\frac{\pi}{2}\lambda-\theta_m) - A_3\cos(\frac{\pi}{2}\lambda+\theta_s) - A_4\sin(\frac{\pi}{2}\lambda+\theta_s)\right)}{D\gamma\sin(\frac{\pi}{2}\lambda)} \tag{160}$$
$$+\frac{\cos\left(\theta_s-\theta_m+\frac{\pi}{2}\lambda\right)\left(B_1+B_2\right) - \sin\left(\theta_s-\theta_m+\frac{\pi}{2}\lambda\right)\left(B_3+B_4\right)}{D\gamma^2\sin(\frac{\pi}{2}\lambda)}$$

$$K_i = K_d\omega^{\lambda+\mu}\frac{\sin(\frac{\pi}{2}\mu)}{\sin(\frac{\pi}{2}\lambda)} - \omega^{\lambda}\frac{I_p(\omega)}{D\sin(\frac{\pi}{2}\lambda)} + \frac{\omega^{\lambda}\left(A_1\cos\theta_m + A_2\sin\theta_m - A_3\cos\theta_s - A_4\sin\theta_s\right)}{D\gamma\sin(\frac{\pi}{2}\lambda)} - \frac{\omega^{\lambda}\left(\cos(\theta_s-\theta_m)(B_1+B_2) - \sin(\theta_s-\theta_m)(B_3+B_4)\right)}{D\gamma^2\sin(\frac{\pi}{2}\lambda)} \tag{161}$$

where

$$A_1 = R_p(\omega)I_m(\omega) + I_p(\omega)R_m(\omega), \qquad A_2 = R_p(\omega)R_m(\omega) - I_p(\omega)I_m(\omega),$$

$$A_3 = R_p(\omega)I_s(\omega) - I_p(\omega)R_s(\omega), \qquad A_4 = R_p(\omega)R_s(\omega) + I_p(\omega)I_s(\omega),$$

$$B_1 = R_p(\omega)\left(-R_m(\omega)I_s(\omega) + I_m(\omega)R_s(\omega)\right), \qquad B_2 = I_p(\omega)\left(R_m(\omega)R_s(\omega) + I_m(\omega)I_s(\omega)\right),$$

$$B_3 = R_p(\omega)\left(R_m(\omega)R_s(\omega) + I_m(\omega)I_s(\omega)\right), \qquad B_4 = I_p(\omega)\left(R_m(\omega)I_s(\omega) - I_m(\omega)R_s(\omega)\right),$$

$$D = \left|G_p(j\omega)\right|^2\left(1 + \frac{1}{\gamma^2}\left|W_m(j\omega)\right|^2 - \frac{2}{\gamma}\left(R_m(\omega)\cos\theta_m - I_m(\omega)\sin\theta_m\right)\right),$$

$$\left|G_p(j\omega)\right|^2 = {R_p}^2(\omega) + {I_p}^2(\omega), \text{ and } \left|W_m(j\omega)\right|^2 = {R_m}^2(\omega) + {I_m}^2(\omega).$$

Thus, all stabilizing FO PID controllers for a fixed K_d value that meet the robust performance constraint (147) can be plotted in a two-dimensional graph using (160) and (161) with K_p and K_i as the two Cartesian axes. If λ=μ=1, which is a conventional IO PID controller, the above results reduce to those presented in [29].

7.2.3 Solution in (K_p, K_d) Plane

Now, the value of K_i will be fixed to determine the solution in the (K_p, K_d) plane. Accordingly, (157) and (158) are rearranged as:

$$\begin{bmatrix} X_{Rp} & X_{Rd} \\ X_{Ip} & X_{Id} \end{bmatrix}\begin{bmatrix} K_p \\ K_d \end{bmatrix} = \begin{bmatrix} Y_R - X_{Ri}K_i \\ Y_I - X_{Ii}K_i \end{bmatrix} \tag{162}$$

Solving (162) for the non-singular case, K_p and K_d are given by

$$\begin{aligned} K_p = -K_i \frac{\sin\left(\frac{\pi}{2}(\lambda+\mu)\right)}{\omega^{\lambda}\sin(\frac{\pi}{2}\mu)} - \frac{R_p(\omega)\sin(\frac{\pi}{2}\mu)+I_p(\omega)\cos(\frac{\pi}{2}\mu)}{D\sin(\frac{\pi}{2}\mu)} \\ + \frac{\left(A_1\cos(\theta_m+\frac{\pi}{2}\mu)+A_2\sin(\theta_m+\frac{\pi}{2}\mu)-A_3\cos(\theta_s-\frac{\pi}{2}\mu)-A_4\sin(\theta_s-\frac{\pi}{2}\mu)\right)}{D\gamma\sin(\frac{\pi}{2}\mu)} \\ - \frac{\cos\left(\theta_m-\theta_s+\frac{\pi}{2}\mu\right)\left(B_1+B_2\right)+\sin\left(\theta_m-\theta_s+\frac{\pi}{2}\mu\right)\left(B_3+B_4\right)}{D\gamma^2\sin(\frac{\pi}{2}\mu)} \end{aligned} \tag{163}$$

$$\begin{aligned} K_d = K_i \frac{\sin(\frac{\pi}{2}\lambda)}{\omega^{\lambda+\mu}\sin(\frac{\pi}{2}\mu)} + \frac{I_p(\omega)}{D\omega^{\mu}\sin(\frac{\pi}{2}\mu)} - \frac{\left(A_1\cos\theta_m+A_2\sin\theta_m-A_3\cos\theta_s-A_4\sin\theta_s\right)}{D\gamma\omega^{\mu}\sin(\frac{\pi}{2}\mu)} \\ + \frac{\left(\cos\left(\theta_m-\theta_s\right)\left(B_1+B_2\right)+\sin\left(\theta_m-\theta_s\right)\left(B_3+B_4\right)\right)}{D\gamma^2\omega^{\mu}\sin(\frac{\pi}{2}\mu)} \end{aligned} \tag{164}$$

Again, all stabilizing FO PID controllers that satisfy the robust performance condition (147) can be found for a fixed K_i value in the (K_p, K_d) plane. If λ=μ=1, which is a conventional IO PID controller, the above results reduce to those presented in [29].

7.2.4 Solution in (K_i, K_d) Plane

Lastly, the (K_i, K_d) plane solution will be determined by fixing the value of K_p. Thus, (157) and (158) can be written as:

$$\begin{bmatrix} X_{Ri} & X_{Rd} \\ X_{Ii} & X_{Id} \end{bmatrix}\begin{bmatrix} K_i \\ K_d \end{bmatrix} = \begin{bmatrix} Y_R - X_{Rp}K_p \\ Y_I - X_{Ip}K_p \end{bmatrix} \tag{165}$$

Solving (165) for the non-singular case, K_i and K_d are given by

$$K_i = -K_p\omega^\lambda \frac{\sin(\frac{\pi}{2}\mu)}{\sin\left(\frac{\pi}{2}(\lambda+\mu)\right)} - \frac{\omega^\lambda\left(R_p(\omega)\sin(\frac{\pi}{2}\mu)+I_p(\omega)\cos(\frac{\pi}{2}\mu)\right)}{D\sin\left(\frac{\pi}{2}(\lambda+\mu)\right)}$$
$$+\frac{\omega^\lambda\begin{pmatrix}A_1\cos(\theta_m+\frac{\pi}{2}\mu)+A_2\sin(\theta_m+\frac{\pi}{2}\mu)\\-A_3\cos(\theta_s-\frac{\pi}{2}\mu)-A_4\sin(\theta_s-\frac{\pi}{2}\mu)\end{pmatrix}}{D\gamma\sin\left(\frac{\pi}{2}(\lambda+\mu)\right)} - \frac{\omega^\lambda\begin{pmatrix}\cos\left(\theta_m-\theta_s+\frac{\pi}{2}\mu\right)(B_1+B_2)\\+\sin\left(\theta_m-\theta_s+\frac{\pi}{2}\mu\right)(B_3+B_4)\end{pmatrix}}{D\gamma^2\sin\left(\frac{\pi}{2}(\lambda+\mu)\right)} \quad (166)$$

$$K_d = -\frac{K_p\sin(\frac{\pi}{2}\lambda)}{\omega^\mu\sin\left(\frac{\pi}{2}(\lambda+\mu)\right)} - \frac{R_p(\omega)\sin(\frac{\pi}{2}\lambda)-I_p(\omega)\cos(\frac{\pi}{2}\lambda)}{D\omega^\mu\sin\left(\frac{\pi}{2}(\lambda+\mu)\right)}$$
$$-\frac{\begin{pmatrix}A_1\cos(\theta_m-\frac{\pi}{2}\lambda)+A_2\sin(\theta_m-\frac{\pi}{2}\lambda)\\-A_3\cos(\frac{\pi}{2}\lambda+\theta_s)-A_4\sin(\frac{\pi}{2}\lambda+\theta_s)\end{pmatrix}}{D\gamma\omega^\mu\sin\left(\frac{\pi}{2}(\lambda+\mu)\right)} + \frac{\begin{pmatrix}\cos\left(\theta_m-\theta_s-\frac{\pi}{2}\lambda\right)(B_1+B_2)\\+\sin\left(\theta_m-\theta_s-\frac{\pi}{2}\lambda\right)(B_3+B_4)\end{pmatrix}}{D\gamma^2\omega^\mu\sin\left(\frac{\pi}{2}(\lambda+\mu)\right)} \quad (167)$$

Likewise, all stabilizing FO PID controllers that meet the robust performance constraint (147) for a fixed K_p value can be determined in the (K_i, K_d) plane using (166) and (167) with K_i and K_d as the two Cartesian axes. For λ=μ=1, the above results reduce to those presented in [29] for the conventional IO PID controller.

It should be noted that all the derivations in this section are based on the frequency response of a system. As a consequence, the controller parameters K_p, K_i, and K_d of the FO PID controllers that not only stabilize a given system but also meet a robust performance constraint can be determined directly from an experimental frequency response if the system transfer function or system parameters are unknown. While the solution was derived in each plane for a fixed value of a third parameter, a complete solution can be constructed by varying the third

parameter for a specified range.

7.3 Example

7.3.1 Problem Formulation

Now, a numerical example will be given to illustrate the application of the results derived in Section II. In order to compare results, we will use the example in [29], in which all IO PID controllers that stabilize the closed-system and satisfy a robust performance constraint were found. The feedback loop now has an unknown time delay of between 0 and 1 second. The nominal model of the system was given by

$$G_{pn}(s) = \frac{-0.5s + 1}{(2s+1)(s+1)} e^{-\tau s} \tag{168}$$

where τ, representing a time delay, was selected to be the mean of the delay, or 0.5 seconds.

The objective of this example is to find all the values of the parameters K_p, K_i and K_d of the FO PID controller (146) that stabilizes the closed-loop system shown in Fig. 24 with the nominal plant (168) and simultaneously satisfies the robust performance constraint (147) where γ=1. As the goal is to find all the parameters K_p, K_i and K_d of the FO PID controller (146) with respect to arbitrary values of the fractional orders λ and μ, a non-optimal FO PID controller was chosen to have λ=0.98 and μ=0.25. Thus, the FO PID controller used is given by

$$G_c(s) = K_p + \frac{K_i}{s^{0.98}} + K_d s^{0.25} \tag{169}$$

Using the method described in [31], the multiplicative weight, $W_m(s)$, was chosen as

$$W_m(s) = \frac{s}{0.3571s + 1.9} \tag{170}$$

to bound the multiplicative errors resulting from the unknown time delay of 0 to 1 second. In addition, the closed-loop system shown in Fig. 24 is required to meet a settling time of 40

seconds, a percent overshoot of 5%, and a steady-state error less than or equal to 1%. Thus, the sensitivity function weight, $W_s(s)$, was determined in accordance with the method in [31] to meet such performance specifications as:

$$W_s(s) = \frac{0.780(s + 0.1314)}{(s + 0.001025)} \tag{171}$$

7.3.2 Robust Performance Region in (K_p, K_i) Plane

In order to find the robust performance region in the (K_p, K_i) plane for the plant transfer function (168) and the FO PID controller transfer function (169), (160) and (161) were used with a fixed value K_d=0.4 when γ=1. All FO PID controllers that satisfy the robust performance condition defined by (147) can be determined by finding an intersection of all the solutions to (160) and (161) for $\theta_s \in [0, 2\pi)$ and $\theta_m \in [0, 2\pi)$ in a given range of frequency ω. Such an intersection lies on or within the boundary set by (154) for $\theta_s \in [0, 2\pi)$ and $\theta_m \in [0, 2\pi)$, thereby constituting a true solution to the robust performance constraint (147). The corresponding nominal stability region can be obtained by setting γ=∞ in (160) and (161), which is the same as that given in [32].

Fig. 25 shows the nominal stability boundaries of the FO PID controller (169) and the IO PID controller for K_d=0.4, respectively. Fig. 26 and Fig. 27 show the robust performance regions of the FO PID controller (169) and the IO PID controller in the (K_p, K_i) plane, respectively.

As can be seen from Fig. 25, both the IO and FO PID controllers provide a large nominal stability region in the (K_p, K_i) plane for K_d=0.4. However, whereas the FO PID controller (169) provides a decent robust performance region in the (K_p, K_i) plane, the IO PID controller does not provide any robust performance region at all. The robust performance region represents all the possible values of K_p and K_i of the FO PID controller (169) for K_d=0.4 that stabilizes the closed-loop system with the nominal plant transfer function (168) and simultaneously satisfy the robust performance condition (147). In particular, the FO PID controller with these parameter values along with the fixed value K_d=0.4 makes the closed-loop system stable for the time delay of the range of 0 to 1 second as well as satisfies the performance specifications of a settling time, a percent overshoot, and a steady state error as mentioned at the beginning of the example.

Accordingly, the IO PID controller is not a plausible choice in this specific example with the time delay uncertainty and performance specifications.

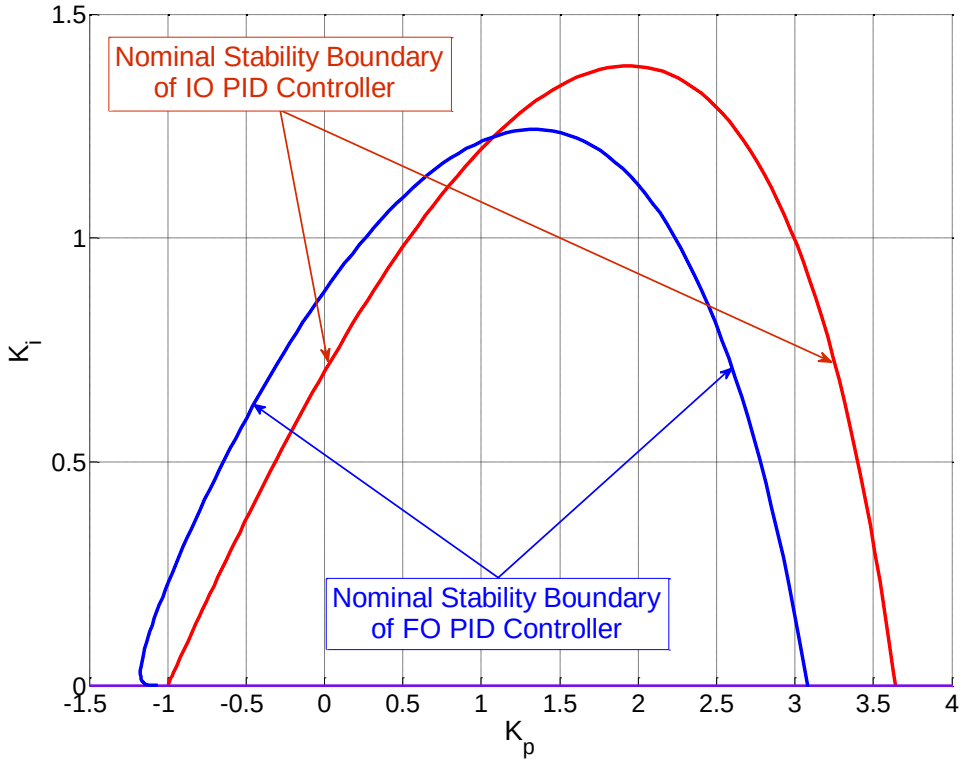

Fig. 25. Nominal stability boundaries of the FO and IO PID controllers in (K_p, K_i) plane for K_d=0.4.

To verify that FO PID controllers lying in such an intersection truly meet the robust performance constraint (147) and the performance specifications, an arbitrary controller was chosen from the robust performance region of the FO PID controller in Fig. 26, which is K_p= 0.0345 and K_i=0.1274, as marked on the plot. Therefore, the chosen FO PID controller is

$$G_{cFO}(s) = 0.0345 + \frac{0.1274}{s^{0.98}} + 0.4s^{0.25} \tag{172}$$

Fig. 28 shows $|W_s(j\omega)S(j\omega)| + |W_m(j\omega)T(j\omega)|$ and illustrates that $\max_{\omega}(|W_s(j\omega)S(j\omega)| + |W_m(j\omega)T(j\omega)|)$ is equal to 0.997, which is less than γ=1. Fig. 29 shows

the corresponding closed-loop step responses with the FO PID controller (172) for the time delays $\tau = 0$, 0.5, and 1 second. Even for the worst case with $\tau = 1$ second, the closed-loop system has a percent overshoot of P.O=3.13%, a 2% settling time of t_s=25.3 seconds, and a zero steady-state error, all of which meet the performance requirements. In other words, the closed-loop system satisfies all the performance specifications for the complete range of the time delay. To generate the closed-loop step response with the FO PID controller (172), the FO PID controller transfer function was approximated using the fractional power pole (FPP) and fractional power zero (FPZ) methods in [34] and [35], respectively.

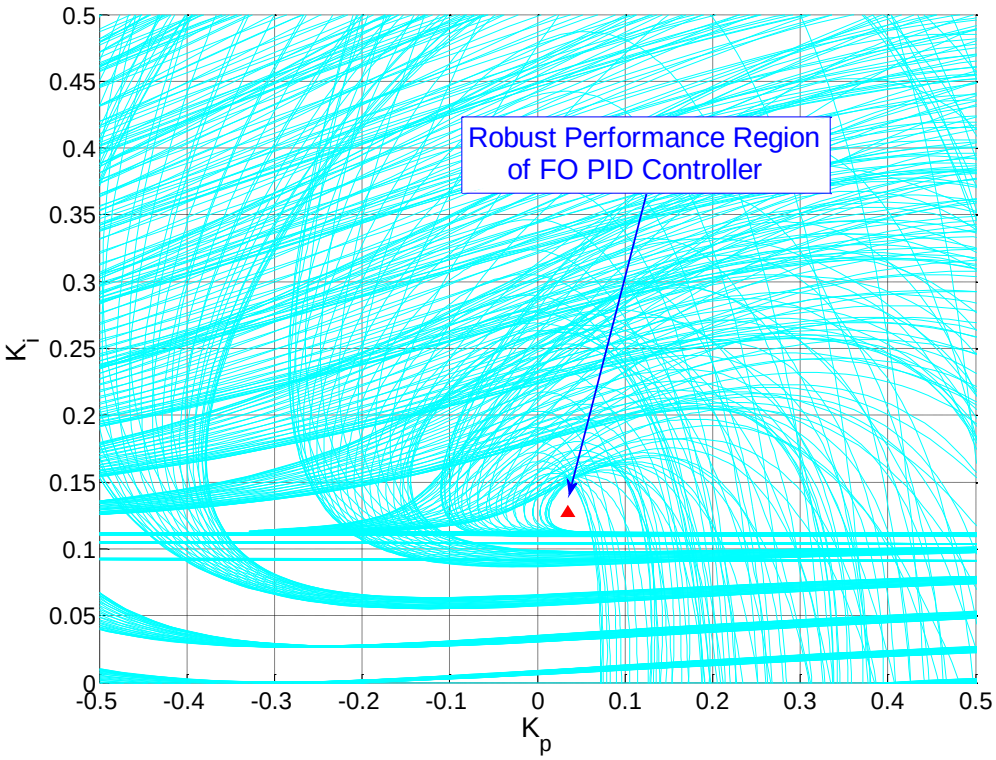

Fig. 26. Robust performance region in (K_p, K_i) plane for the FO PID controller (169) with K_d=0.4.

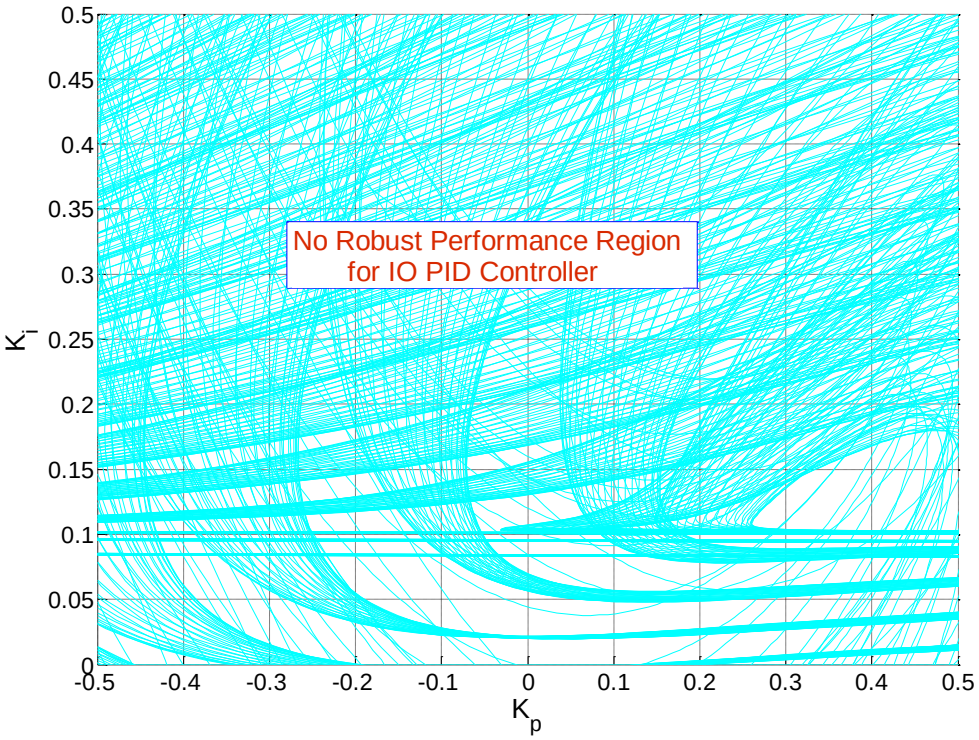

Fig. 27. Robust performance region in (K_p, K_i) plane for the IO PID controller with K_d=0.4.

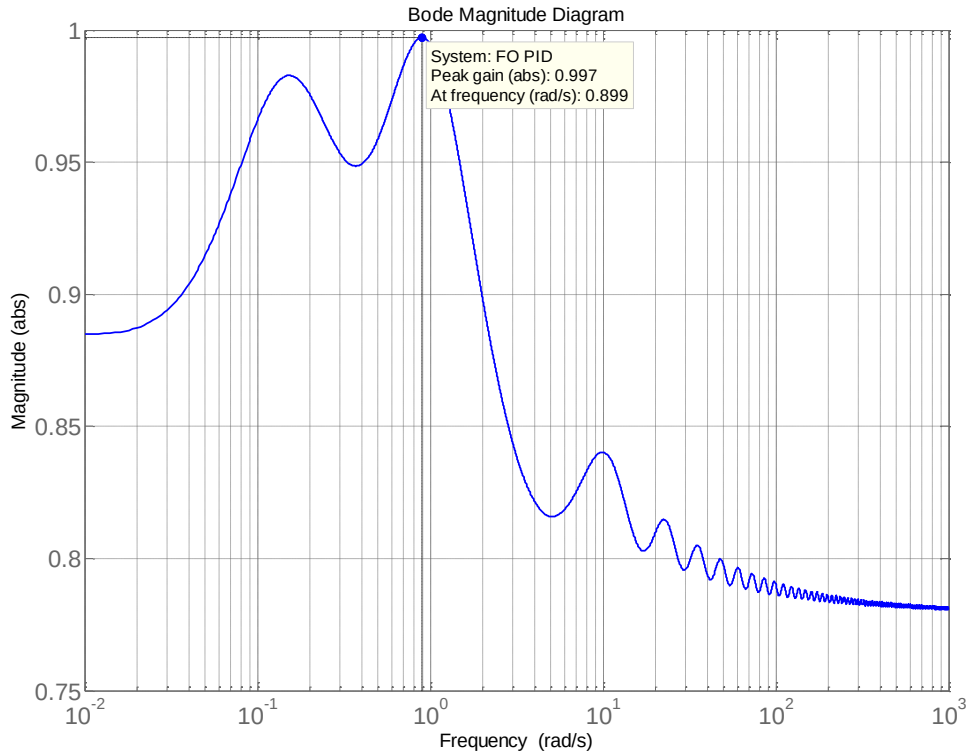

Fig. 28. $\left|W_s(j\omega)S(j\omega)\right|+\left|W_m(j\omega)T(j\omega)\right|$ with the FO PID controller in (172).

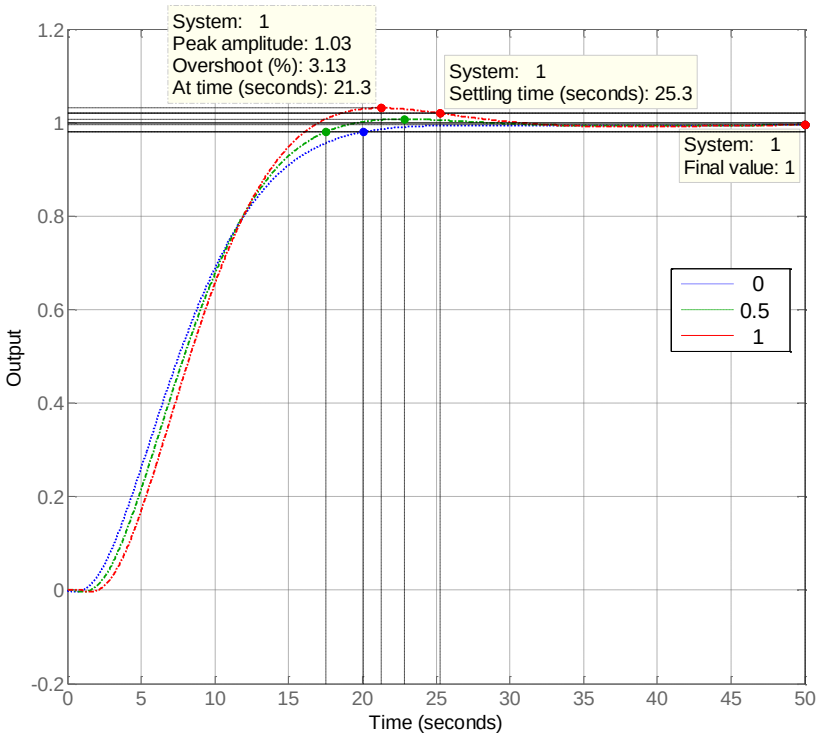

Fig. 29. Closed-loop step responses with the FO PID controller in (172) for the time delays $\tau = 0,\ 0.5,$ and 1second.

7.3.3 Robust Performance Region in (K_i, K_d) Plane

Similarly, the nominal stability boundary and the robust performance region in the (K_i, K_d) plane for the FO PID controller (169) with a fixed value K_p=0.04 were determined by using (166) and (167). As previously, an intersection of all the solutions to (166) and (167) for $\theta_s \in [0, 2\pi)$ and $\theta_m \in [0, 2\pi)$ in a given range of frequency ω is the robust performance region and the corresponding nominal stability boundary was obtained by taking γ=∞ in (166) and (167).

Figs. 30 and 31 show the nominal stability boundary and the robust performance region of the FO PID controller (169) in the (K_i, K_d) plane for K_p=0.04, respectively. To verify that FO PID controllers in such an intersection meet the robust performance constraint (147), an arbitrary controller was chosen from the robust performance region of the FO PID controller in Fig. 31, which is K_i=0.1255 and K_d=0.3887, as marked on the plot. Thus, the chosen FO PID controller is

$$G_{cFO}(s) = 0.04 + \frac{0.1255}{s^{0.98}} + 0.3887 s^{0.25} \tag{173}$$

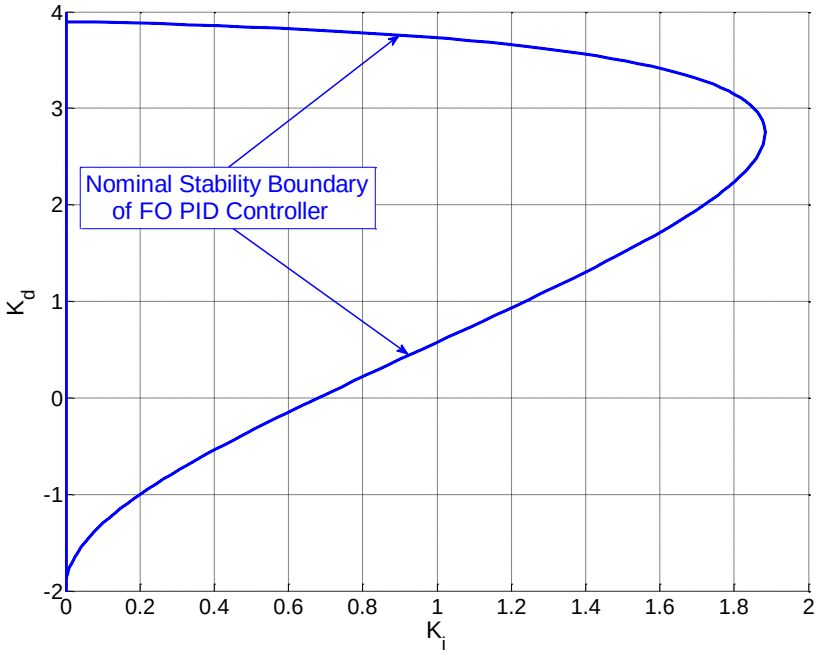

Fig. 30. Nominal stability boundary in the (K_i, K_d) plane for the FO PID controller (169) with K_p=0.04.

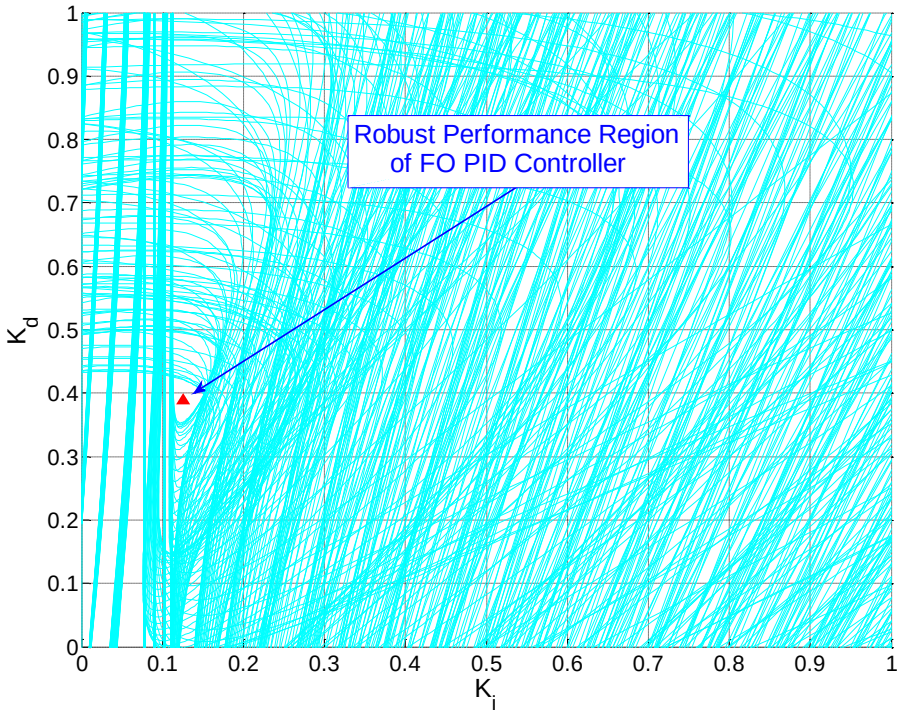

Fig. 31. Robust performance region in (K_i, K_d) plane for the FO PID controller (169) with K_p=0.04.

Fig. 32 shows the corresponding closed-loop step responses with the FO PID controller (173) for the time delays $\tau = 0$, 0.5, and 1 second. As can be seen, all the performance specifications are met for the complete range of the time delay including the worst case with $\tau = 1$ second, which has a percent overshoot of P.O=2.49%, a 2% settling time of t_s=24.4 seconds, and a zero steady-state error.

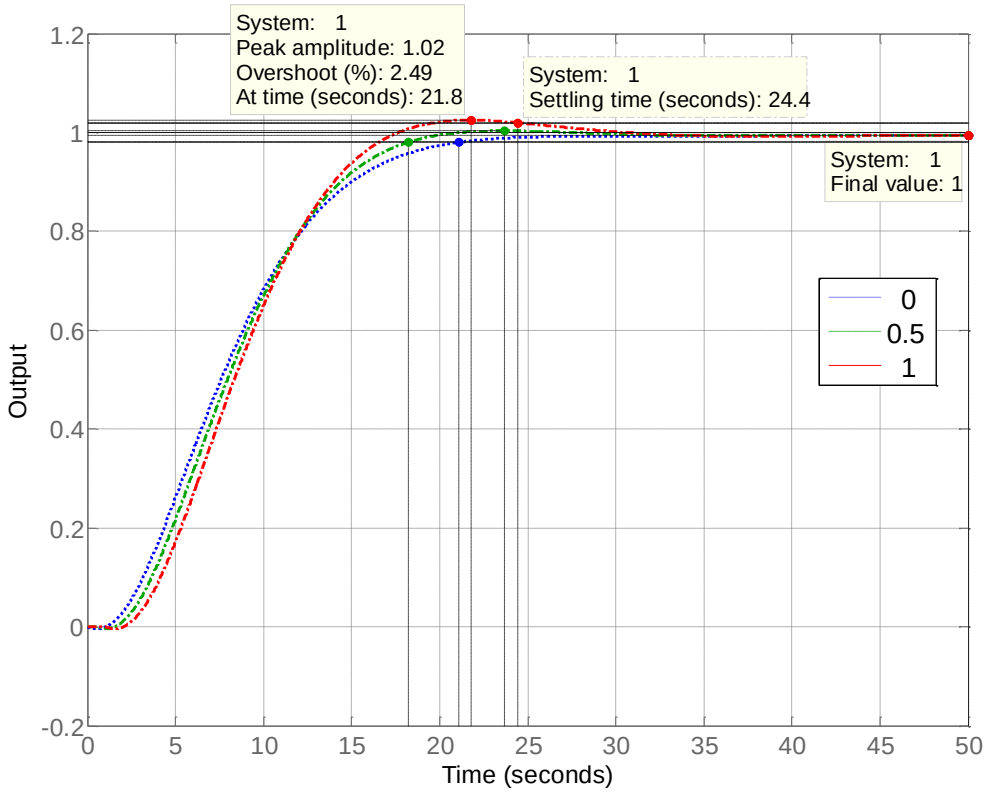

Fig. 32. Closed-loop step response with the FO PID controller in (173) for the time delays $\tau = 0,\ 0.5,$ and 1 second.

7.4 Conclusion

As described in Sections 7.2 and 7.3, a method has been presented for determining all FO PID controllers that not only stabilize a given system with a time delay but also meet a robust performance condition. In particular, FO PID controllers have been designed so that the closed-loop system including the FO PID controller is robustly stable for a time delay uncertainty and meets desired performance specifications, such as a settling time, percent overshoot, and steady state error. As can be seen from the results of the example in Section III, even when there is no

IO PID controller available that satisfies a given robust performance constraint in some cases, FO PID controllers may be able to provide a decent range of solutions. In addition, since the results have been derived based on the frequency response of a system, this method can be applied even when a system transfer function is not available.

CHAPTER 8
WEIGHTED SENSITIVITY DESIGN OF PID CONTROLLERS APPLIED TO A DC MOTOR

8.1 Introduction

As described in Chapters 4 through 7, the methods presented in this dissertation utilize the frequency response of a physical apparatus without relying on the knowledge of the system transfer function. In order to provide applicability and usefulness of the techniques presented in the previous chapters, this chapter provides an example of FO PID controller design with a weighted sensitivity constraint applied to a direct current (DC) motor. In particular, the results set forth in Chapter 5 will be used with the frequency response data directly acquired through experiments on a DC motor. An SRV-02 DC motor from *Quanser Consulting, Inc*. will be used because of a long-time experimental setup in the Department of Electrical Engineering and Computer Science at Wichita State University and versatility and flexibility of its implementation. The Quanser SRV-02 DC motor supports the real-time design and implementation of various control schemes using Matlab and Simulink tools [38].

Therefore, it is the objective of this chapter to find all the numerical values of the parameters K_p, K_i and K_d of FO PID controllers that stabilize a given system and simultaneously meet an H_∞ weighted sensitivity constraint, using measured frequency response of the DC motor without knowing its transfer function. Such parameters K_p, K_i and K_d of FO PID controllers will be determined with respect to arbitrary values of the fractional orders (λ and μ). A single-input single-output (SISO) system is considered, with the motor input voltage as the input and the load shaft position as the output. Detailed experiment setups, measurement of frequency response, and results follow.

8.2 Frequency Response Measurement of SRV-02 DC Motor

8.2.1 Experimental Setup

Consider the closed-loop system shown in Fig. 8 in Chapter 5. In this experiment, the plant is the SRV-02 DC motor system [38] as shown in Fig. 33 below. Note that the SRV-02 DC motor system has low and high-gear configurations as shown in Fig. 34 and that the latter will be used in the experiment. Emami and Watkins used the SRV-02 DC motor in the high-gear

configuration to design a discrete-time PID controller to regulate its shaft position in [39]. Fig. 35 shows complete connections of the hardware components, the SRV-02 motor, Quanser VoltPAQ-X2 (dual-channel power amplifier), Quanser Q8-USB (data acquisition board), and analog sensors adapter.

Fig. 33. Quanser SRV-02 DC motor system.

Fig. 34. Low and high-gear configurations of Quanser SRV-02 DC motor system.

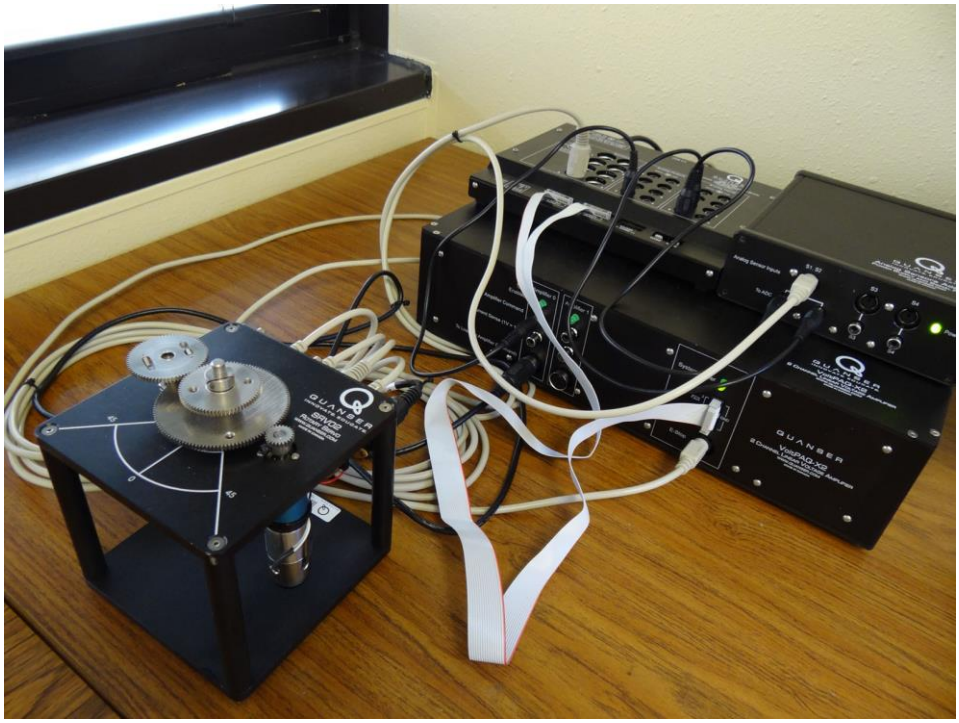

Fig. 35. Hardware connections between SRV-02, amplifier, and data acquisition board.

Fig. 36 shows the Simulink diagram used to conduct the experiments. Inside the *SRV02-ET Position* subsystem, the *SRV02-ET* subsystem contains QUARC® blocks that interface with the DC motor and sensors in the SRV-02 system. The power amplifier is used to drive the motor and the encoder is used to measure the angular position of the load shaft (rad).

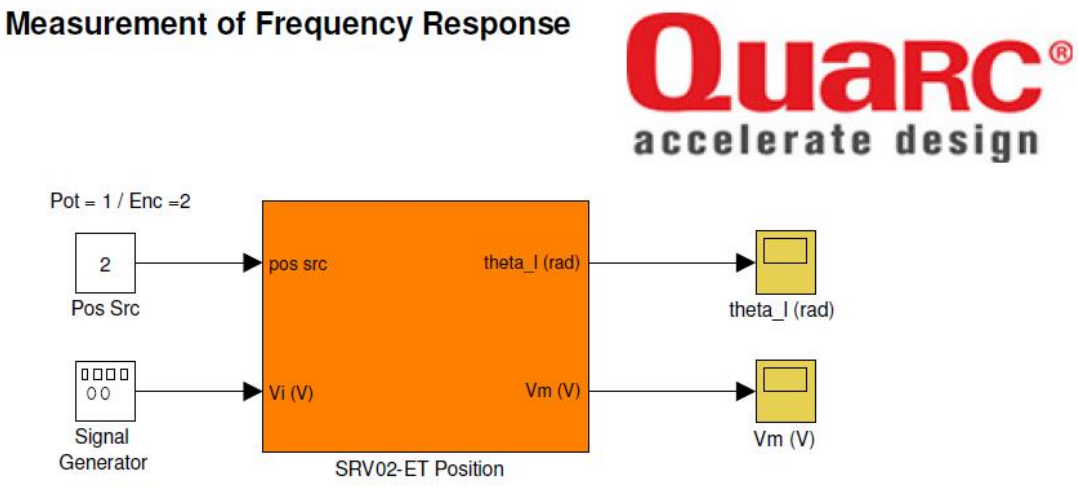

Fig. 36. Simulink model with QUARC® and SRV-02 ET Position block.

8.2.2 Measurement of Frequency Response

In this experiment, the frequency response of the load shaft of the SRV-02 DC motor was measured. The measured frequency response will be used instead of the transfer function to design the controller to regulate the load shaft position of the DC motor in the high-gear configuration. In other words, the technique described in Chapter 5 is applied to the DC motor to find all the possible FO PID controllers that satisfy desired performance specifications using the measured frequency response without the knowledge of the transfer function. As mentioned previously, the encoder was selected in the *Pos Src* source block in Fig. 36 as the sensor to measure the angular position of the load shaft.

The frequency response of the DC motor was obtained by providing a sine wave input signal to the motor and measuring the output sine wave from it. The amplitude of the input sine wave provided by *Signal Generator* block was kept constant at 1 but its frequency was varied. For each frequency point, the amplitude and the peak time of the output sine wave were recorded.

Table 1 shows the amplitude and peak time of the output signal and the peak time of the input signal for frequency points between 0.01 to 100 radians/second. As the input signal has an amplitude of 1, the Bode magnitude plot can be drawn directly from the frequency and the output signal amplitude. The phase (in degrees) was calculated for each frequency by taking the difference in peak time between the input and output signals and multiplying it by a corresponding frequency. Table 2 shows the calculated magnitude in both absolute value and in dB and phase in degrees versus frequency. Then, the data in Table 2 was loaded in MATLAB to store as frequency-response data (FRD) format. Thus, the experimental frequency response of the SRV-02 DC motor was obtained as shown in Fig. 37.

TABLE 1

MEASURED AMPLITUDE AND PEAK TIME OF OUTPUT SIGNAL AND INPUT SIGNAL PEAK TIME VERSUS FREQUENCY

Frequency (rad/s)	Amplitude (Output Signal)	Peak Time (Input Signal)	Peak Time (Output Signal)
0.01	510.049	785.25	944
0.02	256.417	392.5	471.9
0.03	171.0418	261.8	314.8
0.04	127.706905	196.22	235.98
0.05	102.37555	157.02	188.84
0.06	85.5228	130.8	157.32
0.08	63.737585	98.1	118
0.09	57.11085	87.2	104.9
0.1	51.3435	78.54	94.48
0.2	25.588095	39.24	47.22
0.3	17.028095	26.16	31.49
0.4	12.80531	19.62	23.62
0.5	10.231932	15.705	18.91
0.6	8.51273	13.09	15.765
0.8	6.413555	9.82	11.83
0.9	5.698835	8.726	10.516
1	5.129233	7.8525	9.464
2	2.563233	3.928	4.752
3	1.70587	2.62	3.174
4	1.27487	1.964	2.386
5	1.019568	1.571	1.916
6	0.841602	1.31	1.604
7	0.721835	1.122	1.377
8	0.629835	0.982	1.208
9	0.552405	0.874	1.077
10	0.496233	0.786	0.973
20	0.222415	0.393	0.499
30	0.131925	0.262	0.339
40	0.08591	0.3535	0.415
50	0.059825	0.283	0.334
60	0.044475	0.236	0.2805
70	0.034495	0.202	0.241
80	0.02838	0.1772	0.212
90	0.02301	0.15702	0.1885
100	0.018405	0.1412	0.17

TABLE 2

CALCULATED MAGNITUDE AND PHASE

Frequency (rad/s)	Magnitude (abs)	Magnitude (dB)	Phase (Degree)
0.01	510.049	54.1522	-90.9570689
0.02	256.417	48.1789	-90.9857168
0.03	171.0418	44.662	-91.10030838
0.04	127.706905	42.1243	-91.1232267
0.05	102.37555	40.2039	-91.15760417
0.06	85.5228	38.6416	-91.16906333
0.08	63.737585	36.0879	-91.21489996
0.09	57.11085	35.1344	-91.27219575
0.1	51.3435	34.2097	-91.32949154
0.2	25.588095	28.1608	-91.44408313
0.3	17.028095	24.6233	-91.6159705
0.4	12.80531	22.1478	-91.67326629
0.5	10.231932	20.1992	-91.81650577
0.6	8.51273	18.6014	-91.95974525
0.8	6.413555	16.142	-92.13163262
0.9	5.698835	15.1157	-92.30352
1	5.129233	14.201	-92.33216789
2	2.563233	8.1758	-94.42346428
3	1.70587	4.6389	-95.22560536
4	1.27487	2.1093	-96.71529594
5	1.019568	0.1683	-98.83524022
6	0.841602	-1.4979	-101.0697761
7	0.721835	-2.8312	-102.2729877
8	0.629835	-4.0155	-103.5907909
9	0.552405	-5.1548	-104.6794109
10	0.496233	-6.0863	-107.14313
20	0.222415	-13.0567	-121.4670778
30	0.131925	-17.5935	-132.3532782
40	0.08591	-21.3191	-140.9476469
50	0.059825	-24.4623	-146.1042682
60	0.044475	-27.0377	-152.9797631
70	0.034495	-29.2449	-156.4175106
80	0.02838	-30.9398	-159.5114833
90	0.02301	-32.7617	-162.3304363
100	0.018405	-34.7013	-165.0118793

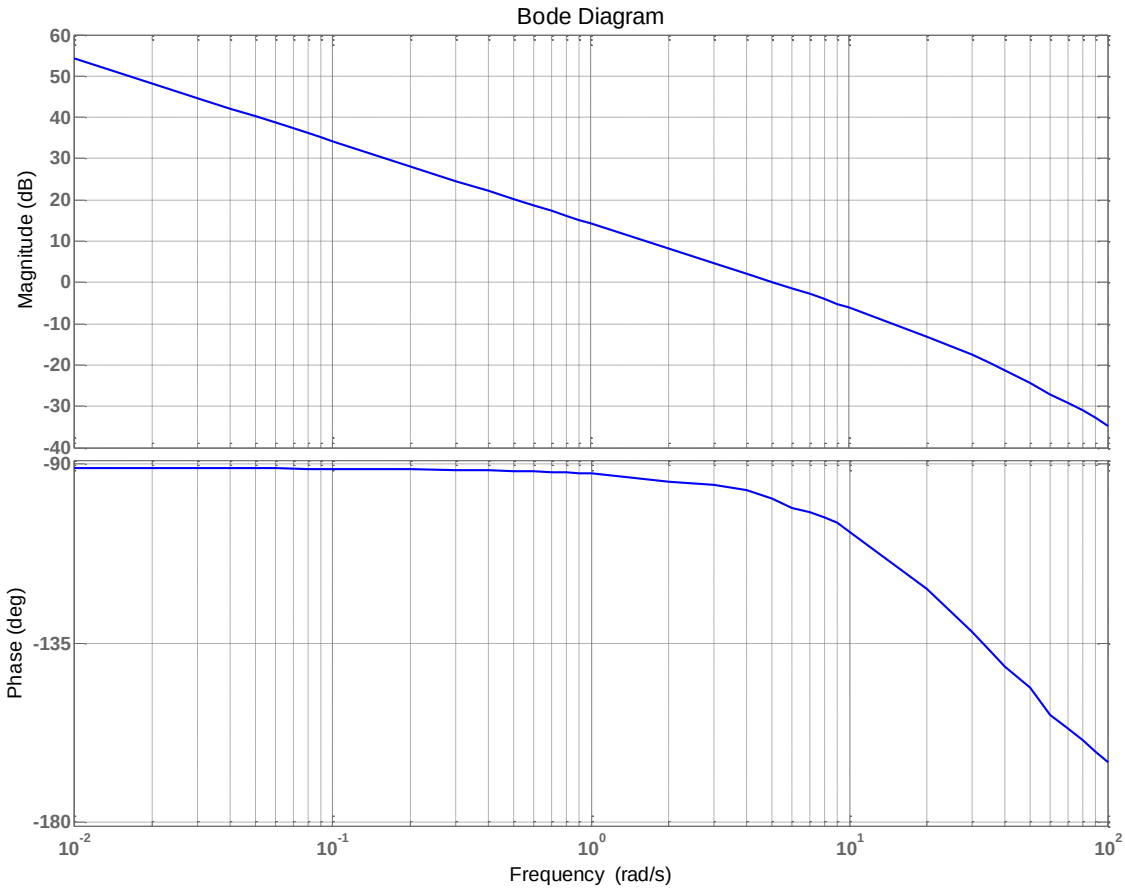

Fig. 37. Experimental frequency response of the SRV-02 DC motor.

8.3 FO PID Controller Design with a Weighted Sensitivity Constraint for a DC Motor

8.3.1 Problem Formulation

The objective of this example is to find all parameters K_p, K_i and K_d of an FO PID controller that stabilize the DC motor represented by the Bode diagram in Fig. 37 and simultaneously satisfy the weighted sensitivity constraint (80) where $\gamma = 1$. In particular, there is no direct knowledge of the transfer function of the DC motor except the measured frequency response thereof. In consideration of practical applicability, an FO PI controller was selected by setting the derivative gain, K_d, equal to zero. As the goal is to find all the parameters K_p and K_i of the FO PI controller with respect to arbitrary values of the fractional order λ, a non-optimal FO PI controller was chosen to have λ=0.2. Thus, the FO PI controller used is given by

$$G_c(s) = K_p + \frac{K_i}{s^{0.2}} \tag{174}$$

In addition, the closed-loop system shown in Fig. 8 is required to meet performance specifications of a settling time of 2 seconds, a percent overshoot of 15%, and a steady-state error less than or equal to 1%. For such performance requirements, the method described in [31] leads to the following sensitivity function weight $W_s(s)$:

$$W_s(s) = \frac{0.69224(s + 3.952)}{(s + 0.02736)} \tag{175}$$

8.3.2 Weighted Sensitivity Region in (K_p, K_i) Plane

In order to find the weighted sensitivity region in the (K_p, K_i) plane for the DC motor with the FO PI controller transfer function (174), (92) and (93) were used with K_d=0 when $\gamma = 1$. As discussed in Chapter 5, all the possible values of the parameters K_p and K_i of the FO PI controller (174) that satisfy the weighted sensitivity constraint (80) can be determined by finding an intersection of all the solutions to (92) and (93) for $\theta_s \in [0, 2\pi)$ in a given range of frequency ω. The corresponding nominal stability region can be obtained by taking $\gamma = \infty$ in (92) and (93).

In Fig. 38, the weighted sensitivity region and the nominal stability boundary of the FO PI controller (174) are shown in the (K_p, K_i) plane. While the nominal stability boundary represents the region for the possible values of K_p and K_i to stabilize the DC motor for K_d=0 in this case, the weighted sensitivity region represents all the possible values of K_p and K_i that not only stabilize the DC motor but also satisfy the weighted sensitivity constraint (80) to meet the performance specifications.

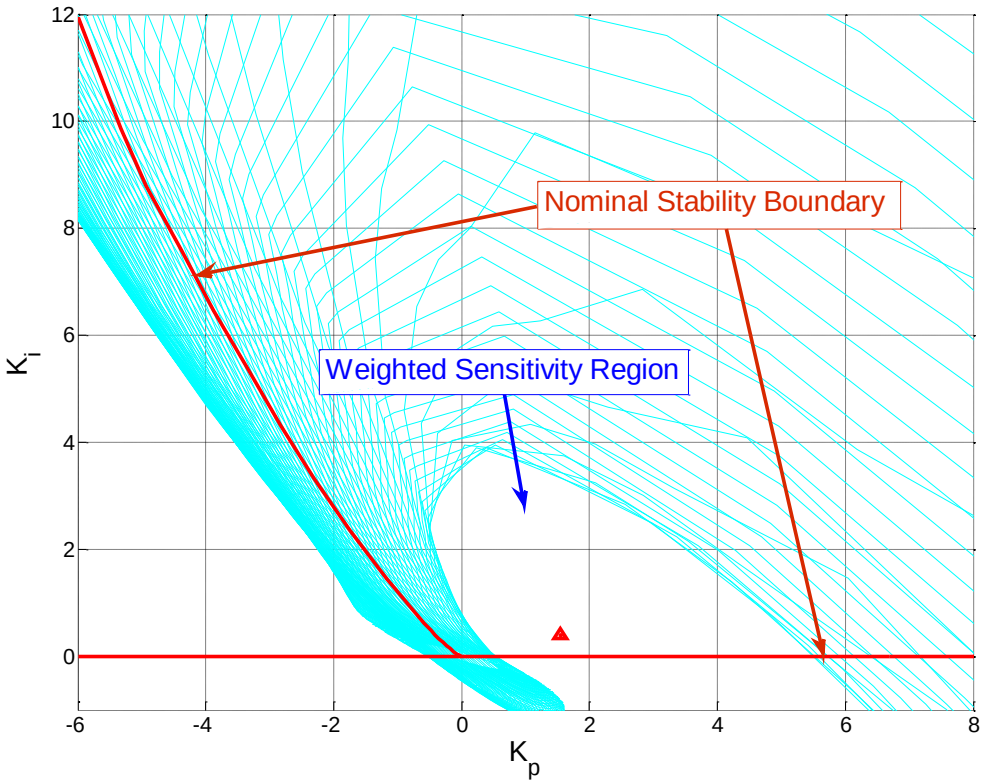

Fig. 38. Nominal stability boundary and weighted sensitivity region in (K_p, K_i) plane for the FO PI controller in (174).

To verify that FO PI controllers lying in the weighted sensitivity region meet the weighted sensitivity constraint (80), an arbitrary controller was chosen from the weighted sensitivity region of the FO PI controller in Fig. 38, which is K_p= 1.55 and K_i= 0.41, as marked on the plot. Therefore, the chosen FO PI controller is

$$G_{cFO}(s) = 1.55 + \frac{0.41}{s^{0.2}} \tag{176}$$

Fig. 39 shows $\left|W_S(j\omega)S(j\omega)\right|$ with the FO PI controller in (176) and illustrates that $\left\|W_S(j\omega)S(j\omega)\right\|_\infty$ is equal to 0.833, which is of course less than $\gamma = 1$. Thus, the weighted sensitivity constraint is met.

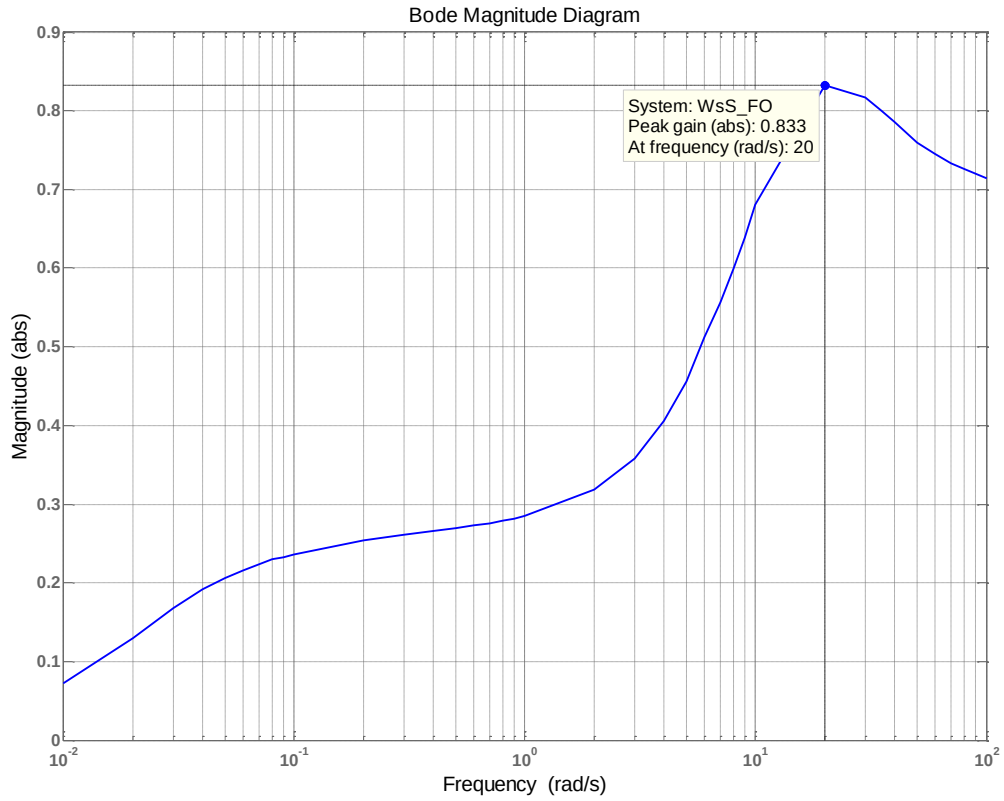

Fig. 39. $\left|W_S(j\omega)S(j\omega)\right|$ with the FO PI controller in (176).

8.4 Implementation of the FO PI Controller on the Quanser SRV-02 DC Motor

8.4.1 Experimental Setup

After designing the FO PI controller (176) for the weighted sensitivity constraint of the closed-loop system containing the Quanser SRV-02 DC Motor, the FO PI controller was implemented on the DC motor to regulate the angular position of the load shaft. The objective of this experiment is to observe the closed-loop position control of the DC motor load shaft for practical applicability. Accordingly, the step response of the closed-loop system was measured for the SRV-02 hardware equipment using the FO PI controller (176).

Before conducting the experiments, the Matlab setup script file was configured according to the SRV-02 DC motor setup, such as for low or high gear configuration, load type, sensor and amplifier types, etc [38]. In the experiment, the settings are as follows: high-gear configuration, no load, encoder as the sensor, and VoltPAQ as the power amplifier.

Fig. 40 shows the Simulink diagram used to implement the closed-loop step response of the DC motor with respect to the angular position of load shaft, using the FO PI controller (176).

As described in Section 8.3.1, the *SRV02-ET Position* subsystem contains QUARC® blocks that interface with the DC motor and sensors in the SRV-02 system. In the Simulink model, the *HIL Initialize* block in the *SRV02-ET* subsystem (which is under the *SRV02-ET Position* subsystem) was configured to have *q8-usb* for the DAQ device board type. The encoder was selected through the *Pos Src* source block as the sensor to measure the angular position of the load shaft.

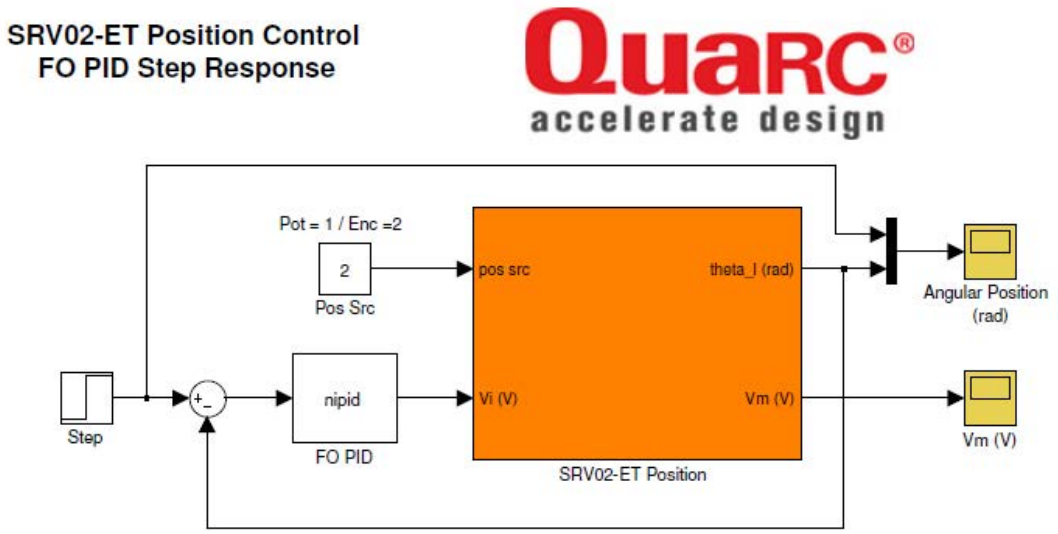

Fig. 40. Simulink model with *FO PID* and *SRV02- ET Position* blocks.

The *Fractional PID* block (the name was changed to *FO PID* block in this experiment for the sake of clarity as shown in Fig. 40) found in a Simulink library called *nintblocks* was used for the implementation of the FO PI controller (176). The *nintblocks* library which also includes *Fractional derivative* block is part of *Ninteger* toolbox in Matlab [40]. The *Ninteger* toolbox is used to implement FO PID controllers and to assess their performance in both the frequency and time domain and may be freely distributed and downloaded from the Internet. Fig. 41 shows *Fractional PID* block parameters window, in which:

- Kp is the proportional gain,
- Kd is the derivative gain,
- vd is the fractional derivative order,
- ki is the integral gain,
- vi is the fractional integral order, and
- n is the number of zeros and poles of the approximation.

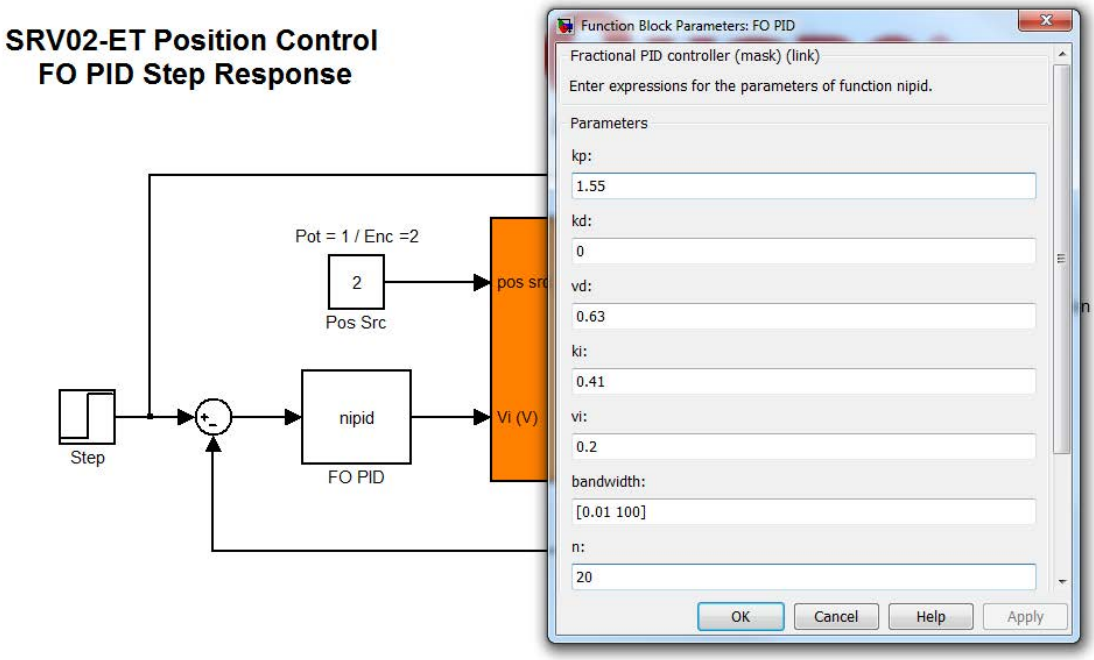

Fig. 41. *Fractional PID* block parameters window.

For FO PI controller (176) implementation, the parameters were set as follows: kp = 1.55, kd = 0, vd = 0.63 (this value does not affect at all because kd is zero), ki = 0.41, vi = 0.2, frequency band [0.01, 100] rad/s, and n=20 as can be seen from Fig. 42. The *Crone* (*Commande robuste d'ordere non-entier*) method was selected in the *FO PID* block to approximate the FO PI controller to have 20 poles and zeros in the approximation within the frequency range [0.01, 100] rad/s.

8.4.2 Step Response of the DC Motor with the FO PI controller

A step reference signal was set with the amplitude of 1 at the step time of 1 second. Then, the Simulink diagram was compiled by clicking *build* in the Quarc pull-down menu, and the experiment began by clicking *start* in the Quarc menu. Fig. 42 shows the step response of the DC motor in relation to the load shaft position (rad) with the FO PI controller (176). As can be seen from Fig. 42, the DC motor shows a 2% settling time (T_s) of 0.255 seconds (the step signal was applied at 1 second) with no overshoot. In light of the performance specifications (T_s = 2 seconds, $\%OS$ = 15%, and e_{ss} (steady-state error) ≤ 1%) mentioned in Section 8.3.1, the FO PI controller (176) can be used satisfactorily.

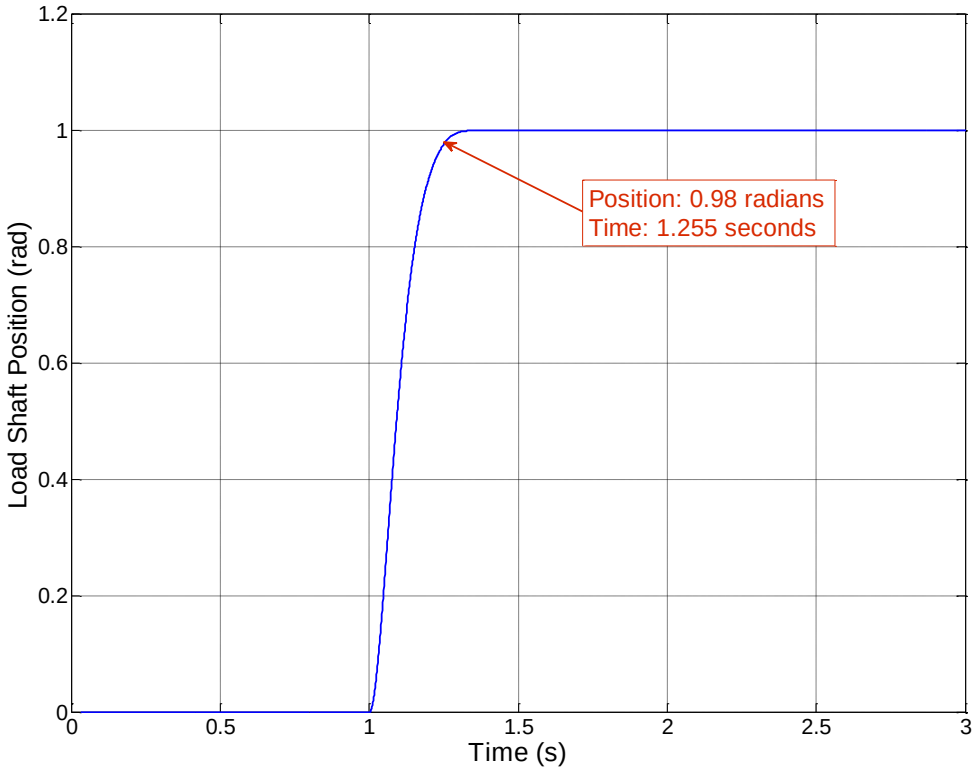

Fig. 42. Measured step response of the DC motor with the FO PI controller in (176).

8.5 Conclusion

As illustrated in Sections 8.2 and 8.3, the method presented in Chapter 5 was applied to a DC motor system to find a weighted sensitivity region for satisfying desired performance specifications of the DC motor. Such weighted sensitivity regions guarantee the stability as well as the robust performance of the closed-loop system containing the DC motor and the FO PI controller. As claimed in Chapters 4 through 7, the technique was successfully applied to the DC motor with only the experimental frequency response without the knowledge of the transfer function. As expected, the FO PI controller was able to provide a large weighted sensitivity region in the (K_p, K_i) plane. In addition, an FO PI controller was implemented on the closed-loop system of the Quanser SRV-02 DC motor to regulate the angular position of the load shaft for practical applicability. The FO PI controller was able to make the DC motor system meet all the performance specifications introduced in in Section 8.3.1.

CHAPTER 9
CONCLUSION AND FUTURE WORK

9.1 Summary

The theoretical and metholological research in this dissertation relates to fundamental control problems of FO PID controllers such as stability, performance, and robustness. First, nominal stability was investigated by finding all the possible FO PID controllers that stabilize a closed-loop system containing a plant transfer function of arbitrary order with a time delay. In particular, all the possible values of the parameters K_p, K_i, and K_d of FO PID controllers were determined with respect to arbitrary values of the fractional orders λ and μ of the FO PID controller. The frequency response of a system was used to derive the results, so that this technique can be applied even when the system parameters such as a transfer function are not known. The findings were presented on the (K_p, K_i), (K_p, K_d), and (K_i, K_d) planes.

In order to satisfy nominal performance requirements such as a settling time, percent overshoot, steady-state error, etc., a sensitivity function weight was introduced and FO PID controllers were sought to meet the weighted sensitivity constraint. This led to a complete set of possible values of FO PID controller parameters that satisfy the given performance specifications. Following the nominal stability and performance, robust stability and performance were investigated. For a robust stability requirement, a multiplicative weight was selected to bound all multiplicative errors of a closed-loop system taking into account a parametric uncertainty of an unknown time delay. Such FO PID controllers allow the closed-loop to remain stable for all the sets of perturbed plants. Nominal performance and robust stability are the prerequisite conditions for the robust performance of a closed-loop system. Though, the closed-loop system was designed only to remain stable in robust stability analysis, it was required not only to remain stable for all the uncertain plants but also to satisfy given performance specifications in the robust performance analysis.

A significant contribution of this research is the establishment of a complete set of solutions for FO PID controllers, with respect to nominal stability and performance and robust stability and performance. Since the results also cover existing solutions applicable only to the conventional IO PID controller, they serve as complete and generalized solutions to PID controllers, whether they are of integer or non-integer.

The use of frequency response of a system has produced interesting and potentially powerful results in applications. That is, the results achieved in this research can be applied even when a system transfer function is not known or unavailable, as long as the experimental frequency data of a system can be obtained. In Chapter 8, this technique was applied to a DC motor system to find weighted sensitivity regions for meeting performance specifications by using only the measured frequency response of the DC motor system without the knowledge of the transfer function thereof.

Many of the control problems encountered in this research have shown promising results for FO PID controllers. This is because FO PID controllers have been able to provide usable solutions even when there is no solution for the conventional IO PID controller. Furthermore, FO PID controllers, in general, exhibit a wider range of solutions and better performance than the IO PID controller, thereby providing more flexibility in design. This is no surprise, considering that integer numbers are a special case of real numbers.

9.2 Future Work

Now that important aspects of PID controllers have been successfully investigated, the focus of my attention at the moment is to apply the results to physical systems. As discussed in Chapter 8, the results in stability, robustness, and performance have been applied to a DC motor system. The next phase of research includes applications of the results presented here to such physical apparatus as a ball and beam system, an inverted pendulum, and a high-fidelity linear cart.

In addition, a unified approach will be investigated for FO PID controllers in both continuous and discrete time with respect to nominal stability, sensitivity, and weighed sensitivity as in the IO PID controller [39]. This unified approach will allow for the use of one technique for both continuous and discrete time PID controller design.

As one of the most helpful environments for students' learning is bridging classroom instruction to the world they live in, it is crucial to motivate students with not only knowledge but also meaningful impact of such knowledge through applications. Development of experiments applicable to classroom instruction is an essential part that will benefit students by providing opportunities for them to witness the powerful potential of the knowledge they learn.

REFERENCES

LIST OF REFERENCES

[1] K. B. Oldham and J. Spanier, *The Fractional Calculus*. New York: Academic Press, 1974.

[2] R. Hilfer (Ed.), *Applications of Fractional Calculus in Physics*. Singapore: World Scientific, 2001.

[3] I. Podlubny, *Fractional Differential Equations, Mathematics in Science and Engineering*. vol. 198, San Diego, Academic Press, 1999.

[4] M. Axtell and E. M. Bise, "Fractional calculus applications in control systems," *Proceedings of the IEEE 1990 National Aerospace and Electronics Conference*, New York, 1990, pp. 563–566.

[5] D. Xue, C. Zhao, and Y. Chen, "Fractional order PID control of a DC-motor with elastic shaft: a case study," *Proceedings of the 2006 American Control Conference*, Minneapolis, Minnesota, USA, 2006.

[6] S. Manabe, "A suggestion of fractional-order controller for flexible spacecraft attitude control," *Nonlinear Dynamics*, vol. 29, no.1-4, 2002, pp. 251-268.

[7] S. Sujoldžić and J. M. Watkins, "Stabilization of an arbitrary order transfer function with time delay using a PID controller," *Proceedings of the 45th IEEE Conference on Decision and Control*, San Diego, CA, USA, 2006, pp. 2427-2432.

[8] T. Emami and J. M. Watkins, "Robust Stability Design of PID Controllers for Arbitrary-Order Transfer Functions with Uncertain Time Delay," *Proc. of the 41st Southeastern Symposium on System Theory*, Tullahoma, TN, 2008, pp. 184-189.

[9] K.S. Miller and B. Ross, *An Introduction to the Fractional Calculus and Fractional Differential Equations*. New York: Wiley, 1993.

[10] Shantanu Das, *Functional Fractional Calculus For System Identification and Controls*. Springer, 2008.

[11] R. Gorenflo and F. Mainardi, "Fractional calculus: Integral and differential equations of fractional order," in *Fractal and Fractional Calculus in Continuum Mechanics*. Berlin: Springer-Verlag, 1997, pp. 223–276.

[12] D. Cafagna, "Fractional Calculus: A Mathematical Tool from the Past for Present Engineers," *IEEE Industrial Electronics Magazine*, Summer 2007, pp. 35-40.

[13] C. Ma, Y. Hori, "Fractional-Order Control: Theory and Applications in Motion Control," *IEEE Industrial Electronics Magazine*, Winter 2007, pp. 6-16.

[14] A. Tustin, J.T. Allanson, J.M. Layton, and R.J. Jake-ways, "The design of systems for automatic control of the position of massive objects," *Proceedings of Institute of Electrical Engineers*, vol. 105-C, no. 1, 1958, pp. 1–57.

[15] A. Oustaloup, X. Moreau, and M. Nouillant, "The CRONE suspension," *Control Eng. Practice*, vol. 4, no. 8, 1996, pp. 1101-1108.

[16] A. Oustaloup, B. Mathieu, and P. Lanusse, "The CRONE control of resonant plants: Application to a flexible transmission," *Eur. J. Contr.*, vol. 1, no. 2, pp. 113-121, 1995.

[17] I. Podlubny. "Fractional-order systems and $PI^{\lambda}D^{\mu}$ controller," *IEEE Transactions on Automatic Control*, vol. 44, no. 1, 1999, pp. 208–214.

[18] C. Ma and Y. Hori, "Backlash vibration suppression control of torsional system by novel fractional order PID^{k} controller," *IEEJ Trans. Ind. Applicat.*, vol. 124-D, no.3, 2004, pp. 312-317.

[19] C. Monje, Y. Chen, et al., *Fractional-order Systems and Controls: Fundamentals and Applications*, Springer, London, 2010.

[20] A. Ruszewski, "Stability regions of closed loop system with time delay inertial plant of fractional order and fractional order PI controller," *Bulletin of the Polish Academy of Sciences, Technical Sciences*, vol. 56, no. 4, 2008, pp. 329-332.

[21] J. Neimark, "D-subdivisions and spaces of quasi-polynomials," *Prikl. Mat. Meth.*, Vol. 13, 1949, pp. 349-380.

[22] Y. I. Neimark, "Robust stability and D-partition," *Automation and Remote Control* 53 (1992) (7), pp. 957-965.

[23] S. E. Hamamci, "An algorithm for stabilization of fractional-order time delay systems using fractional-order PID controllers," *IEEE Transactions on Automatic Control,* vol. 52, no. 10, October 2007.

[24] A. Majid, K. G. Masoud, and S. Nasser, "Design of an H_{∞}-optimal FOPID controller using particle swarm optimization," *Proceedings of the 26th Chinese Control Conference*, Zhangjiajie, Hunan, China, 2007.

[25] M. Saeki, "Fixed structure PID controller design for standard H_{∞} control problem," *Proceedings of the 16th IFAC World Congress*, Prague, Czech Republic, 2005.

[26] Yun Zhang, Lei Jia, and Hongbo Liu, "Robust Stability Analysis of Predictive PID Controller," *Proceedings of the 6th World Congress on Intelligent Control and Automation*, Dalian, China, 2006.

[27] T. Emami and J. M Watkins, "Weighted Sensitivity Design of PID Controllers for Arbitrary-Order Transfer Functions with Time Delay," *Proceedings of the IASTED Conference on Intelligent Systems and Control*, Orlando, FL, November 2008.

[28] T. Emami and J. M Watkins, "Sensitivity Design of PID Controllers for Arbitrary-Order Transfer Functions with Time-Delay Applied to a DC Motor with Communication Delay," *Proceedings of the IEEE Multi Conference on Systems and Control*, San Antonio, TX, 2008.

[29] T. Emami and J. M Watkins, "Robust Performance Characterization of PID Controllers in the Frequency Domain," *Proceedings of the 8th International Conference on Applications of Electrical Engineering*, Houston, TX, April 2009, pp. 121-127.

[30] N. Tan, "Computation of stabilizing PI and PID controllers for processes with time delay," *ISA Trans*., Vol. 44, 2005, pp. 213-223.

[31] S. Skogestad and I. Postlethwaite, *Multivariable Feedback Control Analysis and Design*, John Wiley & Sons, Inc., England, 2005.

[32] Y. K. Lee and J. M. Watkins, "Determination of All Stabilizing Fractional-Order PID Controllers," *Proceedings of the 2011 American Control Conference*, San Francisco, CA, 2011, pp. 5007-5012.

[33] Y. K. Lee and J. M. Watkins, "Determination of All Stabilizing Fractional-Order PID Controllers that Satisfy a Weighted Sensitivity Constraint," *Proceedings of the 51st IEEE Conference on Decision and Control*, Maui, Hawaii, 2012, pp. 254-259.

[34] A. Charef, H. H. Sun, Y. Y. Tsao, and B. Onaral, "Fractal system as represented by a singularity function," *IEEE Transactions on Automatic Control*, vol. 37, no. 9, 1992, pp. 1465-1470.

[35] A. Charef, "Analogue realization of fractional-order integrator, differentiator and fractional $PI^{\lambda}D^{\mu}$ controller," *IEE Proc. Control Theory Appl*. vol. 153, no. 6, November 2006, pp. 714-720.

[36] Y. K. Lee and J. M. Watkins, "Determination of All Robustly Stabilizing Fractional-Order PID Controllers," *Proceedings of the 2012 ASME Dynamic Systems and Control Conference, and 2012 Motion & Vibration Conference*, Ft. Lauderdale, FL, 2012.

[37] Y. K. Lee and J. M. Watkins, "Determination of All Stabilizing Fractional-Order PID Controllers that Satisfy a Robust Performance Constraint," *Proceedings of the 2013 American Control Conference*, Washington, DC, 2013, to be published.

[38] *Quanser Inc*., SRV02 User Manual, 2011.

[39] T. Emami and J. M. Watkins, "A Unified Approach for H_∞ Complementary Sensitivity Design of PID Controllers Applied to a DC Motor with Communication Delay," *Proceedings of the ASME 2009 International Mechanical Engineering Congress & Exposition*, Lake Buena Vista, FL, 2009.

[40] D. Valério and J. S. Costa, "Ninteger: A Non-integer Control Toolbox for MATLAB," *Proceedings of Fractional Differentiation and its applications*, Bordeaux, France, 2004.

APPENDIX

APPENDIX

1. NOMINAL STABILITY OF FO PID CONTROLLERS

The following MATLAB script is for finding the nominal stability boundary of fractional-order (FO) PID controllers in Chapter 4.

1. MATLAB code for Fig. 2

```
clear all;
clc;

% Al is for lambda and Be is for mu
Al = 1.0;
Be = 0.5;

G = tf([4 1],[1 0.4 6])
get(G);
td = 0.8;
set(G,'iodelay',td);

gm = 1;
PM = 0;
pm = PM*(pi/180);

Kdc_min = -0.5;
Kdc_max = 1.5;

ax11 = [-0.5 3.0, -0.5 1.2, -1.4 0.3];

for Kdc = Kdc_min:0.01:Kdc_max;

    if Kdc <= 0.35
        IvW1 = 0.7;
        IvW2 = 5;
    else
        IvW1 = 1;
        IvW2 = 5;
    end
        options = optimset('Display','off');
        wrange = fsolve(@myfunPI, [IvW1 IvW2], options, Kdc, G, pm, gm, Al,
Be);
        wmax = max(wrange);
        wmin = min(wrange);

        if wmin+0.0005 <= wmax
            z = wmin:(wmax-wmin)/100:wmax;
            Gp = frd(G,z);
            Rp = real(Gp);
```

```
Ip = imag(Gp);
magGp = abs(Gp);

zAl = frd(z'.^Al,z);
zBe = frd(z'.^Be,z);

Kp = -(Kdc)*(zBe)*sin((pi/2)*(Al+Be))/sin((pi/2)*Al)-(1/gm)*(Rp*
sin(pm+(pi/2)*Al)-Ip*cos(pm+(pi/2)*Al))/(sin((pi/2)*Al)*
(magGp^2));
Ki = (Kdc)*(zAl*zBe)*sin((pi/2)*Be)/sin((pi/2)*Al)+ (1/gm)*(zAl)
*(sin(pm)*Rp-cos(pm)*Ip)/(sin((pi/2)*Al)*(magGp^2));

y = [Ki.responsedata(:)-0]';
[i,k] = find(abs(diff(sign(y)))>1);

n = sum(i);

if n >0
    wn = zeros(1,n);

    for i = 1:n;
        wn(i) = interp1(y(k(i):k(i)+1),z(k(i):k(i)+1), 0);
    end

    for i = 1:n;
        wnAl(i) = wn(i)'.^Al;
        wnBe(i) = wn(i)'.^Be;

        Gp21(i) = (4*j*wn(i)+1)/((j*wn(i)).^2+0.4*j*wn(i)+6)
       *exp(-0.8*j*wn(i));

        Rp21(i) = real(Gp21(i));
        Ip21(i) = imag(Gp21(i));
        magGp21(i) = abs(Gp21(i));

        Kp21(i) = -(Kdc)*(wnBe(i))*sin((pi/2)*(Al+Be))/
        sin((pi/2)*Al)-(1/gm)*(Rp21(i)*sin(pm+(pi/2)*Al)-Ip21(i)
        *cos(pm+(pi/2)*Al))/(sin((pi/2)*Al)*(magGp21(i)^2));
    end

    if Kp21(1) < Kp21(2)

        figure(2)
        Kp211 = Kp21(1):0.001:Kp21(2);
        Ki1 = Kp211*0;

        line('Xdata',Ki1(1,:),'Ydata',Kdc*ones(size(Kp211)),
        'Zdata',Kp211(1,:),'color','r');
        axis(ax11);
        xlabel('K_i');
        ylabel('K_d');
        zlabel('K_p');
        grid on;
```

```
    zn = wn(1):(wn(2)-wn(1))/100:wn(2);
    Gp22 = frd(G,zn);
    Rp22 = real(Gp22);
    Ip22 = imag(Gp22);
    magGp22 = abs(Gp22);

    znAl = frd(zn'.^Al,zn);
    znBe = frd(zn'.^Be,zn);

    Kp22 = -(Kdc)*(znBe)*sin((pi/2)*(Al+Be))/sin((pi/2)*Al)-
    (1/gm)*(Rp22*sin(pm+(pi/2)*Al)-Ip22*cos(pm+(pi/2)*Al))/
    (sin((pi/2)*Al)*(magGp22^2));
    Ki22 = (Kdc)*(znAl*znBe)*sin((pi/2)*Be)/sin((pi/2)*Al)
    +(1/gm)*(znAl)*(sin(pm)*Rp22-cos(pm)*Ip22)/
    (sin((pi/2)*Al)*(magGp22^2));

    figure(2);
    line('Xdata',Ki22.responsedata(1,:),'Ydata',
    Kdc*ones(size(zn)), 'Zdata',Kp22.responsedata(1,:),
    'color','r');

else
    figure(2)
    Kp211 = Kp21(2):0.001:Kp21(1);
    Ki1 = Kp211*0;

    line('Xdata',Ki1(1,:),'Ydata',Kdc*ones(size(Kp211)),
    'Zdata',Kp211(1,:),'color','r');
    axis(ax11);
    xlabel('K_i');
    ylabel('K_d');
    zlabel('K_p');
    grid on;

    zn1 = wmin:(wn(1)-wmin)/200:wn(1);
    Gp221 = frd(G,zn1);
    Rp221 = real(Gp221);
    Ip221 = imag(Gp221);
    magGp221 = abs(Gp221);

    zn1Al = frd(zn1'.^Al,zn1);
    zn1Be = frd(zn1'.^Be,zn1);

    Kp221 = -(Kdc)*(zn1Be)*sin((pi/2)*(Al+Be))/sin((pi/2)*Al)
    -(1/gm)*(Rp221*sin(pm+(pi/2)*Al)-Ip221*cos(pm+(pi/2)*Al))
    /(sin((pi/2)*Al)*(magGp221^2));
    Ki221 = (Kdc)*(zn1Al*zn1Be)*sin((pi/2)*Be)/sin((pi/2)*Al)
    +(1/gm)*(zn1Al)*(sin(pm)*Rp221-cos(pm)*Ip221)/
    (sin((pi/2)*Al)*(magGp221^2));


    figure(2);
    line('Xdata',Ki221.responsedata(1,:),'Ydata',
    Kdc*ones(size(zn1)),'Zdata',Kp221.responsedata(1,:),
    'color','r');
```

```
                    zn2 = wn(2):(wmax-wn(2))/200:wmax;
                    Gp222 = frd(G,zn2);
                    Rp222 = real(Gp222);
                    Ip222 = imag(Gp222);
                    magGp222 = abs(Gp222);

                    zn2Al = frd(zn2'.^Al,zn2);
                    zn2Be = frd(zn2'.^Be,zn2);

                    Kp222 = -(Kdc)*(zn2Be)*sin((pi/2)*(Al+Be))/sin((pi/2)*Al)
                    -(1/gm)*(Rp222*sin(pm+(pi/2)*Al)-Ip222*cos(pm+(pi/2)*Al))
                    /(sin((pi/2)*Al)*(magGp222^2));
                    Ki222 = (Kdc)*(zn2Al*zn2Be)*sin((pi/2)*Be)/sin((pi/2)*Al)
                    +(1/gm)*(zn2Al)*(sin(pm)*Rp222-cos(pm)*Ip222)
                    /(sin((pi/2)*Al)*(magGp222^2));

                    figure(2);
                    line('Xdata',Ki222.responsedata(1,:),'Ydata',
                    Kdc*ones(size(zn2)),'Zdata',Kp222.responsedata(1,:),
                    'color','r');

                end

            else

                Gpt = freqresp(G,wmin);
                Rpt = real(Gpt);
                Ipt = imag(Gpt);
                magGpt = abs(Gpt);

                Kit = (Kdc)*(wmin.^(Al+Be))*sin((pi/2)*Be)/sin((pi/2)*Al)
                +(1/gm)*(wmin.^Al)*(sin(pm)*Rpt-cos(pm)*Ipt)/(sin((pi/2)*Al)
                *(magGpt^2));

                if Kit > 0

                    figure(2)
                    line('Xdata',Ki.responsedata(1,:),'Ydata',
                    Kdc*ones(size(z)),'Zdata',Kp.responsedata(1,:),
                    'color','r');
                    xlabel('K_i');
                    ylabel('K_d');
                    zlabel('K_p');
                    axis(ax11);
                    grid on
                end
            end
        end

end

title('Stability Space for Varying K_d')
```

2. ROBUSTLY STABILIZING FO PID CONTROLLER DESIGN

The following MATLAB script is for finding the robust stability region of FO PID controllers in Chapter 6.

1. MATLAB code for Fig. 21

```
s = zpk('s')

% integer-order (IO) case
% Al = 1.0;         % the value for alpha
% Be = 1.0;         % the value for beta

% fractional-order (FO) case
Al = 1.32;         % the value for alpha
Be = 0.65;         % the value for beta

G = tf([65.5],[1 34.6 0])
get(G);
td = 0.1;
set(G,'iodelay',td);

Kic = 22;

w = 0.001:0.02:60;
t = 0:0.001:60;

ax2 = [0 9, -0.5 2];

Wm = tf([1 0],[1/2.8 20])

% for robust stability
gamma = 1;

% % for nominal stability
% gamma = inf;

if  mod(Be,2) == 0
    ax21 = [-3 5, -4 5];
    [Kp,Kd] = Kps_Kds_RS_son(Al,Be,G,w,Kic,ax2,ax21,Wm,gamma);
else
    if  Al == 1.0 & Be == 1.0
        [Kp,Kd] = Kpi_Kdi_RS_son(Al,Be,G,w,Kic,ax2,Wm,gamma);
    else
        [Kp,Kd] = Kpf_Kdf_RS_son(Al,Be,G,w,Kic,ax2,Wm,gamma);
    end
end
```

The following is a function file for finding the robust stability region in Fig. 21 for FO PID controllers.

```
function [Kp,Kd] = Kpf_Kdf_RS_son(Al,Be,G,w,Kic,ax2,Wm,gamma);

Gp = frd(G,w);
Rp = real(Gp);
Ip = imag(Gp);
magGp = abs(Gp);

omAl = frd(w'.^Al,w);
omBe = frd(w'.^Be,w);

Wmf = frd(Wm,w);
Rm = real(Wmf);
Im = imag(Wmf);
magWm = abs(Wmf);

if gamma == inf

    for theta = 0:1:2*pi;
        Dp = (omAl)*sin((pi/2)*Be)*(magGp^2)*((1/(gamma^2))*(magWm^2)+1
        -(2/gamma)*(Rm*cos(theta)-Im*sin(theta)));
        Kp = -(Kic)*sin((pi/2)*(Al+Be))/(omAl*sin((pi/2)*Be))-(omAl)*
        (Rp*sin((pi/2)*Be)+Ip*cos((pi/2)*Be)-(1/gamma)*cos((pi/2)*Be+theta)
        *(Rp*Im+Ip*Rm)-(1/gamma)*sin((pi/2)*Be+theta)*(Rp*Rm-Ip*Im))/(Dp);
        Dd = (omAl*omBe)*sin((pi/2)*Be)*(magGp^2)*((1/(gamma^2))*(magWm^2)+1-
        (2/gamma)*(Rm*cos(theta)-Im*sin(theta)));
        Kd = (Kic)*sin((pi/2)*Al)/((omAl*omBe)*sin((pi/2)*Be))+(omAl)*(Ip-
        (1/gamma)*cos(theta)*(Rp*Im+Ip*Rm)-(1/gamma)*sin(theta)
        *(Rp*Rm-Ip*Im))/(Dd);

        figure(21)
        line('Xdata',Kp.responsedata(:),'Ydata',Kd.responsedata(:),'color',
        'r','linestyle','-','linewidth',2.0);
        grid on;
        xlabel('K_p')
        ylabel('K_d')
        axis(ax2);
    end
else

    for theta = 0:0.06:2*pi;
        Dp = (omAl)*sin((pi/2)*Be)*(magGp^2)*((1/(gamma^2))*(magWm^2)+1-
        (2/gamma)*(Rm*cos(theta)-Im*sin(theta)));
        Kp = -(Kic)*sin((pi/2)*(Al+Be))/(omAl*sin((pi/2)*Be)) - (omAl)*
        (Rp*sin((pi/2)*Be)+Ip*cos((pi/2)*Be)-(1/gamma)*cos((pi/2)
        *Be+theta)*(Rp*Im+Ip*Rm)-(1/gamma)*sin((pi/2)*Be+theta)
        *(Rp*Rm-Ip*Im))/(Dp);
        Dd = (omAl*omBe)*sin((pi/2)*Be)*(magGp^2)*((1/(gamma^2))*(magWm^2)+1
        -(2/gamma)*(Rm*cos(theta)-Im*sin(theta)));
        Kd = (Kic)*sin((pi/2)*Al)/((omAl*omBe)*sin((pi/2)*Be))+(omAl)
```

```
        *(Ip-(1/gamma)*cos(theta)*(Rp*Im+Ip*Rm)-(1/gamma)*sin(theta)
        *(Rp*Rm-Ip*Im))/(Dd);

        figure(21)
        line('Xdata',Kp.responsedata(:),'Ydata',Kd.responsedata(:),'color',
        'c','linestyle','-','linewidth',0.5);
        grid on;
        xlabel('K_p')
        ylabel('K_d')
        axis(ax2);
    end
end

hold on

title('FO PID Case in (K_p,K_d) Plane')
```